Technische Universität München

Fakultät für Medizin, Klinikum rechts der Isar

Analysis of PIF-pocket and PH-domain mediated 3-phosphoinositide-dependent protein kinase 1 signaling in pancreatic cancer

Hongkai Yan

Vollständiger Abdruck der von der Fakultät für Medizin der Technischen Universität München zur Erlangung des akademischen Grades eines

Doktors der Medizin (M.D.)

genehmigten Dissertation.

Vorsitzender: Prof. Dr. Lars Maegdefessel
Prüfende/-r der Dissertation:

1. Prof. Dr. Dieter Saur
2. apl. Prof. Dr. Marc Martignoni

Die Dissertation wurde am 03.12.2020 bei der Technischen Universität München eingereicht und durch die Fakultät für Medizin am 08.06.2021 angenommen.

Table of contents

Table of contents I

List of Tables IV

List of Figures V

Abbreviations VI

1. Introduction 1

1.1 Pancreatic ductal adenocarcinoma 1

1.2 Oncogenic KRAS 2

1.3 The PDAC progress stages and related signaling pathways 3

1.4 *Pdk1*^{K465E} mutation and *Pdk1*^{L155E} mutation 6

1.5 Genetically engineered mouse models for PDAC 7

1.6 Aim of this work 8

2. Materials 9

2.1 Technical equipment 9

2.2 Disposables 11

2.3 Reagents and enzymes 12

2.4 Kit 15

2.5 Antibodies 15

2.6 Solutions 16

2.7 Primers 18

2.8 Cell culture 19

2.9 Histology 21

2.10 Software 21

3. Methods 22

3.1 Mouse experiments 22

3.1.1 Mouse strains 22

3.1.2 Genotyping 24
3.1.3 Mouse dissection 24
3.2 Histological analysis 25
3.2.1 Paraffin sections 25
3.2.2 Hematoxylin and eosin (H&E) staining of tissue sections 25
3.2.3 Alcian blue (AB) staining 26
3.2.4 Immunohistochemistry (IHC) 26
3.2.5 Quantification and counting of ADM and PanIN lesions 27
3.2.6 Pathological analysis of staining 27
3.3 Cell culture 27
3.3.1 Generation and culture of primary mouse PDAC cell lines 27
3.3.2 Validation of cell lines 28
3.3.3 Documentation of cell morphology 28
3.3.4 Treatment of cells with tamoxifen 29
3.3.5 MTT assay 29
3.3.6 Clonogenic assay 29
3.3.7 ADM assay 30
3.4 Molecular biology 31
3.4.1 Isolation of genomic DNA 31
3.4.2 Polymerase chain reaction 31
3.4.2.1 Polymerase chain reaction (PCR) condition 31
3.4.2.2 Genotyping PCR 32
3.4.2.3 Recombination PCR 32
3.4.2.4 Touchdown PCR for $Pdk1^{L155E}$ recombination 33
3.4.3 Agarose gel electrophoresis 34
3.5 Western Blot 34
3.5.1 Protein extraction 34
3.5.2 Protein concentration determination 35
3.5.3 SDS polyacrylamide gel electrophoresis (SDS-PAGE) 35
3.5.4 Immunoblot 36

3.6 Statistical analysis 36

4. Results 38

4.1 Validation of *Pdk1* mutation mouse models 38

4.2 The roles of *Pdk1*^{K465E} and *Pdk1*^{L155E} mutations in KRAS^{G12D}-driven cancer ... 41

4.3 Effects of *Pdk1*^{K465E} and *Pdk1*^{L155E} mutations on tumor initiation in KRAS^{G12D}-driven pancreatic tumor mouse model 45

4.4 Analysis of *Pdk1*^{K465E} and *Pdk1*^{L155E} dependent signaling pathways *in vivo* 49

4.5 Inducible induction of PDK1^{K465E} and PDK1^{L155E} mutations *in vivo* and *in vitro* 50

4.6 *Pdk1*^{K465E} and *Pdk1*^{L155E} mutations impair PDAC cell proliferation and colony formation *in vitro* 54

4.7 Longitudinal analysis of PIF-pocket domain and PH-domain dependent downstream signaling *in vitro* 57

5. Discussion 63

5.1 Roles of *Pdk1*^{L155E} *and Pdk1*^{K465E} mutation in KRAS driven pancreatic tumor initiation and development. 63

5.1.1 Role of the PIF-pocket domain of PDK1 for KRAS-driven tumorigenesis . 63

5.1.2 The PH-domain of PDK1 is essential for KRAS-driven PDAC tumorigenesis 65

5.2 Mouse models to test PDAC tumor maintenance 67

5.2.1 The PIF-pocket domain of PDK1 is fundamental for KRAS-driven PDAC cell proliferation and maintenance, and independent of the *p53* status 67

5.2.2 The PH-domain of PDK1 is indispensable for the maintenance of KRAS-driven *p53* wild-type PDAC 68

6. Summary 70

7. Reference 71

8. Acknowledgements 78

List of Tables

Table 1. Technical equipment. 9
Table 2. Disposables..... 11
Table 3. Reagents and enzymes. 12
Table 4. Kit. 15
Table 5. Antibodies..... 15
Table 6. Buffers and solutions for molecular biology..... 16
Table 7. Primers used for genotyping. 18
Table 8. Cell culture media and their components. 19
Table 9. Reagents and kits for cell culture. 20
Table 10. Reagents and kits for histological analysis..... 21
Table 11. Software 21
Table 12. Composition of pre-mix for PCR 31
Table 13. Reaction mix and conditions for standard PCR..... 32
Table 14. Annealing temperatures and PCR products..... 32
Table 15. Annealing temperatures and PCR products..... 33
Table 16. Reaction mix for touch down PCR 33
Table 17. Touchdown PCR program for amplification of DNA 33
Table 18. SDS gel for electrophoresis of proteins..... 36

List of Figures

Figure 1. PI3K and RAS related signaling pathway. 5

Figure 2. The genetic strategy of KC Mouse model with different *Pdk1* mutations... 39

Figure 3. Interpretation of genotyping strategy and PCR results of *Pdk1* constructs 40

Figure 4. Interpretation of recombination PCR strategy and results of *Pdk1* constructs 41

Figure 5. The survival of PDK1^{K465E} and PDK^{L155E} mice in KRAS^{G12D}-driven cancer 43

Figure 6. The body and pancreas weight of KCPDK1^{K465E} and KCPDK^{L155E} mice.... 44

Figure 7. Macroscopic changes in the mouse pancreas at specific time points 45

Figure 8. Pathology changes in the mouse pancreas at specific time points 47

Figure 9. ADM and PanIN formation *in vivo* and *in vitro* 48

Figure 10. *Pdk1^{L155E}* and *Pdk1^{K465E}* mutations related signaling pathway *in vivo*..... 50

Figure 11. DRS mouse model constructions for spatial or temporal manipulation of established KRAS^{G12D}-induced PDAC cells in the *Pdx1-Flp* lineage 51

Figure 12. Analysis of PH-domain and PIF-pocket dependent downstream signaling in vitro 53

Figure 13. *Pdk1^{K465E}* and *Pdk1^{L155E}* mutations impair proliferation and colony formation of *p53* wild-type PDAC cells *in vitro* 55

Figure 14. Context specific effects of *Pdk1^{K465E}* and *Pdk1^{L155E}* mutations on proliferation and colony formation in *p53* deficient PDAC cells *in vitro*..... 56

Figure 15. Time series DRS cell lines treated with TAM or EtOH 58

Figure 16. Logitudinal analysis of PIF-pocket domain of PDK1 downstream signaling in *p53* wild-type and mutant PDAC cells..... 60

Figure 17. Longitudinal analysis of PH-domain of PDK1 downstream signaling in *p53* wild-type and deficient PDAC cells 62

Abbreviations

Abbreviations

°C	degree Celsius
AB	alcian blue
ADM	acinar-to-ductal-metaplasia
AKT	protein kinase B
Amp	ampicillin
ANOVA	analysis of variance
APS	ammonium persulphate
BDNF	Brain-derived neurotrophic factor
Bp	base pairs
BPE	bovine pituitary extract
BRSK	BR serine/threonine kinase
BSA	bovine serum albumin
CDKN2A	cyclin-dependent kinase inhibitor 2A
cDNA	complementary desoxyribonucleic acid
Cers	ceramide synthase
CK19	cytokeratin 19
Cm	Centimeter
DAB	3, 3 -diaminobenzidine
DMEM	Dulbecco´s modified Eagle medium
DMEM	Dulbecco´s modified Eagle medium
DMSO	Dimethylsulfoxide
DMSO	Dimethylsulfoxide
DMSO	Dimethylsulfoxide
DNA	deoxyribonucleic acid
dNTP	deoxynucleoside triphosphate
DRS	dual-recombinase system
DTT	Dithiothreitol

DTT	1,4-Dithiothreito
ECM	extracellular matrix
EDTA	ethylenediaminetetraacetic acid
EDTA	Ethylenediaminetetraacetic acid
EGF	epidermal growth factor
EGFP	enhanced green fluorescent protein
ELISA	enzyme-linked immunosorbent assay
EMT	epithelial mesenchymal transition
ER	estrogen receptor
ERK	extracellular signal-related kinase
ES	embryonic stem
EtOH	ethanol
FCS	fetal calf serum
FOXO	forkhead box O protein
FSF	frt-stop-frt
G	gram
GAPDH	Glyceraldehyde 3-phosphate dehydrogenase
GEF	guanine nucleotide exchange factor
GEMM	genetically engineered mouse model
GSK3	glycogen synthase kinase 3
H	hour
H&E	hematoxylin and eosin
HBSS	Hanks' balanced salt solution
HCl	Hydrochloric acid
i.p.	intraperitoneal
IHC	immunohistochemistry
IPMN	intraductal papillary mucinous neoplasm
ITS-X	Insulin,-Transferrin-Selenium-Ethanolamine
Kb	kilo base pair

KO	knock-out
Kras	v-Ki-ras2 Kirsten rat sarcoma viral oncogene homolog
L	liter
LOH	loss of heterozygosity
LSL	loxP-stop-loxP
M	mol / molar
MAPK	mitogen-activated protein kinase
MCN	mucinous cystic neoplasm
Mek	mitogen-activated protein kinase kinase
Mg	milligram
Min	minute
Ml	milliliter
mM	millimole
Mm	millimeter
MMF	midazolam, medetomidine, fentanyl
mRNA	messenger ribonucleic acid
mTOR	mammalian target of rapamycin
mTORC1	mammalian target of rapamycin complex 1
MTT	3-(4,5-dimethyl-2-thiazolyl)-2,5-diphenyl-tetrazolium bromide
Mut	mutated
MW	molecular weight
NaCl	Sodium chloride
NaOH	Sodium hydroxide solution
Ng	nanogram
Nm	nanometer
nM	nanomole
o/n	over night
OD	optical density
P	phospho

PAGE	polyacrylamide gel electrophoresis
PanIN	pancreatic intraepithelial neoplasia
PBS	phosphate buffered saline
PBST	phosphate buffered saline with 0.1% Tween-20
PCNA	proliferating cell nuclear antigen
PCR	polymerase chain reaction
PDAC	pancreatic ductal adenocarcinoma
PDK1	3-phosphoinositide-dependent protein kinase 1
Pdx1	pancreatic and duodenal homeobox 1
PFA	paraformaldehyde
PH	pleckstrin homology
PI3K	phosphoinositide 3-kinase
PIF	PDK1 interacting fragment
PIP_2	phosphatidylinositol 4,5-bisphosphate
PIP_3	phosphatidylinositol 3,4,5-trisphosphate
PKB	Protein kinase B
PKC	Protein kinase C
PPT	pancreatic primary tumor
PTEN	phosphatase and tensin homolog
Ptf1a	pancreas transcription factor subunit alpha
R26	Rosa26
RAF	Rapidly Accelerated Fibrosarcoma
RNA	ribonucleic acid
Rpm	revolutions per minute
rRNA	ribosomal ribonucleic acid
RSK2	p90 Ribosomal protein S6 kinase-2
RT	room temperature
S6K	p70 Ribosomal protein S6 kinase
S6R	Phospho-S6 Ribosomal Protein

SBTI	soybean trypsin inhibitor
SD	standard deviation
SDS	Sodium dodecyl sulphate
Sec	seconds
SEM	standard error of the mean
SGK3	Serum/Glucocorticoid Regulated Kinase Family Member 3
SMAD4	mothers against decapentaplegic homolog 4
TAE	tris-acetate-EDTA
TAM	tamoxifen
TCA	tricarboxylic acid
TE	tris-EDTA buffer
TEMED	N,N,N',N'-tetramethylethylenediamine, 1,2-bis(dimethylamino)-ethane
TGFα	transforming growth factor α
Tnc	tenascin C
P53 / TP53 / Trp53	transformation related protein 53
Tris	tris-(hydroxymethyl)-aminomethan
tTA	tetracycline transactivator
U	unit of enzyme activity
UV	ultraviolet
V	volt
VEGF	vascular endothelial growth factor
w/v	weight per volume
WB	western blot
Wt	wild-type
µg	microgram
Ml	microliter
µm	micrometer
µM	micromole
4-OHT	4-hydroxytamoxifen

1. Introduction

1.1 Pancreatic ductal adenocarcinoma

Pancreatic ductal adenocarcinoma (PDAC) is a highly lethal disease and is the seventh leading cause of cancer deaths worldwide (Christenson et al., 2020). Considering the rising incidence of PDAC and that it has the highest case-fatality rate of the solid tumors, it is critical to design effective therapeutic strategies. Factors such as metabolism (Son et al., 2013), heterogeneity (Neuzillet et al., 2019), and microenvironment (Zhang et al., 2020) integral in PDAC pathogenesis have been vigorously explored.

Pancreatic cancer is not readily detected in the beginning, because it remains asymptomatic until an advanced stage in most cases. By the time patients have developed diabetes or abdominal pain, PDAC has already progressed to the advanced stage, and only those aware they present high-risk factors and participate in an annual screening are discovered in the early stage (Li et al., 2013). Risk factors include family history (Hruban et al., 2010), cigarette smoking (Iodice et al., 2008), chronic pancreatitis (Raimondi et al., 2010), and diabetes mellitus (Bosetti et al., 2014). This latent character renders it difficult to study the entire progress of PDAC from tumor initiation to tumor maintenance.

Worldwide, the prognosis of PDAC is poor. Based on GLOBOCAN 2018 estimates, there were 458,918 new pancreatic cancer cases and 432,242 deaths from the disease in 2018 (Bray et al., 2018). Despite advancements in diagnosis and surgery, the 5-year survival rate remains at approximately 9% (Bray et al., 2018).

The cost of PDAC treatment is another crucial challenge for both individual patients and the broader economy. Economic research has determined that the average inflation-adjusted cost per patient for pancreatic cancer has decreased from USD 37,000 to USD 10,000 between 2009 and 2016. During the same period, with reasonable pharmacotherapy, prescription drug spending increased from USD 2,400 to USD 5,300 per person (Hirsch et al., 2020). This increase indicates that drug

efficiency plays an important role in the cost of pancreatic cancer treatment and demonstrates that a highly cost-effective option is needed for both individual patients and the nation. It is crucial to study cancer-related signaling pathways to advance potential PDAC treatment strategies and effective drug discoveries.

1.2 Oncogenic KRAS

In humans, three *RAS* genes, *HRAS*, *KRAS,* and *NRAS,* encode four ~21 kDa small GTPases. *KRAS* is one of the most frequently mutated oncogenes in cancer and its protein cycles between an inactive GDP bound state and an active GTP bound state (Bourne et al., 1990; Field et al., 1987; Wittinghofer and Pai, 1991). The majority of *KRAS* mutations occur at codons 12, 13, and 61, leading to constitutive activation. Constitutive activation subsequently causes abnormal behavior. Researchers have reported that *KRAS* mutations influence pancreatic tumorigenesis, malignancy and response to therapy (Corcoran et al., 2011; Kelber et al., 2012; Ying et al., 2012). Numerous pathways related to KRAS include RAS/RAF/MEK/ERK, PI3K/PDK1/AKT, STAT3, Rac and Rho, Rassf1, NF1, p120GAP, and PLC-e, but the two major pathways seem to be RAS/RAF/MEK/ERK and PI3K/PDK1/AKT (Castellano and Downward, 2011; Eser et al., 2014; Pylayeva-Gupta et al., 2011). The RAS/RAF/MEK/ERK pathway, also known as the mitogen-activated protein kinase (MAPK) pathway, was the first identified RAS effector cascade (Moodie et al., 1993; Vojtek et al., 1993; Warne et al., 1993; Zhang et al., 1993).

In the pancreas, most studies have reported that ERK activation may influence growth, proliferation, and regeneration as ERK1/2 is recognized as a master regulator of the cell cycle focused on the G1 to S phase transition (Meloche and Pouysségur, 2007). As the inhibition of MEK/ERK leads to a high dependence of PDAC cells on autophagy for survival, combined treatment of MEK/ERK inhibitors and autophagy inhibitors is a potential treatment approach (Bryant and Stalnecker, 2019). In the PI3K/PDK1/AKT pathway, PI3K converts phosphatidylinositol 4,5-bisphosphate (PIP_2) to phosphatidylinositol 3,4,5-triphosphate (PIP_3). This reaction is suppressed by the tumor suppressor phosphatase and tensin homolog (PTEN). The second messenger

PIP_3 binds to proteins containing pleckstrin homology (PH) domains (Cantley, 2002) and thereby recruits 3-phosphoinositide-dependent protein kinase 1 (PDK1) and AKT to the plasma membrane. The AKT T308 is activated by phosphorylation, and together with AKT S473 phosphorylation, could provide AKT full function. Several studies have demonstrated constitutive activation of AKT in PDAC is associated with poor prognosis and chemoresistance (Liu et al., 2007; Massihnia et al., 2017).

Besides well-known related pathways, recent studies have described new mechanisms of KRAS induced tumorigenesis by analyzing its effects on the components of the tumor microenvironment. Tumor microenvironment includes inflammatory and immune cells, and other resident or recruited stromal cells, such as fibroblasts, endothelial cells, adipocytes, pericytes, and components of the extracellular matrix (ECM) (Hanahan and Coussens, 2012). Cancer cells bearing *KRAS*-mutations affect many aspects of the microenvironment, such as tumor growth (Laklai et al., 2016), metastasis (Tauriello and Batlle, 2016), and drug resistance (Jiang and Hegde, 2016).

1.3 The PDAC progress stages and related signaling pathways

The mechanisms behind PDAC progression are extremely complicated. With oncogene activation and mutation or loss of suppressor genes, normal cells start to transition to tumor cells with nuclear and architectural atypia. The most common mechanism for tumor progression is the accumulation of mutated genes, gene deletions, or translocations (Martincorena and Campbell, 2015).

Acinar-to-ductal metaplasia (ADM) has been suggested as an initiating event in human and murine PDAC formation (Aichler et al., 2012). Several distinct precursor lesions were discovered in the subsequent step, and they could affect the biological behavior of tumor cell, effects of therapeutics, and prognosis. The precursor lesions include pancreatic intraepithelial neoplasia (PanIN), intraductal papillary mucinous neoplasm (IPMN), mucinous cystic neoplasm (MCN) (Matthaei et al., 2011), and atypical flat lesions (Esposito et al., 2012). The most common precursor lesion associated with PDAC is PanIN (Basturk et al., 2015).

According to the nuclear and architectural atypia, PanINs are generally classified into three different stages: PanIN-1, PanIN-2, and PanIN-3 (Hruban et al., 2000). Normal ductal structures consist of cuboidal to low-columnar epithelium without cytoplasmatic mucin. ADM is a morphologic and transcriptional conversion, which would alter cells from acinar to duct-like and it is considered the main origin of pancreatic pre-neoplastic lesions (Chuvin et al., 2017). PanIN-1A lesions are ductal structures characterized by a flat epithelium consisting of tall columnar cells with basally located nuclei and by abundant mucin. PanIN-1B lesions acquire a papillary, micropapillary or basally pseudostratified architecture. These low-grade PanINs are common and present in up to 40% of non-malignant pancreata in patients older than 50 years (Hruban et al., 2004; Schneider et al., 2005). Frequent papillae and nuclear abnormalities such as pleomorphism, loss of polarity and hyperchromatism are the main characteristics of the PanIN2 lesions (Reichert and Rustgi, 2011; Zamboni et al., 2013). PanIN-3 lesions are characterized by papillary or micropapillary structure with dystrophic goblet cells, and there will be nuclear and structural abnormalities, such as abnormal mitosis and budding of cells into the lumen of ducts (Hassid et al., 2014).

Another typical characteristic of PanIN progression is the consecutive accumulation of genetic alterations. Mutationally activated *KRAS* is the most common genetic hallmark of PDAC and it presents in more than 90% of the PanINs (Kanda et al., 2012) and invasive PDAC (Biankin et al., 2012; Jones et al., 2008). Subsequently, inactivating mutations of the tumor suppressor gene cyclin-dependent kinase inhibitor 2A (*CDKN2A*) can be detected in low-grade PanIN-1 and PanIN-2 (Bardeesy et al., 2006). Mutations or deletions of tumor suppressor *TP53* (*Trp53* in mouse) and *SMAD4* appear later and can be found in more than half of the PanIN3 lesions and 50–75% of pancreatic tumors.

Our lab has proven that PDK1 is an essential factor for $KRAS^{G12D}$-driven pancreatic cancer development (Eser et al., 2013). In this thesis, the precise function and downstream signaling of PDK1 are dissected. An overview of RAS-related signaling networks in pancreatic cancer is shown in Figure 1 (Eser et al., 2014; Mann et al., 2016; Son et al., 2013; Ying et al., 2012; Zurashvili et al., 2013). Many researchers

have also reported that the PH (pleckstrin homology) domain affects the PI3K/PDK1/AKT pathway (Bayascas et al., 2008) and that the PIF (PDK1 interacting fragment)-pocket domain directly relates PDK1 to RSK2, S6K, S6R, SGK3 and PKC (Biondi et al., 2000; Biondi et al., 2001; Biondi et al., 2002). The activity of S6K is controlled by multiple phosphorylation events, of which the phosphorylation at T229 by PDK1 and T389 by mTOR are the most critical for its function (Alessi et al., 1997; Pullen et al., 1998). Subsequent activation of S6K phosphorylates the S6R protein (Peterson and Schreiber, 1998). Researchers reported that S6R S235/S236 was one of the downstream targets of S6K1, but also an exclusive target of RSK2 (Al-Ali et al., 2017; Roux et al., 2007).

Therefore, the downregulation of S6R S235/S236 activation, might be a result of PI3K/PDK1/AKT/mTORC1/S6K1 pathway (S6K1 T389) downregulation or PIF-pocket dependent pathway (S6K1 T229 and RSK2 S227) downregulation (Figure 1).

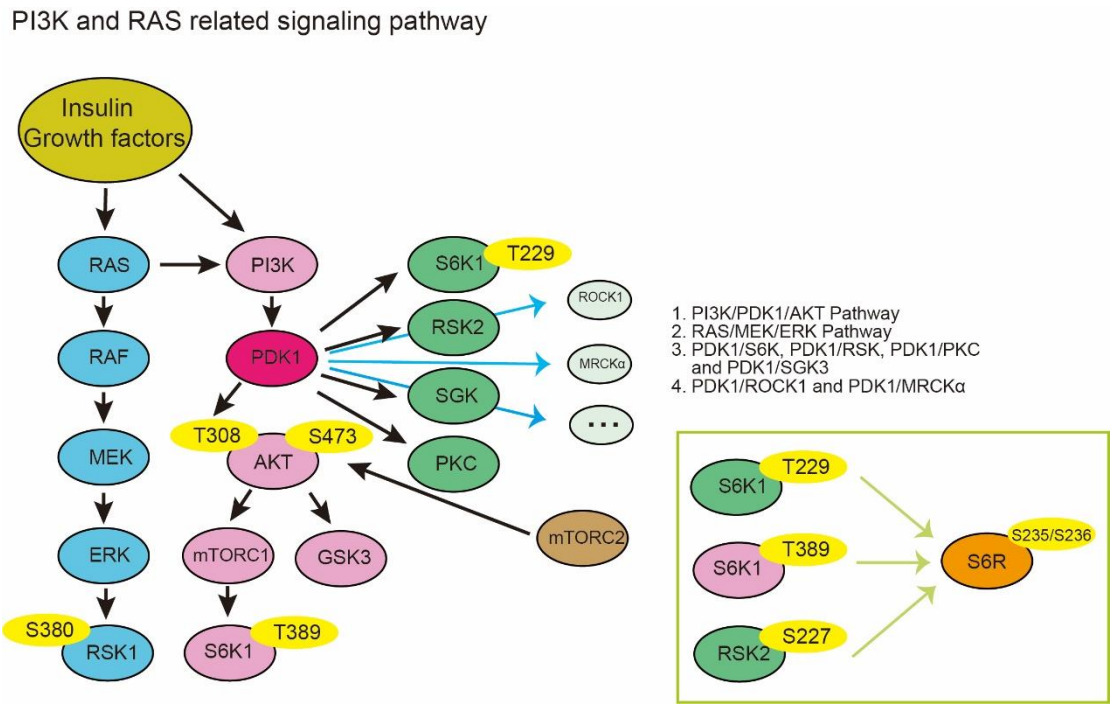

Figure 1. PI3K and RAS related signaling pathway.

The PI3K/PDK1/AKT, RAS/RAF/MEK/ERK, PIF-pocket dependent pathway (PDK1/S6K1, PDK1/RSK2, PDK1/PKC, and PDK1/SGK3), mTORC2/AKT, PDK1/RPCK1, and PDK1/MRCKα related pathway which may be related to PDK1 downstream signaling (left). Three proteins which could influence the phosphorylation of S6R S235/S236 (bottom

right).

1.4 *Pdk1*^{K465E} mutation and *Pdk1*^{L155E} mutation

Pdk1^{K465E} and *Pdk1*^{L155E} mutation were generated by researchers to explore PDK1 downstream signaling. The *Pdk1*^{K465E} mutation was used to abrogate phosphoinositide binding in the PH-domain of PDK1 without affecting domain stability (Bayascas et al., 2008). The *Pdk1*^{L155E} sequence carries a point mutation in *Pdk1* that blocks activation of the PIF-pocket dependent signaling pathway (Bayascas et al., 2006; Mora et al., 2004).

The PH-domain mutation inhibits the PI3K/PDK1/AKT pathway (Bayascas et al., 2008). The AKT signaling pathway plays a vital role in controlling cellular responses to insulin as well as in proliferation and survival (Wullschleger et al., 2011). PDK1^{K465E} may influence many other pathways. BDNF-mediated AKT activation reduces activation of S6K, and AKT/mTORC1/BRSK pathway inhibition is affected by PDK1^{K465E} (Zurashvili et al., 2013). In addition, Zurashvili and colleagues showed that PDK1^{K465E} is essential for neuronal differentiation (Zurashvili et al., 2013). Najafov et al reported that AKT was efficiently activated by PIF-pocket dependent PtdIns(3,4,5)P3 mechanisms (Najafov et al., 2012). *Pdk1*^{K465E} mice were used to inhibit AKT activation and revealed crosstalk between AKT and PTEN (Wullschleger et al., 2011).

Researchers also reported that the PIF-pocket dependent pathway directly included RSK2, S6K, S6R, SGK3, and PKC (Biondi et al., 2000; Biondi et al., 2001; Biondi et al., 2002) which are important for the cell's biological behavior. For example, S6K plays important roles in cell growth, proliferation, and cell differentiation by regulating ribosome biogenesis, protein synthesis, cell cycle progression, and metabolism (Shin et al., 2011). Several studies have revealed that the inactivation of the PIF-pocket dependent pathway leads to mental or metabolic diseases, for example, SGK1 is involved in the development and complications of diabetes and neurological disorders (Lang et al., 2009; Lang et al., 2010), and loss-of-function mutations in *RSK2* are responsible for the Coffin–Lowry syndrome which causes severe mental problems

(Hanauer and Young, 2002).

1.5 Genetically engineered mouse models for PDAC

Genetically engineered mouse models (GEMMs) driven by oncogenic *Kras* have been created to mimic human pancreatic cancer. Although there are differences between mice and humans, these mouse models provide opportunities to explore the role of central genes and pathways in PDAC initiation, development, and maintenance (Rangarajan and Weinberg, 2003). The Cre/lox system is a commonly used site-specific recombinase technology for GEMMs and this system consists of a single enzyme, Cre recombinase, that recombines a pair of short target sequences called the lox sequences (Sauer, 1987). Flp/frt system is another site-specific recombinase technology similar to Cre/lox system(Senecoff et al., 1988). GEMMs used for this project were based on a latent oncogenic $Kras^{G12D}$ allele silenced by a *loxP*-stop-*loxP* (*LSL*) cassette at the endogenous locus (*LSL-*$Kras^{G12D}$ mouse line) (Jackson et al., 2001). *Ptf1a-Cre* (Nakhai et al., 2007) or *Pdx1-Cre* (Gannon et al., 2000) were used to activate oncogenic *Kras* in the pancreas by Cre-mediated recombination of the *LSL* cassette. *Pdx1* is expressed at embryonic day E8.5 (Offield et al., 1996) and *Ptf1a* at E10.5 (Kawaguchi et al., 2002). Both two types of Cre are mainly expressed in pancreatic acini, ducts, and islets. However, *Pdx1-Cre* is also expressed in the bile duct, duodenum, and stomach, while *Ptf1a-Cre* is expressed in the brain and the retina. The KC (*Ptf1a*$^{Cre/+}$*; LSL-*$Kras^{G12D/+}$) mouse model can fully recapitulate the different stages of PanIN progression (Jackson et al., 2001). Using this model, the researchers can study the tumor initiation of PDAC.

In this thesis, $Pdk1^{K465E}$ and $Pdk1^{L155E}$ alleles were crossed in KC mouse model to study PDK1 downstream signaling. Considering the expression of only $Pdk1^{L155E}$ in the global mouse model is lethal for the embryo, a ”minigen” method is used to enable tissue specific expression (Bayascas et al., 2006). The minigen contains the the cDNA corresponding to exons 3–14, the intronic sequence 5’ to exon 3 to allow splicing, and a poly-A tail 3' of exon 14 to prevent further translation. The minigen lies behind exon 2 in the *Pdk1* gene locus and is flanked by two loxP sites. This leads to an expression

of *Pdk1*^{wt} without Cre-mediated recombination. After this recombination, minigen is cut out and *Pdk1*^{L155E} is expressed. With minigen method, mice with *Pdk1*$^{L155E/L155E}$ is available (Bayascas et al., 2006).

Since *Pdk1* deletion and *Pdk1*^{L155E} expression starts after Cre expression in the KC mouse model with *Pdk1*^{lox} and *Pdk1*^{L155E}, it is not possible to achieve spatial or temporal manipulation. Thus, a dual-recombinase system (DRS) mouse model was created in our lab by combining both the Flp/frt and Cre/loxP recombination systems (Schönhuber et al., 2014). The latent oncogenic *Kras*^{G12D} allele was silenced by an *frt*-stop-*frt* (*FSF*) cassette at the endogenous locus (*FSF-Kras*^{G12D} mouse line) in the pancreas. To subsequently manipulate Flp-recombined cells with the Cre/loxP system, a latent tamoxifen-inducible *CreER*^{T2} allele, silenced by an *FSF* cassette, under the control of a strong *CAG* promoter, was generated as a knock-in sequence at the *Rosa26* locus (*FSF-R26*^{CreER}). By tamoxifen application, the system allows temporal and space-specific secondary genetic manipulation (Schönhuber et al., 2014). Based on this genetic strategy, *Pdk1*^{lox}, *Pdk1*^{K465E}, and *Pdk1*^{L155E} alleles were crossed into the DRS mouse model. *p53*^{frt} was also crossed into these models to detect the interactions.

1.6 Aim of this work

Previous work from the lab showed that PDK1 in the PI3K/PDK1 axis is essential for PDAC initiation (Eser et al., 2013), but the precise PDK1 downstream substrates and signaling pathways, and their role for PDAC initiation and tumor maintenance are still not clear. Thereby, the aim of this study is to analyze PDK1 downstream signaling pathways in vitro and in vivo using genetically engineered mouse models and to provide basic information for improved strategies to block tumor initiation, development, or maintenance.

2. Materials

2.1 Technical equipment

Table 1. Technical equipment.

Device	Source
96-well magnetic ring-stand	Applied Biosystems, Inc., Carlsbad, CA, USA
Analytical balance A 120 S	Sartorius AG, Göttingen
Analytical balance BP 610	Sartorius AG, Göttingen
Aperio AT2 Digital Whole Slide Scanner	Leica Microsystems GmbH, Wetzlar
Autoclave 2540 EL	Tuttnauer Europe B.V., Breda, The Netherlands
AxioCam HRc	Carl Zeiss AG, Oberkochen
AxioCam MRc	Carl Zeiss AG, Oberkochen
Bag sealer Folio FS 3602	Severin Elektrogeräte GmbH, Sundern
Centrifuge Avanti® J25	Beckman Coulter GmbH, Krefeld
Centrifuge Rotina 46R	Andreas Hettich GmbH & Co. KG, Tuttlingen
CLARIOstar Microplate Reader	BMG LABTECH, Ortenberg, Germany
CO_2 incubator HERAcell®	Heraeus Holding GmbH, Hanau
CO_2 incubator MCO-5AC 17AI	Sanyo Sales & Marketing Europe GmbH, Munich
Dewar carrying flask, type B	KGW-Isotherm, Karlsruhe
Electrophoresis power supply Power Pac 200	Bio-Rad Laboratories GmbH, Munich
Gel Doc™ XR+ system	Bio-Rad Laboratories GmbH, Munich
Glass ware, Schott Duran®	Schott AG, Mainz
Heated paraffin embedding module EG1150 H	Leica Microsystems GmbH, Wetzlar
HERAsafe® biological safety cabinet	Thermo Fisher Scientific, Inc., Waltham, MA, USA
Hiseq2000 platform	Illumina, San Diego, CA, USA
Hiseq2500 platform	Illumina, San Diego, CA, USA
Homogenizer SilentCrusher M with tool 6F	Heidolph Instruments GmbH & Co. KG, Schwabach
Horizontal gel electrophoresis system	Biozym Scientific GmbH, Hessisch Oldenburg
Horizontal shaker	Titertek Instruments, Inc., Huntsville, AL, USA

Incubator shaker Thermoshake	C. Gerhardt GmbH & Co. KG, Königswinter
Laminar flow HERAsafe	Heraeus Holding GmbH, Hanau
Li-Cor Odyssey Fc Dual-Mode Imaging System	Li-Cor Biosciences, Lincoln, NE, USA
Magnetic stirrer, Ikamag® RCT	IKA® Werke GmbH & Co. KG, Staufen
Microcentrifuge 5415 D	Eppendorf AG, Hamburg
Microcentrifuge 5417 R	Eppendorf AG, Hamburg
Microscope Axio Imager.A1	Carl Zeiss AG, Oberkochen
Microscope Axiovert 25	Carl Zeiss AG, Oberkochen
Microscope DM LB	Leica Microsystems GmbH, Wetzlar
Microtome Microm HM355S	Thermo Fisher Scientific, Inc., Waltham, MA, USA
Microwave	Siemens AG, Munich
Mini centrifuge MCF-2360	LMS Consult GmbH & Co. KG, Brigachtal
Mini Trans-Blot® Cell and Criterion™ Blotter	Bio-Rad Laboratories GmbH, Munich
Mini-PROTEAN® Tetra Cell	Bio-Rad Laboratories GmbH, Munich
Multipette® stream	Eppendorf AG, Hamburg
Neubauer hemocytometer, improved	LO-Laboroptik GmbH, Bad Homburg
PALM laser-capture microdissection system	Carl Zeiss AG, Oberkochen
Paraffin tissue floating bath Microm SB80	Thermo Fisher Scientific, Inc., Waltham, MA, USA
pH meter 521	WTW Wissenschaftlich-Technische Werkstätten GmbH, Weilheim
Pipettes Reference®, Research®	Eppendorf AG, Hamburg
Pipetus®	Hirschmann Laborgeräte GmbH & Co. KG, Eberstadt
Power supplies E844, E822, EV243	Peqlab Biotechnologie GmbH, Erlangen
Qubit® 2.0 Fluorometer	Invitrogen GmbH, Karlsruhe
Spectrophotometer NanoDrop 1000	Peqlab Biotechnologie GmbH, Erlangen
Surgical instruments	Thermo Fisher Scientific, Inc., Waltham, MA, USA
Thermocycler T1	Biometra GmbH, Göttingen
Thermocycler T100	Biometra GmbH, Göttingen

Thermocycler Tgradient	Biometra GmbH, Göttingen
Thermocycler Tpersonal	Biometra GmbH, Göttingen
Thermocycler UNO-Thermoblock	Biometra GmbH, Göttingen
Thermomixer compact	Eppendorf AG, Hamburg
Tissue processor ASP300	Leica Microsystems GmbH, Wetzlar
Tumbling Table WT 17	Biometra GmbH, Göttingen
UVP UVsolo touch	Analytik Jena US, Upland, CA, USA
Vortex Genius 3	IKA® Werke GmbH & Co. KG, Staufen
Water bath 1003	GFL Gesellschaft für Labortechnik mbH, Burgwedel

2.2 Disposables

Table 2. Disposables

Disposable	Source
Amersham Hybond™-N membrane	GE Healthcare Europe GmbH, München
Blood glucose test strips	Abbott GmbH & Co. KG, Ludwigshafen
Canonical tubes, 15 ml	Greiner Bio-One, Frickenhausen
Canonical tubes, 50 ml	Sarstedt AG & Co., Nümbrecht
Cell culture plastics	Becton Dickinson GmbH, Franklin Lakes, NJ, USA; Greiner Bio-One GmbH, Frickenhausen; TPP Techno Plastic Products AG, Trasadingen, Switzerland
Cell scrapers	TPP Techno Plastic Products AG, Trasadingen, Switzerland
Cell strainer, 100 µm, yellow	BD Biosciences, Franklin Lakes, NJ, USA
Chromatography paper, 3 mm	GE Healthcare Europe GmbH, Munich
Combitips BioPur®	Eppendorf AG, Hamburg
Conical tubes, 15 mL	TPP Techno Plastic Products AG, Trasadingen, Switzerland
Conical tubes, 50 mL	Sarstedt AG & Co., Nümbrecht
Cover slips	Gerhard Menzel, Glasbearbeitungswerk GmbH & Co. KG, Braunschweig
CryoPure tubes	Sarstedt AG & Co., Nümbrecht
Disposable scalpels	Feather Safety Razor Co., Ltd., Osaka, Japan

Filtropur S 0.2	Sarstedt AG & Co., Nümbrecht
Filtropur S 0.45	Sarstedt AG & Co., Nümbrecht
Glass slides Superfrost® Plus	Gerhard Menzel, Glasbearbeitungswerk GmbH & Co. KG, Braunschweig
MicroAmp® optical 96-well reaction plate	Applied Biosystems, Inc., Carlsbad, CA, USA
Microtome blades S35, C35	Feather Safety Razor CO, LTD., Osaka, Japan
Pasteur pipettes	Hirschmann Laborgeräte GmbH & Co. KG, Eberstadt
PCR reaction tubes	Eppendorf AG, Hamburg
Petri dishes	Sarstedt AG & Co., Nümbrecht
Phase lock gel light tubes	5 Prime GmbH, Hamburg
Pipette tips	Sarstedt AG & Co., Nümbrecht
Reaction tubes, 0.5 mL, 1.5 mL and 2 mL	Eppendorf AG, Hamburg
Safe seal pipette tips, professional	Biozym Scientific GmbH, Hessisch Oldenburg
Safe-lock reaction tubes BioPur®	Eppendorf AG, Hamburg
Serological pipettes	Sarstedt AG & Co., Nümbrecht
Single use needles Sterican® 27 gauge	B. Braun Melsungen AG, Melsungen
Single use syringes Omnifix®	B. Braun Melsungen AG, Melsungen
Spectra/Mesh® polypropylene filters	Spectrum Laboratories, Inc., Rancho Dominguez, CA, USA
Tissue embedding cassette system	Medite GmbH, Burgdorf
Transfer membrane Immobilon-P	Millipore GmbH, Schwalbach am Taunus

2.3 Reagents and enzymes

Table 3. Reagents and enzymes.

Reagent	Source
1 kb DNA extension ladder	Invitrogen GmbH, Karlsruhe
1,4-Dithiothreitol (DTT)	Carl Roth GmbH + Co. KG, Karlsruhe
2-Mercaptoethanol, 98%	Sigma-Aldrich Chemie GmbH, Munich
2-Propanol (isopropanol)	Carl Roth GmbH, Karlsruhe
4-hydroxytamoxifen (4-OHT)	Sigma-Aldrich Chemie GmbH, Steinheim

Agarose	Sigma-Aldrich Chemie GmbH, Munich
Ammonium persulfate	Sigma-Aldrich Chemie GmbH, Munich
Ampicillin sodium salt	Carl Roth GmbH + Co. KG, Karlsruhe
BBXF agarose gel loading dye mixture	BIO 101, Inc. Carlsbad, CA, USA
Blotting grade blocker non-fat dry milk	Bio-Rad Laboratories GmbH, Munich
Bovine serum albumin (BSA), fraction V	Sigma-Aldrich Chemie GmbH, Munich
Bradford reagent	Serva Electrophoresis GmbH, Heidelberg
Chloramphenicol	AppliChem GmbH, Darmstadt
Color Prestained Protein Standard, Broad Range (10-250 kDa)	Bio-Rad Laboratories GmbH, Munich
Complete, EDTA-free, protease inhibitor cocktail tablets	Roche Deutschland Holding GmbH, Grenzach-Wyhlen
Dimethylsulfoxide (DMSO)	Carl Roth GmbH, Karlsruhe
dNTP mix, 10 mM each	Fermentas GmbH, St. Leon-Rot
Dodecylsulfate Na-salt in pellets (SDS)	Serva Electrophoresis GmbH, Heidelberg
Dulbecco's phosphate buffered saline, powder	Biochrom AG, Berlin
Ethanol, 100%	Merck KGaA, Darmstadt
Ethidium bromide	Sigma-Aldrich Chemie GmbH, Munich
Ethylenediaminetetraacetic acid (EDTA)	Invitrogen GmbH, Karlsruhe
Forene® isoflurane	Abbott GmbH & Co. KG, Ludwigshafen
Gel loading dye, blue	New England Biolabs GmbH, Frankfurt am Main
Gelatine	Carl Roth GmbH, Karlsruhe
GelStar® nucleic acid gel stain	Biowhittaker Molecular Applications, Rockland, ME, USA
GeneRuler™ 100bp DNA ladder	Fermentas GmbH, St. Leon-Rot
Glucose	Sigma-Aldrich Chemie GmbH, Steinheim
Glycerol	Sigma-Aldrich Chemie GmbH, Munich
Glycin Pufferan®	Carl Roth GmbH + Co. KG, Karlsruhe

Histosec® pastilles (without DMSO)	Merck KGaA, Darmstadt
HotStarTaq DNA polymerase	Qiagen GmbH, Hilden
Hydrochloric acid (HCl)	Merck KGaA, Darmstadt
Isotonic sodium chloride solution	Braun Melsungen AG, Melsungen
Magnesiumchloride	Carl Roth GmbH, Karlsruhe
Methanol	Merck KGaA, Darmstadt
N,N-dimethylformamide	Sigma-Aldrich Chemie GmbH, Munich
Nonidet P40	Roche Deutschland Holding GmbH, Grenzach-Wyhlen
Odyssey blocking reagent	LI-COR Corp. Offices, Lincoln, NE, USA
Peanut oil	Sigma-Aldrich Chemie GmbH, Munich
PfuUltra™ high fidelity DNA polymerase	Agilent Technologies, Inc., Santa Clara, CA, USA
Phosphatase inhibitor mix I	Serva Electrophoresis GmbH, Heidelberg
Precision Plus Protein™ all blue standard	Bio-Rad Laboratories GmbH, Munich
Proteinase K, recombinant, PCR grade	Roche Deutschland Holding GmbH, Grenzach-Wyhlen
REDTaq® ReadyMix™ PCR reaction mix	Sigma-Aldrich Chemie GmbH, Munich
RnaseA	Fermentas GmbH, St. Leon-Rot
RNase-free DNase set	Qiagen GmbH, Hilden
Rotiphorese® gel 30	Carl Roth GmbH + Co. KG, Karlsruhe
Saponin	Sigma-Aldrich Chemie GmbH, Steinheim
Sodium chloride (NaCl)	Merck KGaA, Darmstadt
Sodium dodecyl sulphate (SDS)	Carl Roth GmbH, Karlsruhe
Sodium hydroxide solution (NaOH)	Merck KGaA, Darmstadt
Spectra Multicolor Broad Range Protein ladder	Fermentas GmbH, St. Leon-Rot
Tamoxifen	Sigma-Aldrich Chemie GmbH, Munich
TE buffer, pH 8.0	AppliChem GmbH, Darmstadt
TEMED	Carl Roth GmbH, Karlsruhe

Tris hydrochloride	J.T.Baker® Chemicals, Phillipsburg, NJ, USA
Tris Pufferan®	Carl Roth GmbH + Co. KG, Karlsruhe
Tween® 20	Carl Roth GmbH, Karlsruhe

2.4 Kit

Table 4. Kit.

Kit	Source
QIAamp DNA mini kit	Qiagen GmbH, Hilden
QIAamp DNA micro kit	Qiagen GmbH, Hilden
QIAquick® gel extraction kit	Qiagen GmbH, Hilden
QIA shredder	Qiagen GmbH, Hilden
Qubit® dsDNA BR assay kit	Invitrogen GmbH, Karlsruhe
Quick Blunting™ kit	New England Biolabs GmbH, Frankfurt
RNeasy Mini kit	Qiagen GmbH, Hilden
Venor® *GeM* mycoplasma detection kit	Minerva Biolabs GmbH, Berlin

2.5 Antibodies

Table 5. Antibodies.

Antibody	Source
Akt, #9272	Cell Signaling Technology, Inc., Danvers, MA, USA
Anti-mouse IgG (H+L) (DyLight® 680 Conjugate) #5470	Cell Signaling Technology, Inc., Danvers, MA, USA
Anti-mouse IgG (H+L) (DyLight® 800 Conjugate) #5257	Cell Signaling Technology, Inc., Danvers, MA, USA
Anti-rabbit IgG (H+L) (DyLight® 680 Conjugate) #5366	Cell Signaling Technology, Inc., Danvers, MA, USA
Anti-rabbit IgG (H+L) (DyLight® 800 Conjugate) #5151	Cell Signaling Technology, Inc., Danvers, MA, USA
Biotinylated anti-goat IgG (H+L)	Vector Laboratories, Inc., Burlingame, CA, USA
Biotinylated anti-mouse IgG (H+L)	Vector Laboratories, Inc., Burlingame, CA, USA
Biotinylated anti-rabbit IgG (H+L)	Vector Laboratories, Inc., Burlingame, CA, USA
Biotinylated anti-rat IgG (H+L)	Vector Laboratories, Inc., Burlingame, CA, USA

GAPDH (14C10) Rabbit mAB, #2118	Cell Signaling Technology, Inc., Danvers, MA, USA
GSK3beta, #9315	Cell Signaling Technology, Inc., Danvers, MA, USA
p44/42 MAPK (ERK1/2), #4695	Cell Signaling Technology, Inc., Danvers, MA, USA
p70 S6 Kinase, #9202	Cell Signaling Technology, Inc., Danvers, MA, USA
pAKT (S473) D9E, #4060	Cell Signaling Technology, Inc., Danvers, MA, USA
pAKT (T308) 244F9, #4056	Cell Signaling Technology, Inc., Danvers, MA, USA
pGSK3beta (S9), #9323	Cell Signaling Technology, Inc., Danvers, MA, USA
p-p44/42 MAPK (T202/Y204), #4370	Cell Signaling Technology, Inc., Danvers, MA, USA
p-p70 S6 Kinase (T389), #9234	Cell Signaling Technology, Inc., Danvers, MA, USA
p-p90-RSK (S380), #9341	Cell Signaling Technology, Inc., Danvers, MA, USA
pRSK2 (S227), #3556	Cell Signaling Technology, Inc., Danvers, MA, USA
pS6 Ribosomal Protein (S235/236), #4858	Cell Signaling Technology, Inc., Danvers, MA, USA
RSK1/RSK2/RSK3, #9355	Cell Signaling Technology, Inc., Danvers, MA, USA
S6-ribosomal Protein (5G10), #2217	Cell Signaling Technology, Inc., Danvers, MA, USA
α-Tubulin, #T6199	Sigma-Aldrich Chemie GmbH, Munich
β-actin (13E5) Rabbit mAb, #4970	Cell Signaling Technology, Inc., Danvers, MA, USA

2.6 Solutions

All buffers were prepared with bidistilled H2O.

Table 6. Buffers and solutions for molecular biology.

Buffer	Component
10x Gitschier's buffer	670 mM Tris, pH 8.8 166 mM (NH4)2SO4 67 mM MgCl2
IP buffer, pH 7.9	50 mM HEPES 150 mM NaCl 1 mM EDTA 0.5% Nonidet P40

	10% Glycerol Phosphatase inhibitor (add prior to use) Protease inhibitor (add prior to use)
6x Loading buffer orange G	60% Glycerol 60 mM EDTA 0.24% Orange G
5x Protein loading buffer (Laemmli), pH 6.8	10% SDS 50% Glycerol 228 mM Tris hydrochloride 0.75 mM Bromphenol blue 5% 2-Mercaptoethanol
Running buffer	25 mM Tris 192 mM Glycine 0.1% SDS
Separating gel buffer	1.5 M Tris, adjusted to pH 8.8 with HCl
Soriano lysis buffer	0.5% Triton® X-100 1% 2-Mercaptoethanol 1x Gitschier's buffer 400 µg/mL Proteinase K (add prior to use)
Stacking gel buffer	0.5 M Tris, adjusted to pH 6.8 with HCl
SucRot solution (for PCR)	1.5 mg/mL Cresol red 100 mM Tris, pH 9.0 30% Saccharose
Transfer buffer, pH 8.3	25 mM Tris 192 mM Glycine 20% Methanol
50x Tris acetate EDTA (TAE) buffer, pH 8.5	2 M Tris 50 mM EDTA 5.71% Acetic acid

2.7 Primers

Oligonucleotides were synthesized by Eurofins MWG GmbH (Ebersberg) and diluted in H_2O to a concentration of 10 µM.

Table 7. Primers used for genotyping.

PCR name	Primer name	Sequence (5´ to 3´)
Ptf1a^{Cre}	p48-Cre-GT-LP-URP	CCTCGAAGGCGTCGTTGATGGACTGCA
	p48-Cre-GT-wt-UP	CCACGGATCACTCACAAAGCGT
	p48-Cre-GT-mut-UP-neu	GCCACCAGCCAGCTATCAA
LSL-Kras^{G12D}	Kras-WT-UP1	CACCAGCTTCGGCTTCCTATT
	Kras-URP-LP1	AGCTAATGGCTCTCAAAGGAATGTA
	KrasG12Dmut-UP	CCATGGCTTGAGTAAGTCTGC
Pdk1^{lox}	PDK1-UP	ATCCCAAGTTACTGAGTTGTGTTGGAAG
	PDK1-LP	TGTGGACAAACAGCAATGAACATACACGC
Pdk1^{K465E}	PDK_K465E_For	GGGTGAAGCATGGAATCTGTGTCTT
	PDK_K465E_Rev	GCCAGGATACCTAAGAGTACCTAGAA
Pdk1^{L155E}	Pdk_L155E_P1	GGAACTTACTCTGTAGACCAGGCTG
	Pdk_L155E_P2	GACGTGTCCTAATACTACCACAAGTGGC
Pdx1^{Flp}	pdx5ut-scUP	CGTTGTAAGGGATGATGGTGAACT
	Flpopt-scLP	AGAGAGAAAATTGAAACAAGTGCAGGT
	Gabra-UP	AACACACACTGGAGGACTGGCTAGG
	Gabra-LP	CAATGGTAGGCTCACTCTGGGAGATGATA
FSF-Kras^{G12D}	Kras-WT-UP1	CACCAGCTTCGGCTTCCTATT
	Kras-URP-LP1	AGCTAATGGCTCTCAAAGGAATGTA
	R26-Tva-SA-mut	GCGAAGAGTTTGTCCTCAACC
R26-CAG	R26-td-E-mutLP	TCAATGGGCGGGGGTCGTT
	R26-Tva-GT-UP	AAAGTCGCTCTGAGTTGTTAT
	R26-Tva-GT-WT-LP	GGAGCGGGAGAAATGGATATG
FSF	pGL3-pA-pause-4645-UP	TGAATAGTTAATTGGAGCGGCCGCAATA

	Cre-neu-LP	CAGGGTGTTATAAGCAATCCC
CreER^{T2}	Cre-ER-T2-sc-UP3	GAATGTGCCTGGCTAGAGATC
	Cre-ER-T2-sc-LP1	GCAGATTCATCATGCGGA
Trp53^{frt}	p53-ftr1	CAAGAGAACTGTGCCTAAGAG
	p53-frt2	CTTTCTAACAGCAAAGGCAAGC
FSF-R26CAG-CreER^{T2}	caggs-sc-UP4	GTTCGGCTTCTGGCGTGT
recombination	Cre-Stop-del-LP2	CGATCCCTGAACATGTCCATC
FSF-Kras^{G12D} recombination	Kras-FSF-del-LP2	AGAATACCGCAAGGGTAGGTGTTG
	Kras-FSF-del-UP4	TGTAGCAGCTAATGGCTCTCAAA
Trp53^{frt} recombination	p53-ftr1	CAAGAGAACTGTGCCTAAGAG
	p53-frt3	ACTCGTGGAACAGAAACAGGCAGA
Pdk1^{lox} recombination	Pdk1-i4-UP2	CCCTCTAGCAAATGTTCTGTCTGGAATGTCT
	Pdk del UP	CTATGCTGTGTTACTTCTTGGAGCACAG
	Pdk LP	TGTGGACAAACAGCAATGAACATACACGC
Pdk1^{L155E} recombination	Pdk1155i2E5	CACACTCCAGAGATCCGATATCA
	Pdk1MGex4+5	GCATAACTAAGGCCAAAATACAGCTT
	Pdk1ex4muti4-LP	CATTGACCATGCAAAGGATACACTC

2.8 Cell culture

All the cell lines used for this project were isolated from primary tumor mice.

Table 8. Cell culture media and their components.

Medium	Components
Cancer cell medium	DMEM 10% FCS (Biochrom AG) 1% Penicillin/Streptomycin
Freezing medium	70% DMEM 20% FCS 10% DMSO

ADM medium	Waymouth's medium 0.1% BSA 0.2 mg/ml SBTI 0.5% Pen/Strep 1% ITS-X 50 µg/ml BPE 0.1% FCS 0.25 µg/ml Fungizone

Table 9. Reagents and kits for cell culture.

Reagent / Kit	Source
4-hydroxytamoxifen(4-OHT) (≥70% Z isomer)	Sigma-Aldrich Chemie GmbH, Munich
Collagenase type 2	Worthington Biochemical Corporation, Lakewood, NJ, USA
Dulbecco's modified eagle medium (DMEM) with L-glutamine	Invitrogen GmbH, Karlsruhe
Dulbecco's phosphate buffered saline (PBS)	Invitrogen GmbH, Karlsruhe
Fetal calf serum (FCS)	Biochrom AG, Berlin
Fungizone® antimycotic	Invitrogen GmbH, Karlsruhe
Giemsa solution	Sigma-Aldrich Chemie GmbH, Munich
L-Glutamine 200 mM	Invitrogen GmbH, Karlsruhe
MTT reagent	Sigma-Aldrich Chemie GmbH, Munich
Penicillin (10000 units/mL) / Streptomycin (10000 µg/mL) solution	Invitrogen GmbH, Karlsruhe
Trypsin, 0.05% with 0.53 mM EDTA 4Na	Invitrogen GmbH, Karlsruhe
Venor® *GeM* mycoplasma detection kit	Minerva Biolabs GmbH, Berlin
Waymouth's medium	Thermo Fisher Scientific, Inc., Waltham, MA, USA
Soy bean Trypsin Inhibitor (SBTI)	Sigma-Aldrich Chemie GmbH, Steinheim
Insulin-Transferrin-Selenium-Ethanolamine (ITS -X)	Thermo Fisher Scientific, Inc., Waltham, MA, USA
bovine pituitary extract (BPE)	Thermo Fisher Scientific, Inc., Waltham, MA, USA

2.9 Histology

Table 10. Reagents and kits for histological analysis.

Reagent / Kit	Source
Acetic acid (glacial)	Merck KGaA, Darmstadt
Alcian blue 8GX	Sigma-Aldrich Chemie GmbH, Munich
Aluminium sulfate	Honeywell Specialty Chemicals Seelze GmbH, Seelze
Antigen unmasking solution, citric acid based	Vector Laboratories, Inc., Burlingame, CA, USA
Avidin/biotin blocking kit	Vector Laboratories, Inc., Burlingame, CA, USA
DAB peroxidase substrate kit, 3,3'-diaminobenzidine	Vector Laboratories, Inc., Burlingame, CA, USA
Donkey serum D9663	Sigma-Aldrich Chemie GmbH, Munich
Eosine	Waldeck GmbH & Co KG, Münster
Goat serum G9023	Sigma-Aldrich Chemie GmbH, Munich
Hematoxylin	Merck KGaA, Darmstadt
Hydrogen peroxide 30%	Merck KGaA, Darmstadt
Pertex mounting medium	Medite GmbH, Burgdorf
Rabbit serum R9133	Sigma-Aldrich Chemie GmbH, Munich
Roti® Histofix 4%	Carl Roth GmbH + Co. KG, Karlsruhe
Roti® Histol	Carl Roth GmbH + Co. KG, Karlsruhe
Vectastain® elite ABC kit	Vector Laboratories, Inc., Burlingame, CA, USA

2.10 Software

Table 11. Software

Software	Source
Adobe illustrator CC	Adobe, San Jose, CA, USA
AxioVision 4.8	Carl Zeiss AG, Oberkochen
CLARIOStar MARS	BMG Labtech, Offenburg
Excel	Microsoft Corporation, Redmont, WA, USA
Gel Doc	Bio-Rad Laboratories GmbH, Munich

GraphPad Prism 6	La Jolla, CA, USA
ImageScope v12.3	Leica Biosystems, Wetzlar
LAS X	Leica Biosystems, Wetzlar
li-Cor Odyssey® v1.2	Li-Cor Biosciences, Lincoln, NE, USA
SnapGene	GSL Biotech LLC，San Diego，CA, USA

3. Methods

3.1 Mouse experiments

All animal related works were conducted according to the European guidelines for the care and use of laboratory animals and were approved by the local animal authorities (Regierung von Oberbayern). Mice were on a mixed C57BL6/J;129/S6 background.

3.1.1 Mouse strains

Conditional Cre/loxP mouse models were used in this research. In the mouse models, targeted genes can be flanked by loxP sites or silenced by the LSL cassette. The tissue specific promoter allows the conditional inactivation or activation of the target gene. An inducible dual-recombinase system (DRS) by combining Flp/frt and Cre/loxP to improve GEMMs of pancreatic cancer were used in this study as well. Flp/frt recombination system is designed for tumor initiation and Cre/loxP recombination system is constructed for the spatial or temporal secondary manipulation of cancer cells *in vitro* or *in vivo*.

***Ptf1a*^{Cre}** (Nakhai et al., 2007).

The *Ptf1a* is a subunit of the pancreas transcription factor (Ptf) and plays a fundamental role in exocrine pancreas development in mice. Ptf1a is required for the formation of pancreatic acinar and ductal cells. Cre recombinase, controlled by the *Ptf1a* promoter, is specifically expressed in pancreatic precursor cells.

LSL-Kras^{G12D} (Hingorani et al., 2003; Jackson et al., 2001).

This knock-in mouse line has a G12D (Substitution - Missense, position 12, glycine to aspartate) point mutation similar to the mutation in human tumors. After Cre-mediated *LSL* cassette deletion, the GTPase activity is impaired resulting in constitutive Kras signaling.

Pdk1^{lox} (Lawlor et al., 2002).

In this mouse strain, exon 3 and exon 4 of the *Pdk1* locus are flanked by *loxP* sites, permitting conditional deletion of *Pdk1*.

Pdk1^{K465E} (Bayascas et al., 2008)

In this mouse line, there is a mouse K465E(Substitution - Missense, position 465, lysine to glutamic) point mutationa in exon 12 of the *Pdk1* gene. This mutation abrogates phosphoinositide binding in PH-domain without affecting the stability of the domain.

Pdk1^{L155E} (Bayascas et al., 2006)

This knock-in mouse line carris a point mutation L155E (Substitution - Missense, position 155, leucine to glutamic) in exon 4 of the *Pdk1* gene. The minigen, composed of exons 3-14 without the mutation, is in front of exon4. Minigen cassette is flanked by *loxP* sites and ends with a stop codon. The Cre-mediated minigen cassette deletion leads to an expression of the *Pdk1^{L155E}* mutant and thus inhibits of the PIF-dependent signaling pathway.

Pdx1-Flp (Schönhuber et al., 2014).

This transgenic mouse strain is generated in the laboratory of Prof. Dieter Saur. The Flp recombinase is expressed under the control of the *Pdx1* (Pancreatic and Duodenal Homeobox 1) promotor, which is active in early stage of embryogenesis in both endocrine and exocrine cells and in adult pancreatic acini, ducts and islets.

FSF-Kras^{G12D} (Schönhuber et al., 2014).

This knock-in mouse strain was generated in the laboratory of Prof. Dieter Saur. After Flp-mediated *FSF* cassette deletion, oncogenic *Kras^{G12D}* allele from its endogenous locus can be activated resulting in constitutive Kras signaling.

FSF-R26^{CreER} (Schönhuber et al., 2014).

This mouse strain was generated in the laboratory of Prof. Dieter Saur. In this mouse line, ***FSF-R26^{CreER}*** is constructed as a knock-in at the *Rosa26* locus. *CreER^{T2}* allele is a latent tamoxifen-inducible silenced by the FSF cassette. After Flp-mediated *FSF* cassette deletion, *CreER^{T2}* allele is under the control of the strong *CAG* promoter. With tamoxifen induction, the system allows spatial or temporal manipulation by Cre.

Trp53$^{frt/+}$ (Lee et al., 2012).

Exons 2 to 6 of the *Trp53* gene are flanked by *frt* sites. Trp53 is a suppressor gene and will be deleted by Flp expression.

3.1.2 Genotyping

Mice were genotyped at the age of 2–3 weeks. Ear tissue after earmark clipping was taken as biopsies for genotyping. The wound was stanched by pressure with tissue paper and disinfected with silver nitrate applicator if needed. DNA was isolated from the biopsies as described in 3.4.1 and PCR are described in sections 3.4.2.

3.1.3 Mouse dissection

To dissect the tumor mouse or time point mouse, mouse was first anesthetized with medetomidine-midazolam-fentanyl (MMF) abdominal injection or isoflurane inhalation. Then the cervical dislocation was performed to euthanize the mouse. After the mouse was fixed on the dissection table and disinfected with 70% ethanol, the operation procedure was carried out as sterile as possible. Pancreatic tissue samples for DNA

were directly snap frozen; sample for RNA was homogenized immediately in 600 µL RLT buffer with 1% 2-mercaptoethanol; and samples for protein isolation were homogenized in 500 µL IP buffer containing 1% phosphatase and 4% proteinase inhibitors. Both samples were stored at -80 °C. For histological analysis, spleen, liver, lung, heart, stomach, intestine, kidneys and part of pancreas were fixed overnight in 4% Roti® Histofix. When a pancreatic tumor, metastasis or ascites was observed, primary cell lines were isolated. For primary murine tumor cell line isolation, pancreatic tissue samples or metastasis samples were firstly transferred to sterile PBS and then cut into small pieces with sterile scalpels and incubated away from light in 5 ml cell culture medium containing 200 U/ml collagenase type II at 37°C for 24h-36h digestion. After digestion, the cells were suspended and subsequently centrifuged for 5 min at 1000rpm. The supernatant was discarded, and the cells were cultured in a small cell culture flask. For ascites isolation, ascites was taken from the peritoneal cavity and directly cultured in medium. Cell culture is described in 3.3.1.

3.2 Histological analysis

3.2.1 Paraffin sections

Tissue samples for histological analysis were fixed in 4% Roti® Histofix for 24 h. Then the tissue samples were washed by PBS and stored in 4℃ in PBS. Afterwards, the samples were dehydrated with the tissue processor ASP300, embedded in paraffin and stored at room temperature until further experiments. For following stainings, series of 2.5–3 µm thick serial sections were cut using the microtome Microm HM355S.

3.2.2 Hematoxylin and eosin (H&E) staining of tissue sections

First, paraffin-embedded sections were dewaxed by incubation in Roti® Histol (2 x 5 min). Second, the sections were rehydrated in a decreasing ethanol series (2 x 99%, 2 x 96% and 2 x 80%) and washed with dH_2O. Third, sections were placed into hematoxylin for 5 s and subsequently bathed in tap water for around 5 min. Forth,

sections were stained in eosin for 20 s and subsequently washed in dH_2O. Fifth, sections were dehydrated in an increasing ethanol series (2 x 80%, 2 x 96% and 2 x 99%) and Roti® Histol (2 x 5 min) . Final step, sections were mounted with Pertex mounting medium.

3.2.3 Alcian blue (AB) staining

Paraffin-embedded sections were dewaxed and rehydrated as described in 3.2.2. Then alcian blue staining was performed by incubating the slides in aqueous alcian blue solution for 5 min. After washing them in water, sections were counterstained with nuclear fast red solution for 5 min, dehydrated and mounted as described in 3.2.2.

3.2.4 Immunohistochemistry (IHC)

Paraffin-embedded tissue sections were dewaxed and rehydrated as described in 3.2.2. For antigen retrieval, sections were boiled in citric acid-based antigen unmasking solution using a microwave for 10 min. After 20 min cooling down at RT, the sections were rinsed with water and incubated in 3% H_2O_2 away from light for 15 min to inhibit endogenous peroxidase activity. Then, the sections were washed 1 time with water and 3 times with PBS. According to DAB staining manufacturer's protocol, the sections were blocked for 1 h in 3-5% serum and Avidin in PBS. The sections were washed again 3 times with PBS and incubated with the first antibody diluted in 3–5 % serum in PBS at dilution ranges from 1:50 to 1:500 at 4 °C overnight. The avidin/biotin blocking kit was generally applied. The next day, the sections were washed 3 times with PBS before incubating with the biotinylated secondary antibody, which was diluted in 3–5 % serum in PBS 1:500, at RT for 1 h. After washing, the Vectastain® elite ABC kit and the DAB peroxidase substrate kit were used for detection according to manufacturer's protocol. Finally, the slides were counterstained with hematoxylin, dehydrated and mounted as described in 3.2.2.

3.2.5 Quantification and counting of ADM and PanIN lesions

At least three H&E stained slices from three animals per time point and genotype were used for analysis of ADM formation and PanIN lesion formation. The lesion number in each 20x magnification field was counted. Identification of ADM and PanIN lesions was performed according to established grading for PanIN lesions in mice (Hruban et al., 2006).

3.2.6 Pathological analysis of staining

For documentation of the staining results from H&E staining and IHC as well as for counting positive cells, slides were scanned with bright field by Aperio AT2 Digital Whole Slide Scanner and stored by software Image Scope.

3.3 Cell culture

Primary murine pancreatic cancer cells were established from tumor mice as described before and were maintained in cancer cell medium (DMEM supplemented with 10% FCS and 1% penicillin/streptomycin) at 37 °C, 5% CO_2 and 100% humidity.

3.3.1 Generation and culture of primary mouse PDAC cell lines

Two different pieces of tumor tissue were used to isolate primary murine tumor cells. All the cell culture procedures were taken place under a cell culture fume hood used only for primary cell culture. After the cells were 80%-90% confluent in the small flask, we passaged the cells to middle flask and started to use normal cell culture fume hood and incubator. For passaging, the medium was aspirated and cells were washed with PBS, and then detached by incubation with trypsin/EDTA at 37 °C for around 5 min. 10 ml of cancer cell medium was used to stopped trypsinization and transfer the cell suspension to a middle flask. Cell number was determined by a Neubauer hemacytometer.

For cryopreservation, after trypsinization, cells were taken up in cancer cell culture medium and then centrifuged at 1000 rpm at 4℃ for 5 min. The supernatant was

discarded, and the cell pellet was resuspended in ice-cold freezing medium (70% DMEM, 20% FBS and 10% DMSO). Then the cells were transferred to CryoPure tubes, frozen in a freezing container at -80 °C for 24 h and subsequently stored in liquid nitrogen tank for long-term storage.

To thaw a frozen cell line, cell stock was taken from liquid nitrogen tank and thawed in a 37 °C water bath. Cells were then transferred into a new 15ml falcon containing 10 ml cancer cell medium and centrifuged at 1000 rpm at 4℃ for 5 min. Later on, the supernatant was aspirated, and cells were cultured in cancer cell medium in a new small flask.

3.3.2 Validation of cell lines

The cell lines were validated by regenotyping and mycoplasma test. Regenotyping was performed as described in section 3.4.2. For mycoplasma test, cells were cultured in DMEM with 10% FBS (without penicillin-streptomycin) for at least 7 days until the medium appeared yellow. 2 ml medium was collected and centrifuged for 2 min at 250 rcf. The supernatant was collected in a new tube and was centrifuged for 10 min at maximum speed (about 16,000 rcf) in a table centrifuge. The supernatant was discarded, and the pellet was resuspended in 50 µL PBS and heated up to 95 °C for 2 min. The resulting sample was used as template for Mycoplasma PCR. Mycoplasma PCR was performed as Table 13. using 60 °C as the annealing temperature. PCR product was analysed by electrophoresis as described in 3.4.3. Samples negative for mycoplasma show no band, and a typical positive band appears at 500 bp. All cell lines used in this project had the correct genotypes and were free from mycoplasma.

3.3.3 Documentation of cell morphology

Bright-field pictures of cell lines were documented with a camera connected to a phase-contrast microscope and Carl Zeiss AxioVision Rel. 4.8 software. Shading correction and white balance adjustment were performed before image acquisition.

3.3.4 Treatment of cells with tamoxifen

4-Hydroxytamoxifen (4-OHT) is an active metabolite of the antiestrogen, tamoxifen (TAM), in humans and other mammals. To activate $CreER^{T2}$ in cell culture experiments, pancreatic cancer cells were treated with 600 nM 4-OHT for $CreER^{T2}$ heterozygous or 100 nM 4-OHT for $CreER^{T2}$ homozygous. Ethanol (EtOH) was used as vehicle. To delete *loxP*-flanked targeted sequences, the TAM treatment would last for 8 days. DNA samples, protein samples and pictures for time series analysis were collected at day 1, day 2, day 4, day 6, day 8. Subsequently, cells were seeded for a variety of assays (as described in chapters 3.3.2 to 3.3.6).

3.3.5 MTT assay

The MTT assay is used to measure the proliferation character of cells by determining the activity of cytosolic and mitochondrial dehydrogenases. Yellow 3-(4,5-dimethyl-2-thiazolyl)-2,5-diphenyl-tetrazolium bromide (MTT) is absorbed by the cells and converted into water-insoluble dark blue formazan by NADH-dependent reductases.

Dilute the cells concentration to 5000 cells/ml, 10000 cells/ml and 20000 cells/ml. Thereafter, to get 500 cells/well, 1000 cells/well and 2000 cells/well, 100ul of different cells concentration were seeded triplicates in 96-well plates after pretreatment with 4-OHT or EtOH. Each day at the same time, 10 µL MTT reagent was added to each well (final concentration of MTT dye: 0.5 mg/mL) and incubated for 4 h at 37 °C. After removing the medium, the water-insoluble formazan crystals were solubilized by adding 200 µL of ethanol/DMSO mix (1:1) and the 96-well plate was shaken for 10 min at RT. The optical density at a wavelength of 600 nm was determined by the plate spectrophotometer Anthos 2001. The MTT assay was performed on five consecutive days to quantify the cell proliferation.

3.3.6 Clonogenic assay

First, cells (2000 cells/well) were seeded on a 6-well plate. About 1-2 weeks after

seeding, cells showed evenly spread visible colonies. Then, cell culture medium was aspirated, and cells were fixed in cold 99% methanol shaking at RT for 30 min. After methanol was removed, colonies were stained with Giemsa solution (diluted 1:20 in distilled water) on an orbital shaker overnight. The next day, Giemsa solution was removed, and colonies were washed with distilled water and air dried later.

3.3.7 ADM assay

Pancreatic acinar cells were isolated from mice less than 12 weeks old. After the mice were opened as described in “mouse dissection”, 2.5 ml of a solution of 1.33 mg/ml collagenase P in HBSS was injected into the pancreas and another 5 ml collagenase P solution was used to digest the pancreas. After 30 min digestion in 37℃ water bath，10 ml HBSS with 5% FCS was applied to stop the digestion. The cell suspension was stand still for 10 min on ice for sedimentation of the cellular fraction. Next, the supernatant and remaining fat tissue were aspirated and the cells were washed 2 times with 10 ml of 5% FCS in HBSS. After that, the cells were centrifuged at 1000 rpm at 4°C for 3 min and resolved in 10 ml of 5% FCS in HBSS. To get rid of clumps and islet cells, the pipette resuspension solution was filtered through a 100 µm mesh into a new falcon. Afterwards, the cell suspension was gently dropped onto 20 ml of 30% FCS in HBSS and centrifuged at 1000 rpm at 4°C for 3 min. After aspiring the supernatant, the pellet was resuspended in 2 ml recovery medium and put into 6-well plate and recovery at 37℃ for 1 h. During this time, the plate was moved from time to time to avoid cell attachment. In a new falcon, 10% 10xPBS, 1.3% 1N NaOH, 32.1% dH_2O and 56.6% rat tail collagen type I were added in order to prepare the collagen solution. Then, 100 µl collagen solution was added to wells of 48 well plate. After coagulation of the bottom layer, the cells were diluted 1:1 in collagen and seed 100 µl per well above the bottom layer. After the coagulation of the cell layer, 100 ul collagen solution was added above to form the up layer. 400 µl cell culture medium was gently added to the wells after coagulation of the up layer. From then, medium was changed every 24 h and cells were observed daily.

3.4 Molecular biology

3.4.1 Isolation of genomic DNA

Genomic DNA for subsequent genotyping and recombination PCR analysis was isolated by adding 50 µL of Soriano lysis buffer to a small piece of tissue or a cell pellet. Lysis was performed in a thermocycler at 55 °C for 90 min. Then, proteinase K was inactivated for 15 min at 95 °C. After vortex, the samples were centrifuged at 14000 rpm at 4 °C for 10 min. Then, the DNA-containing supernatant was transferred into a new tube and stored at -20 °C.

3.4.2 Polymerase chain reaction

A PCR pre-mix was prepared for standard genotyping or recombination PCR (Mullis et al., 1986) (see Table 12).

Table 12. Composition of pre-mix for PCR

Solution	Volume for one reaction
distilled water	4.375 µL
10x buffer S	2.5 µL
30% sucrose	2.5 µL
SucRot	2.5 µL
PeqTaq	0.125 µL
dNTPs (10 µM each)	0.5 µL

3.4.2.1 Polymerase chain reaction (PCR) condition

The standard PCR reaction compositions and conditions are shown in Table 13. Primer amounts were optimized depending on the final amount of PCR product. If necessary, DMSO was added to improve PCR outcome. PCR products were stored at 4 °C until further analysis by gel electrophoresis.

Table 13. Reaction mix and conditions for standard PCR

Reaction Mix		Conditions		
12.5 µl	REDTaq® Ready Mix™	95°C	5 min	
0.25 - 2 µl	Forward primer (10 µM)	95°C	45 sec	
0.25 - 2 µl	Reverse primer (10 µM)	55°C - 64°C	1 min	40x
1 µl	DNA templete	72°C	1min, 30 sec	
ad 25 µl	H_2O	72°C	---	

3.4.2.2 Genotyping PCR

DNA template, which isolated as described in 3.4.1, was used to genotype each mouse or cell lines. Specific primers were designed for each allele (Table 7). Annealing temperatures and PCR products are described in Table 14.

Table 14. Annealing temperatures and PCR products

PCR name	Annealing temperature	PCR products bp
Ptf1a^{Cre}	60 ℃	400 mut / 600 wt
LSL-Kras^{G12D}	55 ℃	170 mut / 270 wt
Pdk1^{lox}	63 ℃	280 mut / 200 Pdk1$^{L155E/K465E/wt}$
Pdk1^{K465E}	63 ℃	236 mut / 196 Pdk1$^{lox/wt}$
Pdk1^{L155E}	63 ℃	212 mut / 171 Pdk1$^{lox/wt}$
Pdx1^{Flp}	56 ℃	620 mut / 300 internal control
FSF-Kras^{G12D}	55 ℃	351 mut / 270 wt
R26-CAG	62 ℃	450 mut / 650 wt
FSF	60 ℃	600 mut
CreER^{T2}	55 ℃	190 mut
Trp53^{frt}	57 ℃	292 mut / 258 wt

mut = mutated allele; wt = wild-type allele; rec = mutated allele after recombination

3.4.2.3 Recombination PCR

To check the recombination condition of sequences flanked by *loxP* or *frt* sites, a

piece of pancreas tissue or a cell pellet was lysed as described in Table 15.

mut = mutated allele; wt = wild-type allele; rec = mutated allele after recombination; uns = unspecific

Table 15. Annealing temperatures and PCR products

PCR name	Annealing temperature	PCR products bp
FSF-R26CAG-CreER^{T2} recombination	60 ℃	490 rec
FSF-Kras^{G12D} recombination	60 ℃	196 rec
Trp53^{frt} recombination	55 ℃	352 rec
Pdk1^{lox} recombination	63 ℃	250 rec /300 uns/380 mut
Pdk1^{L155E} recombination	Touch down ℃	1077 rec / 811 mut

3.4.2.4 Touchdown PCR for Pdk1^{L155E} recombination

To check *Pdk1^{L155E}* recombination, genomic DNA was used for a touchdown PCR. (Table 16 and Table 17)

Table 16. Reaction mix for touch down PCR

Reaction Mix	
12.5 µl	REDTaq® Ready Mix™
0.5 µl	Forward primer (10 µM)
0.5 µl	Non-Rec Reverse primer (10 µM)
0.5 µl	Rec Reverse primer (10 µM)
1 µl	DNA template
ad 25 µl	H_2O

Table 17. Touchdown PCR program for amplification of DNA

Temperature	Time	
95 ℃	2 min	
95 ℃	30 s	
68 ℃	2 min	1x
95 ℃	30 s	
67 ℃	30 s	

68 ℃	2 min	
95 ℃ 66 ℃ 68 ℃	30 s 30 s 2 min	2x
95 ℃ 65 ℃ 68 ℃	30 s 30 s 2 min	2x
95 ℃ 64 ℃ 68 ℃	30 s 30 s 2 min	38x
68 ℃ 22 ℃	5 min ---	

3.4.3 Agarose gel electrophoresis

1.5% or 2% agarose gels were prepared to separate the PCR products by electrophoresis. Agarose was dissolved in 1x TAE buffer by boiling in a microwave for 7 min. After the buffer cooled down by a magnetic stirrer, ethidium bromide was added before the gel was poured in a chamber placed with combs. The combs were removed after gelling. For PCR analysis, 12.5 µl of PCR products were loaded into the wells and separated in 1× TAE buffer by electrophoresis at 110 V for 1-1.5 h or until the bands were separated sufficiently. Thereafter, DNA bands were visualized by UV light and documented with Gel Doc XR+ system.

3.5 Western Blot

3.5.1 Protein extraction

For protein isolation of pancreas tissue, the samples were collected before as in chapter 3.1.3. For protein isolation from cell lines, protein was collected until the cells reached about 70–80% confluency in 10 cm dishes. After medium was aspirated,

cells were washed twice with sterile PBS. After washing, protein was lysed in IP buffer containing 1% phosphatase and 4% proteinase inhibitors by a cell scraper and snap frozen in Dewar carrying flask containing liquid nitrogen. The lysate was stored at -80 °C for long term storage.

3.5.2 Protein concentration determination

To measure the protein concentration for further experiments, the homogenized protein solution was thawed on ice. For protein solution collected from tissue, it had to be lysed on ice for another 30 min. To remove the debris, the lysate solution was centrifuged at 4 °C, 13200 rpm for 20 min and the supernatant was collected into a new reaction tube.

The protein concentrations of cell lysates were determined by using the Bradford assay (Bradford, 1976). The standard curve for protein concentration's calculation was constructed with a series of BSA dilution. 1 µL of the protein solution was added to 300 µL Bradford reagent (diluted 1:5 in water) in a well of a 96-well plate and each sample was triplicate. After 10 min of incubation, absorbance was measured at 600 nm with the microplate reader ClarioStar MARS. Then, IP buffer containing phosphatase and proteinase inhibitors was added in protein solution to adjust protein concentration to a same level. Protein samples were subsequently denatured by laemmli buffer (diluted 1:5 in samples) (Laemmli, 1970) at 95 °C for 5 min and stored at -20 °C.

3.5.3 SDS polyacrylamide gel electrophoresis (SDS-PAGE)

To separate the proteins by size, standard sodium dodecyl sulphate polyacrylamide gel electrophoresis (SDS-PAGE) was performed. First, a 10% or 12% separating gel was prepared according to table 18, 10% APS and TEMED were added at last. Then, the gel was poured into a gel caster and covered with 2-propanol until it polymerized. Next, the stacking gel was prepared according to table 18 and added to the gel caster. After polymerization, 60-70 µg protein samples were loaded into the gel's wells.

SDS-PAGE would run first at 80V in running buffer for 0.5 h. After the protein electrophorese into the separating gel, the voltage was adjusted to 110V for around 1 h depending on the molecular weight of the interesting protein.

Table 18. SDS gel for electrophoresis of proteins

Compounds	10% separating gel	12% separating gel	Stacking gel
H_2O	2050 ul	1700 ul	1500 ul
Separating gel buffer	1300 ul	1300 ul	-
Stacking gel buffer	-	-	650 ul
Rotiphorese® gel 30	1650 ul	2000 ul	375 ul
10% SDS	50 ul	50 ul	25 ul
10% APS	25 ul	25 ul	12.5 ul
TEMED	7.5 ul	7.5 ul	5 ul

3.5.4 Immunoblot

After the SDS-PAGE, transmembrane was performed at 300mA for 2 h in transfer buffer. The proteins were electro-blotted in a Bio-rad tank blot system on the NC membranes. Then, the membranes were blocked in 5% BSA (diluted in PBS-Tween) at RT for 60 min to prevent unspecific binding of the antibody. The primary antibody was diluted to different concentration in 5% BSA (diluted in PBS-Tween) depending on the efficiency. Thereafter, the membrane was incubated at 4 ℃ overnight with primary antibody of the interesting protein. After 3 times washing with PBS-Tween for 5 min, the membranes were incubated with the secondary antibody (diluted in 5% BSA) for 1 h at RT in darkness. Membranes were again washed 3 times with PBS-Tween. Finally, the membranes were scanned at 700 nm and/or 800 nm wavelength using Odyssey® Fc Imaging System from LI-COR Biosciences. The results were documented and analysed by the Odyssey® Fc Imaging System later on.

3.6 Statistical analysis

Graphical depiction, data correlation and statistical analysis were performed with GraphPad Prism 6. Figure assembly was done with Adobe illustrator CC 2017.

Biological replicates were reported, and data were expressed as mean values ± SEM. To calculate statistical differences between certain data sets, Student's t test was applied for normally distributed samples. A two-way analysis of variance (ANOVA) test was used to analyze the statistical difference between treatments like results of cells treated with TAM / EtOH. For survival analysis, Kaplan-Meier and Log rank test were done for statistical analysis of survival curves. $p < 0.05$ was considered to be statistically significant. If more than one statistical test was performed on a single data set, a Bonferroni-correction was applied to account for the increased possibility of false-positive results.

4. Results

4.1 Validation of *Pdk1* mutation mouse models

We designed a Cre/loxP-based mouse model KCPDK1^{lox} (*Ptf1a$^{Cre/+}$;LSL-Kras$^{G12D/+}$; Pdk1$^{lox/lox}$*) to explore the function of PDK1. Researchers in our group found that *Pdk1* knock-out blocked PanIN and PDAC development completely in the KRAS^{G12D}-driven mouse model *in vivo* and tumor cell proliferation in 2D cell culture (Eser et al., 2013). PH-domain (Bayascas et al., 2008) and PIF-pocket domain (Bayascas et al., 2006; Mora et al., 2004) are two major domains of PDK1 which are supposed to control different downstream signaling pathways (Figure 2B). Mouse models were generated to better dissect the two different functional domains of PDK1, KCPDK1^{K465E} (*Ptf1a$^{Cre/+}$;LSL-Kras$^{G12D/+}$;Pdk1$^{lox/\ K465E}$*), and KCPDK1^{L155E} (*Ptf1a$^{Cre/+}$;LSL-Kras$^{G12D/+}$; Pdk1$^{lox/L155E}$*) (Figure 2A). Wild-type PDK1 is represented by PDK1^{wt} in Figure 2B. In addition to mice generation, genotyping PCR was applied, the results of which are shown in Figure 3. *Pdk1^{lox}* genotyping PCR could detect *Pdk1^{lox}* at 280 bp, but not *Pdk1^{L155E}*, *Pdk1^{K465E}*, and *Pdk1^{wt}* alleles since these alleles would show the same bands at 200 bp (Figure 3A). *Pdk1^{K465E}* genotyping PCR is able to detect *Pdk1^{K465E}* allele at 236 bp. The products of other alleles in this genotyping PCR were the same size at 196 bp (Figure 3B). The results were similar for *Pdk1^{L155E}* genotyping PCR, which showed *Pdk1^{L155E}* allele at 212 bp and other alleles at 171 bp (Figure 3C). Before the experiments, recombination PCR was used to test the recombination of the targeted sequence. *Pdk1^{lox}* and *Pdk1^{L155E}* alleles, which would recombine after Cre expression, were activated by the Cre/loxP system, but *Pdk1^{K465E}* and *Pdk1^{wt}* alleles would not be adjusted. The *Pdk1^{lox}* recombination PCR could detect the difference between *Pdk1^{lox}* (380 bp) and *Pdk1$^{lox\Delta}$* (250 bp) (Δ, recombination), but not other alleles (Figure 4A). For *Pdk1^{L155E}* allele, the *Pdk1^{L155E}* recombination PCR could distinguish the *Pdk1^{L155E}* band (811 bp) from the *Pdk1$^{L155E\Delta}$* band (1077 bp). No other band was shown to represent other alleles because the *Pdk1^{L155E}* recombination primers could not bind to the DNA template of them (Figure 4B). Validated by genotyping PCR and recombination PCR, the mouse lines were expanded, and the

materials, like pancreas tissue, for the subsequent experiments were collected.

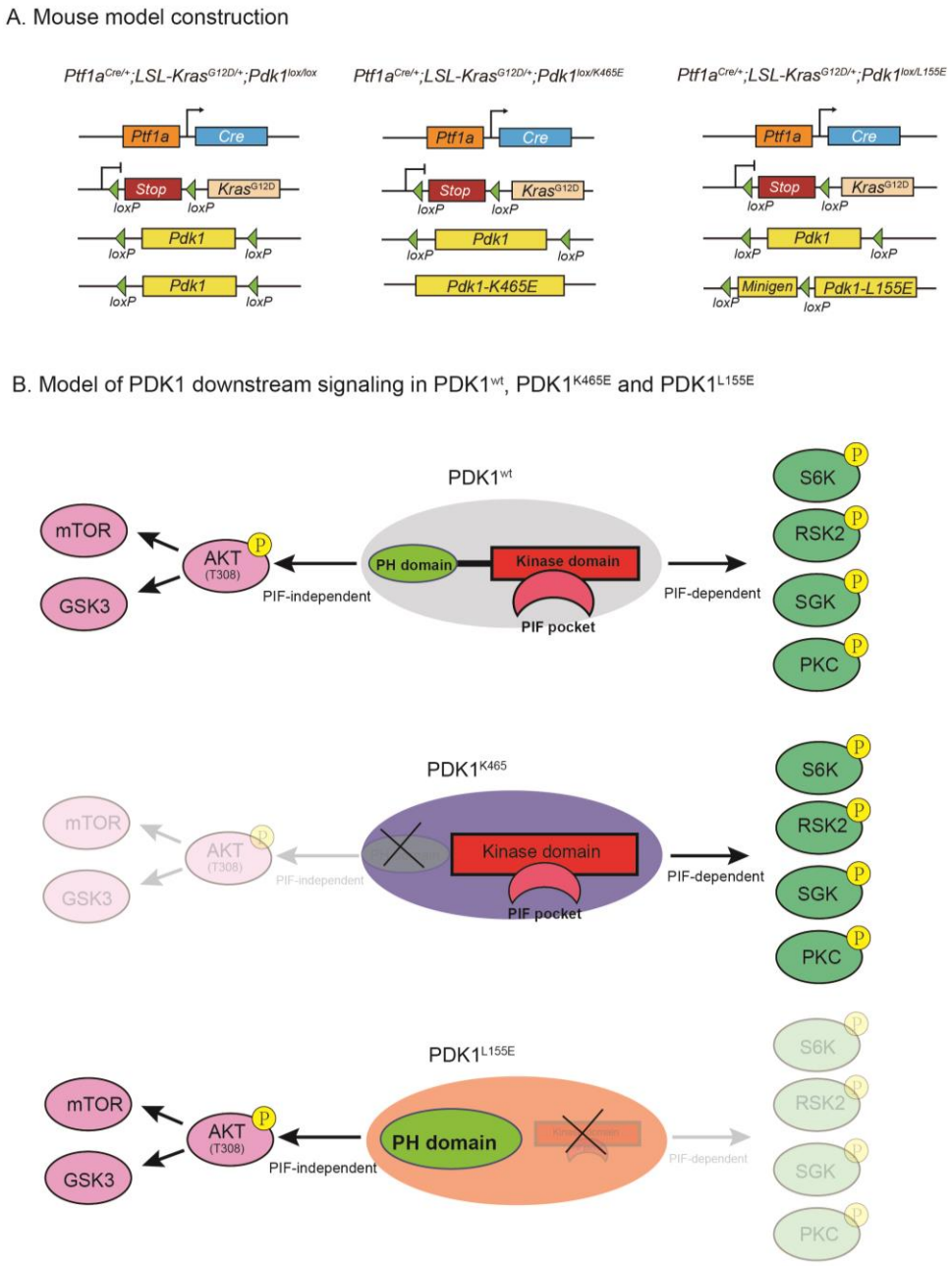

Figure 2. The genetic strategy of KC Mouse model with different *Pdk1* mutations

(A) The genetic strategy used to study the role of the PI3K substrate PDK1 in $Kras^{G12D}$-driven pancreatic cancer formation (left). The same genetic strategy was used to study $PDK1^{K465E}$ (middle) and $PDK1^{L155E}$ mutation (right).

(B) Model of PDK1 downstream signaling in PDK1, $PDK1^{K465E}$, and $PDK1^{L155E}$. The domain and downstream signaling pathway regulated by normal wild-type PDK1 ($PDK1^{wt}$) (top), the $PDK1^{K465E}$ mutation inhibited pathway (middle), and the $PDK1^{L155E}$ mutation inhibited pathway (bottom).

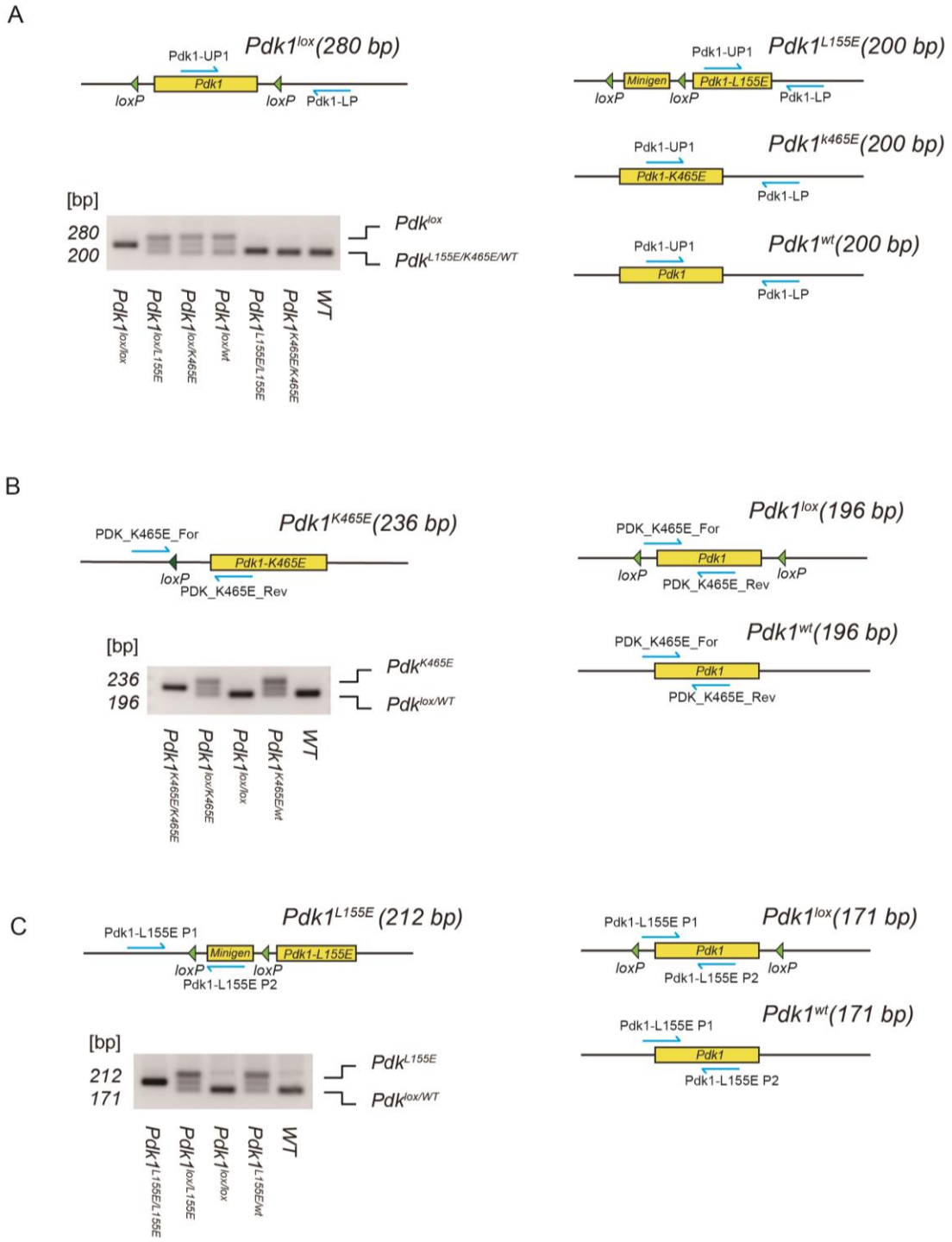

Figure 3. Interpretation of genotyping strategy and PCR results of *Pdk1* constructs

(A) The genotyping strategy to detect the *Pdk1*^{lox} allele (top left). The genotyping strategy for other *Pdk1*^{L155E}, *Pdk1*^{K465E}, and *Pdk1*^{wt} alleles (top right). The PCR products of *Pdk1*^{lox} (280 bp), *Pdk1*^{L155E} (200 bp), *Pdk1*^{K465E} (200 bp), and *Pdk1*^{wt} (200 bp) (bottom left). bp, base pair.

(B) The genotyping strategy to detect the *Pdk1*^{K465E} allele (top left). The genotyping strategy for other *Pdk1*^{lox} and *Pdk1*^{wt} alleles (top right). The PCR products of *Pdk1*^{K465E} (236 bp), *Pdk1*^{lox} (196 bp), and *Pdk1*^{wt} (196 bp) (bottom left). bp, base pair.

(C) The genotyping strategy to detect the *Pdk1*^{L155E} allele (top left). The genotyping strategy for other *Pdk1*^{lox} and *Pdk1*^{wt} alleles (top right). The PCR products of *Pdk1*^{L155E} (212 bp), *Pdk1*^{lox} (171 bp), and *Pdk1*^{wt} (171 bp) (bottom left).

bp, base pair.

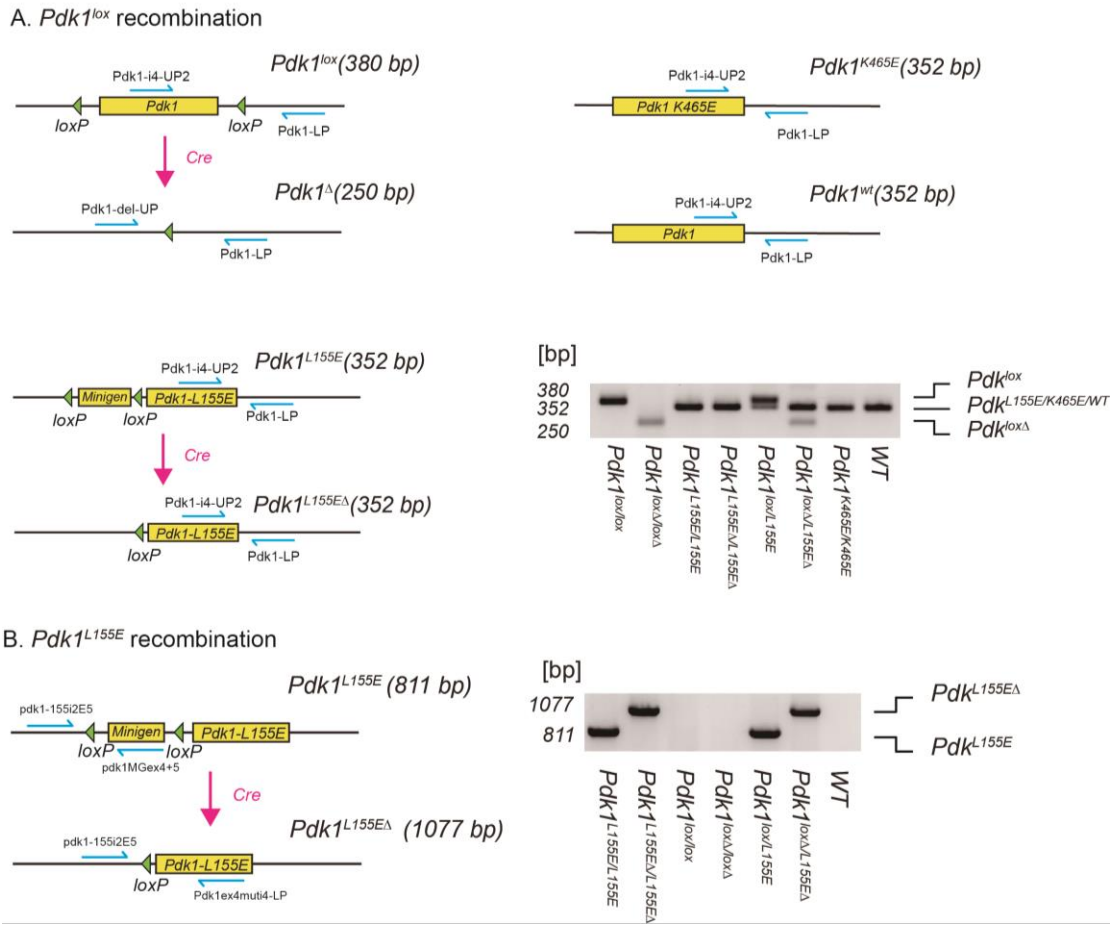

Figure 4. Interpretation of recombination PCR strategy and results of *Pdk1* constructs

(A) The genotyping strategy to detect *Pdk1*^{lox} recombination after Cre expression (top left). The same genotyping strategy for *Pdk1*^{L155E} recombination after Cre expression (bottom left). The same genotyping strategy for other *Pdk1*^{K465E} and *Pdk1*^{wt} alleles (top right). The PCR product of *Pdk1*^{lox} (380 bp), *Pdk1*$^{lox\Delta}$ (380 bp), *Pdk1*^{L155E} (352 bp), *Pdk1*$^{L155E\Delta}$ (352 bp), *Pdk1*^{K465E} (200 bp), and *Pdk1*^{wt} (200 bp) (bottom right). bp, base pair; *Δ*, recombined allele.

(B) The genotyping strategy to detect *Pdk1*^{L155E} recombination after Cre expression (left). The PCR products of *Pdk1*^{lox}*(none), Pdk1*$^{lox\Delta}$*(none), Pdk1*^{wt}*(none)*, *Pdk1*^{L155E} (811 bp) and *Pdk1*$^{L155E\Delta}$ (1077 bp) (bottom right). bp, base pair; *Δ*, recombined allele.

4.2 The roles of *Pdk1*^{K465E} and *Pdk1*^{L155E} mutations in KRAS^{G12D}-driven cancer

Experiments using the KC mouse model were performed to test the roles of *Pdk1*^{K465E} and *Pdk1*^{L155E} mutations in tumor progression in KRAS^{G12D}-driven cancer. Aging the well-established KC mouse model, we observed that the survival time in wild-type, KCPDK1$^{lox/lox}$, and KCPDK1$^{lox/K465E}$ mice were significantly longer than that of KC mice,

indicating that the *Pdk1*^{K465E} mutation regulated downstream signaling pathway was worthy of study since *Pdk1*^{K465E} mutation might affect tumor progression (Figure 5A). However, for KCPDK1$^{K465EK/465E}$ mice, the survival time was similar to that of KC mice (Figure 5A). Hingorani, Gabriel and other authors reported that nearly all KC mice would develop tumors (Ariston Gabriel et al., 2020; Hingorani et al., 2003). For the KCPDK1$^{K465E/K465E}$ mice, only 10% of the mice developed a tumor, as determined by our pathological analysis (Fig. 5C). Although the survival time was similar, the tumor was not the main reason for scarifying the animals. Reasons for terminating the experiment are depicted in Fig. 5C. Besides, the survival time of KCPDK1$^{lox/L155E}$ and KCPDK1$^{L155E/L155E}$ mice was significantly shorter than other genotypes (Figure 5B). Furthermore, none of these mice were sacrificed because of a tumor: the main reason was “bad condition and enlarged appendix” (Figure 5C). The results indicated that no tumors developed in KCPDK1$^{lox/L155E}$, and KCPDK1$^{L155E/L155E}$ mice. Our analysis therefore showed that the *Pdk1*^{K465E} mutation substantially blocked PDAC development, whereas the *Pdk1*^{L155E} mutation led to various other conditions, mainly weight loss, hutching and reduced activity.

Mouse body weight data and pancreas weight data of 3, 6, 9, and 12 months are collected to analyze general mouse condition and pancreatic abnormality. Bodyweight at 3, 6, 9, and 12 months showed no significant differences between groups (Figure 6A), suggesting that mice were growing naturally. However, the pancreas weight percentage (pancreas weight / total body weight) of KC mice were significantly greater than those of KCPDK1$^{lox/L155E}$ and KCPDK1$^{lox/K465E}$ mice in the first 6 months. And KCPDK1$^{lox/L155E}$ and KCPDK1$^{lox/K465E}$ mice were not significantly different from wt mice (Figure 6B), meaning there might be pancreatic atrophy and/or a block of neoplasia in KCPDK1$^{lox/L155E}$ and KCPDK1$^{lox/K465E}$ mice in the early age.

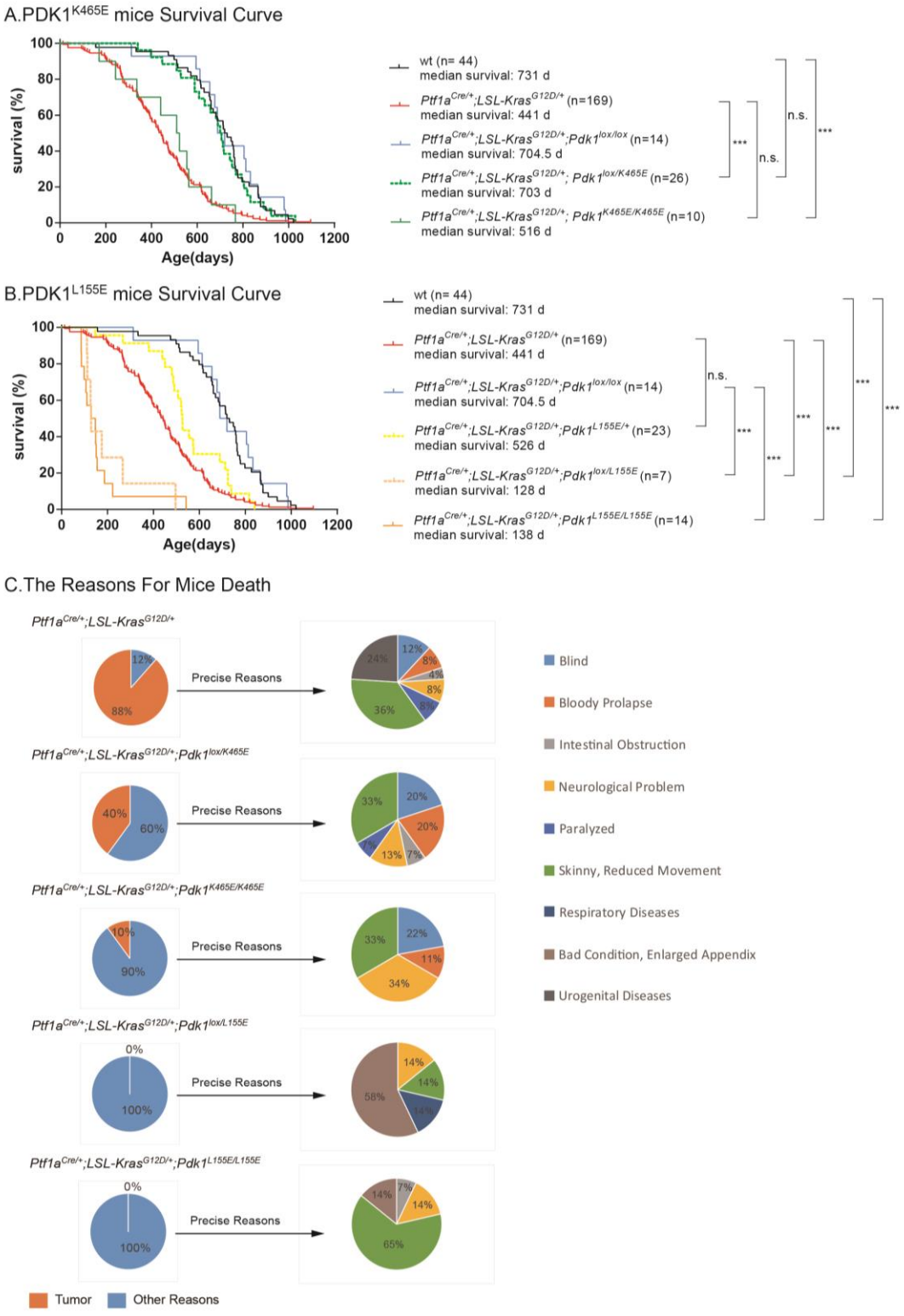

Figure 5. The survival of PDK1^{K465E} and PDK^{L155E} mice in KRAS^{G12D}-driven cancer

(A) Survival curve of KCPDK1^{K465E} mice and other comparable mice. Kaplan-Meier survival analysis of the indicated genotypes. + denotes the wild-type allele, *** p<0.001, log-rank test.

(B) Survival curve of KCPDK1^{L155E} mice and other comparable mice. Kaplan-Meier survival analysis of the indicated genotypes. + denotes the wild-type allele; n.s., not significant; *** p<0.001; log-rank test.

(C) The reasons for the death of mice. *Ptf1a$^{Cre/+}$;LSL-Kras$^{G12D/+}$* (n=169); *Ptf1a$^{Cre/+}$;LSL-Kras$^{G12D/+}$;Pdk1$^{lox/K465E}$* (n=25);

Ptf1a$^{Cre/+}$;*LSL-Kras*$^{G12D/+}$; *Pdk1*$^{K465E/K465E}$ (n=10); *Ptf1a*$^{Cre/+}$; *LSL-Kras*$^{G12D/+}$; *Pdk1*$^{lox/L155E}$ (n=7); *Ptf1a*$^{Cre/+}$; *LSL-Kras*$^{G12D/+}$; *Pdk1*$^{L155E/L155E}$ (n=14).

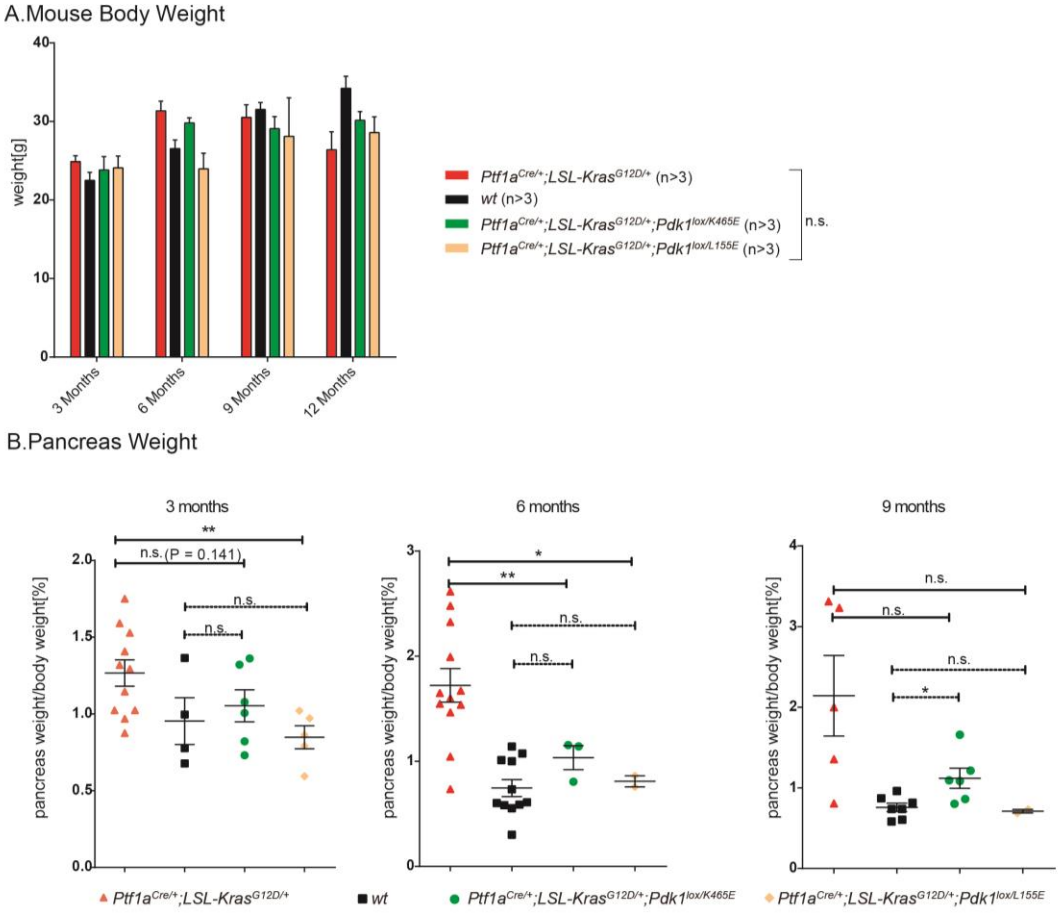

Figure 6. The body and pancreas weight of KCPDK1^{K465E} and KCPDK^{L155E} mice

(A) Bodyweight of the *Ptf1a*$^{Cre/+}$;*LSL-Kras*$^{G12D/+}$ mice; wild-type (wt) mice; *Ptf1a*$^{Cre/+}$;*LSL-Kras*$^{G12D/+}$;*Pdk1*$^{lox/K465E}$ mice and *Ptf1a*$^{Cre/+}$;*LSL-Kras*$^{G12D/+}$;*Pdk1*$^{lox/L155E}$ mice at the age of 3, 6, 9, and 12 months. There were more than 3 animals in each group. n.s., not significant; mean ± SEM; two-tailed Student's t-test.

(B) Percentage of the pancreas in the total body weight of *Ptf1a*$^{Cre/+}$;*LSL-Kras*$^{G12D/+}$ mice; wild-type (wt) mice; *Ptf1a*$^{Cre/+}$;*LSL-Kras*$^{G12D/+}$;*Pdk1*$^{lox/K465E}$ mice and *Ptf1a*$^{Cre/+}$;*LSL-Kras*$^{G12D/+}$;*Pdk1*$^{lox/L155E}$ mice at the age of 3, 6, and 9 months. *Ptf1a*$^{Cre/+}$;*LSL-Kras*$^{G12D/+}$;*Pdk1*$^{lox/L155E}$ mice at 6 months (n=2); *Ptf1a*$^{Cre/+}$;*LSL-Kras*$^{G12D/+}$;*Pdk1*$^{lox/L155E}$ mice at 9 months (n=2); the other groups (n > 3). * p<0.05, ** p<0.01, n.s., not significant; mean ± SEM; two-tailed Student's t-test.

4.3 Effects of *Pdk1*^{K465E} and *Pdk1*^{L155E} mutations on tumor initiation in KRAS^{G12D}-driven pancreatic tumor mouse model

A comparison of mice at different time points is a general method to observe tumorigenesis. Preselected mice were euthanized at 3, 6, and 12 months. Macroscopic pictures of the pancreas and spleen were taken at each time point (Figure 7). By visual inspection, the KC mice pancreas showed nodular changes in morphology, while the pancreas of the KCPDK1^{K465E} and KCPDK1^{L155E} mice were still normal. The results indicated no obvious abnormal macroscopic changes occurred in the pancreas in KCPDK1^{K465E} and KCPDK1^{L155E} mice at these time points (Figure 7).

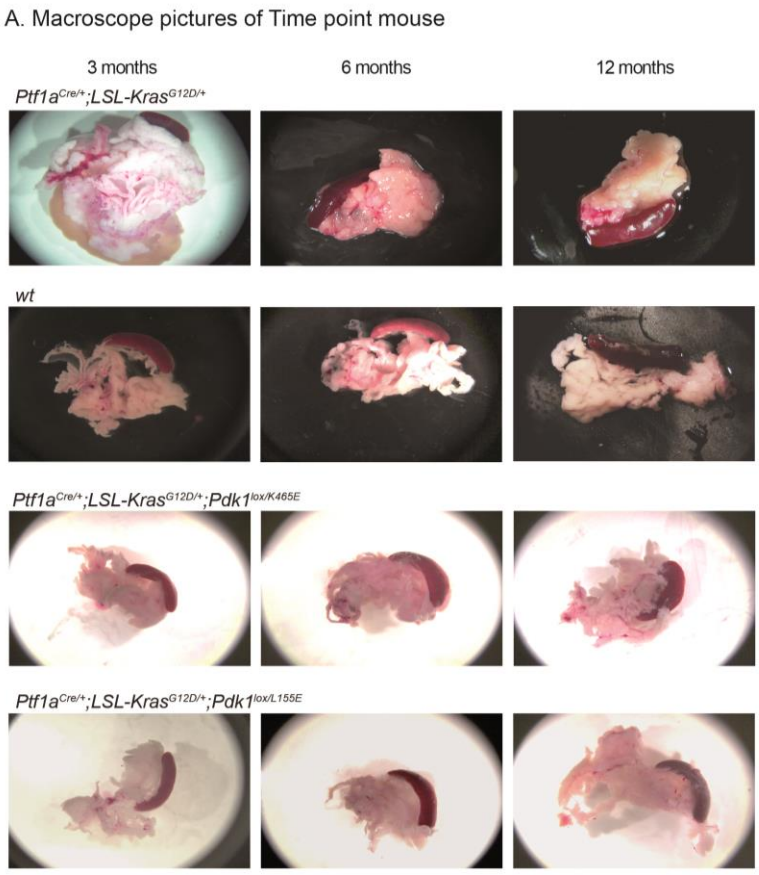

Figure 7. Macroscopic changes in the mouse pancreas at specific time points

(A) Representative macroscopic images of the pancreas in mice with the indicated genotypes at 3, 6, and 12 months old as time points (images from Felix Hesse, Doctoral dissertation, 2020).

To further analyze the pathological changes, hematoxylin and eosin (HE) staining and alcian blue (AB) staining were performed at each time point, and all the slices were scanned integrally. HE staining was used to evaluate the normal structures of the

pancreas. AB staining was used for better assessment of PanIN due to the increased mucin production of the PanIN lesions (Figure 8A). Many researchers reported that PDAC tumorigenesis had begun with ADM and PanIN. In our project, the ADM lesion and PanIN lesions in HE and AB stained slices were counted manually (Figure 8A). At least three slices from three animals per time point and genotype were used for analysis of ADM formation and PanIN lesion formation. The average lesion number in 20x magnification field was counted as result. Besides, pancreatic atrophy was observed in KC, KCPDK1^{K465E}, and KCPDK1^{L155E} mice. Notably, the incidence rate of pancreatic atrophy was higher in KCPDK1^{L155E} mice compared with other groups after 6 months old (Figure 8B).

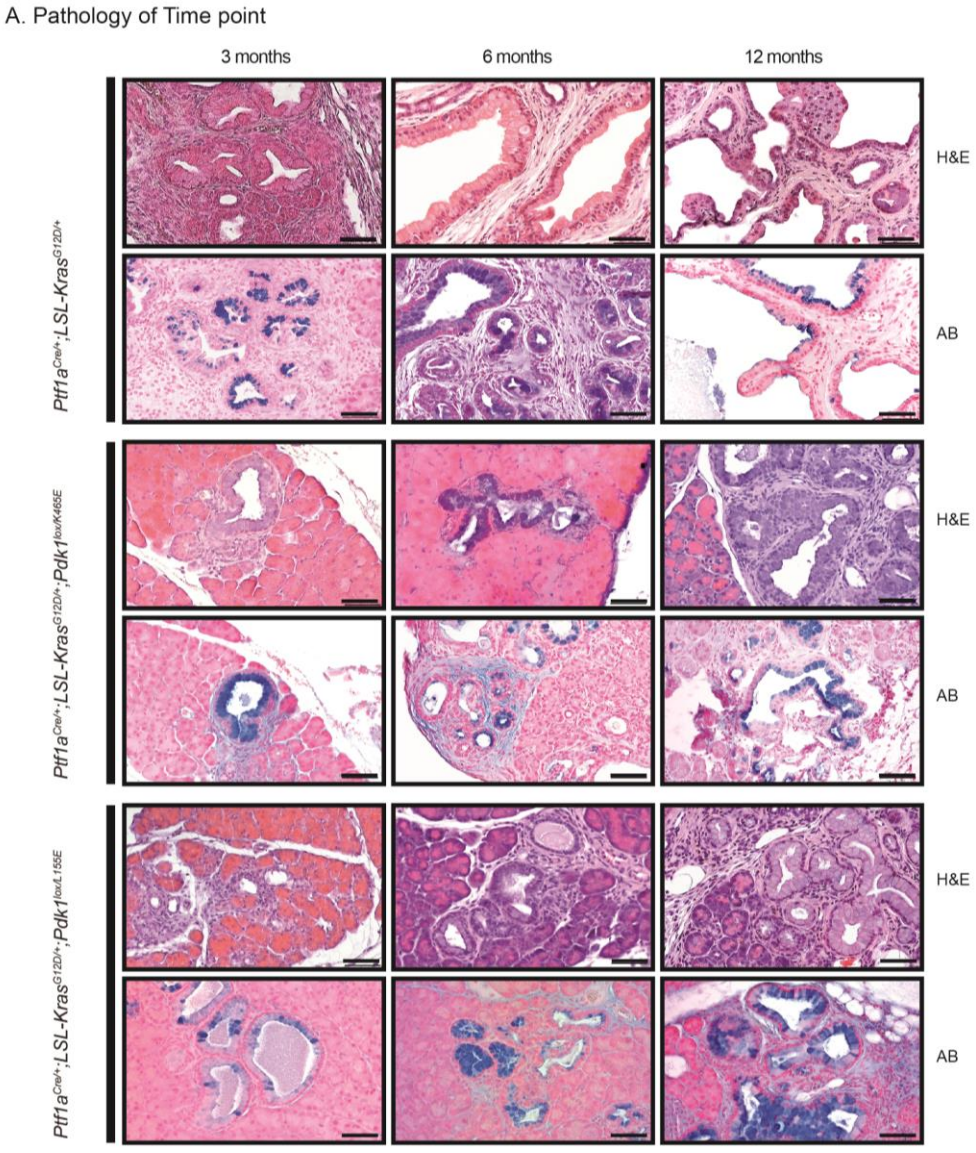

(Figure 8 continued on next page)

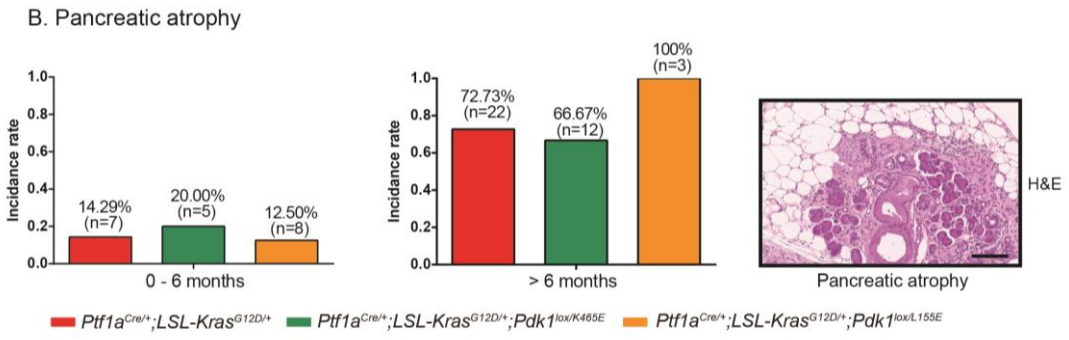

Figure 8. Pathology changes in the mouse pancreas at specific time points

(A) Representative H&E and Alcian blue staining of *Ptf1a*$^{Cre/+}$*;LSL-Kras*$^{G12D/+}$*;Pdk1*$^{lox/K465E}$ mice (top), *Ptf1a*$^{Cre/+}$*;LSL-Kras*$^{G12D/+}$ *;Pdk1*$^{lox/L155E}$ mice (middle); and *Ptf1a*$^{Cre/+}$ *;LSL-Kras*$^{G12D/+}$ mice (bottom) at 3, 6, and 12 months. Scale bar 50μm (images from Felix Hesse, Doctoral dissertation, 2020).

(B) The percentage of mice with pancreatic atrophy in *Ptf1a*$^{Cre/+}$*;LSL-Kras*$^{G12D/+}$ mice, *Ptf1a*$^{Cre/+}$*;LSL-Kras*$^{G12D/+}$*; Pdk1*$^{lox/K465E}$ mice, and *Ptf1a*$^{Cre/+}$*;LSL-Kras*$^{G12D/+}$*;Pdk1*$^{lox/L155E}$ mice, before 6 months and after 6 months. Representative H&E staining of pancreatic atrophy (right). Scale bar 50μm.

For KC mice, the initiation of ADM and PanIN-1A lesions was rapid in the first 9 months, and as time passed, ADM and PanIN lesions gradually developed into high-grade PanIN lesions. At 12 months, the number of ADM lesions of KC mice were less than in KCPDK1^{K465E} or KCPDK1^{L155E} mice, but PanIN lesions were still more than in KCPDK1^{K465E} or KCPDK1^{L155E} mice (Figure 9A).

For KCPDK1^{K465E} mice, ADM lesions were significantly less than those in KC mice in the first 6 months. And PanIN-1A lesions were significantly less than in KC mice in 12 months (Figure 9A).

For KCPDK1^{L155E} mice, the number of ADM lesions were not significantly different from KC mice. But the number of PanIN-1A lesions in KCPDK1^{L155E} mice were significantly down-regulated than those in KC mice at 6 months and 12 months (Figure 9A).

These results suggest that *Pdk1*^{K465E} mutation blocks the ADM and PanIN process, and *Pdk1*^{L155E} mutation blocks the PanIN formation but not ADM. An assay was performed to test the ADM process *in vitro* using 3-month-old mice to support the results *in vivo*. The acinar cells were isolated from pancreatic tissue and cultured for 5 days. Then, acinar cells and ductal cells were counted manually after 5 days in cell culture. Cells isolated from KCPDK1^{K465E} mice showed less ADM during these 5 days than KC mice (*p*-value is 0.093) (Figure 9B). Considering all evidence, *Pdk1*^{K465E}

mutation inhibits the ADM process both *in vivo* and *in vitro*. Furthermore, both *Pdk1*^{K465E} and *Pdk1*^{L155E} mutations reduce the PanIN formation *in vivo*.

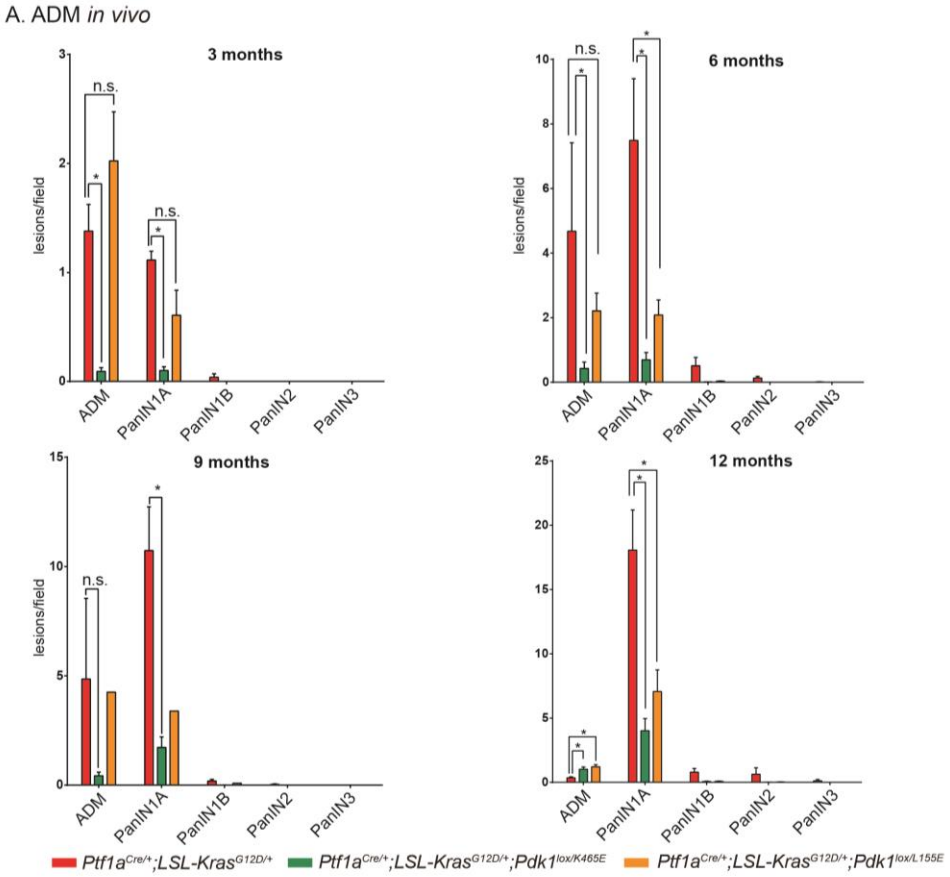

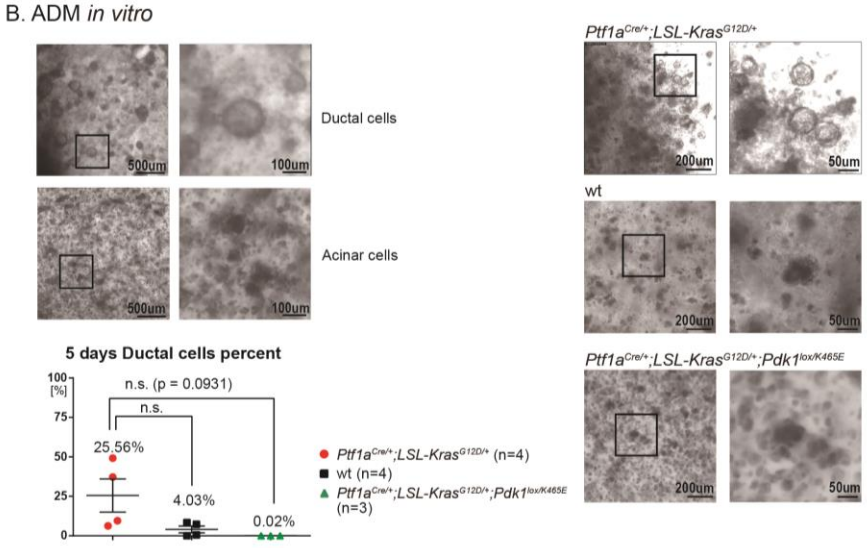

Figure 9. ADM and PanIN formation *in vivo* and *in vitro*

(A) The number of ADM and PanIN lesions in *Ptf1a*$^{Cre/+}$*;LSL-Kras*$^{G12D/+}$ mice, *Ptf1a*$^{Cre/+}$*;LSL-Kras*$^{G12D/+}$*;Pdk1*$^{lox/K465E}$ mice, and *Ptf1a*$^{Cre/+}$*;LSL-Kras*$^{G12D/+}$*;Pdk1*$^{lox/L155E}$ mice at 3, 6, 9, and 12 months. PanIN lesions were divided into PanIN-1A, PanIN-1B, PanIN-2, and PanIN-3 according to the specific pathology changes. * p<0.05, ** p<0.01, n.s., not significant; mean ± SEM; two-tailed Student's t-test.

(B) Acinar and ductal cells representative image (top left). Scale bar 500um and 100um. Representative images of ADM assay results of *Ptf1a*$^{Cre/+}$;*LSL-Kras*$^{G12D/+}$ mice, wt mice, and *Ptf1a*$^{Cre/+}$;*LSL-Kras*$^{G12D/+}$;*Pdk1*$^{lox/K465E}$ mice (right). Scale bar 200um and 50um. Results after quantification (bottom left). n.s., not significant; mean ± SEM; two-tailed Student's t-test.

4.4 Analysis of *Pdk1*^{K465E} and *Pdk1*^{L155E} dependent signaling pathways *in vivo*

Former researchers reported that *Pdk1*^{K465E} mutation was found to inhibit the AKT T308 phosphorylation and thus inactivate the PI3K/PDK1/AKT pathway (Bayascas et al., 2008) and *Pdk1*^{L155E} mutation was found to inhibit the function of the PIF-pocket domain, which down-regulated the phosphorylation of RSK2 S227, S6K1 T229, S6R S235/S236 and SGK3, among others (Bayascas et al., 2006; Mora et al., 2004). In our experiment, the effect of the *Pdk1*^{K465E} and *Pdk1*^{L155E} mutation was tested by IHC using pancreas tissue from the respective mice at endpoint. For the PI3K/PDK1/AKT signaling pathway, both PH-domain and PIF-pocket domain activated the PI3K/PDK1/AKT signaling pathway, confirmed by AKT T308 phosphorylation in all groups of IHC sections (Figure 10). For the PIF-pocket dependent pathways, *Pdk1*^{L155E} mutation down-regulated RSK2 S227 phosphorylation, but SGK3 T320 phosphorylation was similar in all groups.

These results suggest that the PIF-pocket domain related PDK1/RSK2 pathway is inhibited by *Pdk1*^{L155E} mutation *in vivo*.

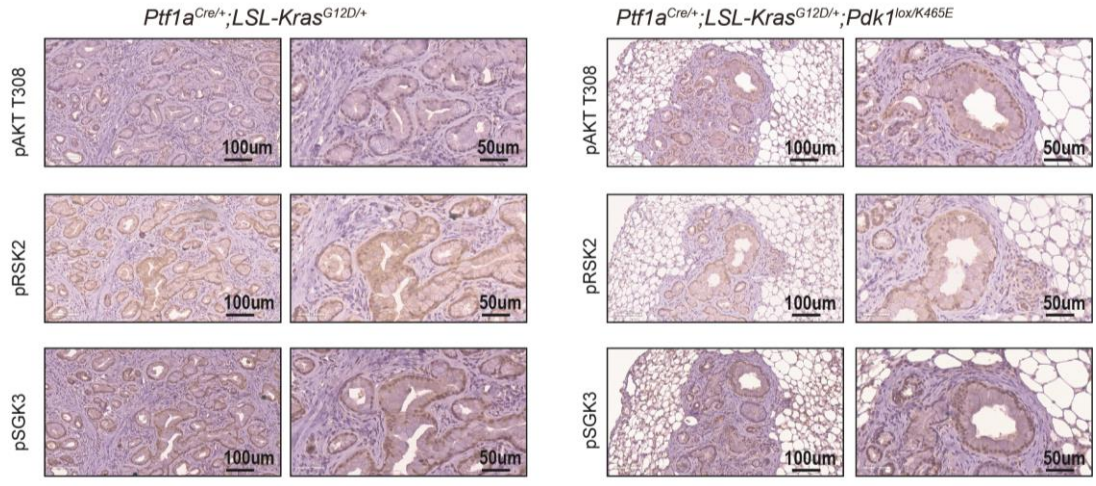

(Figure 10 continued on next page)

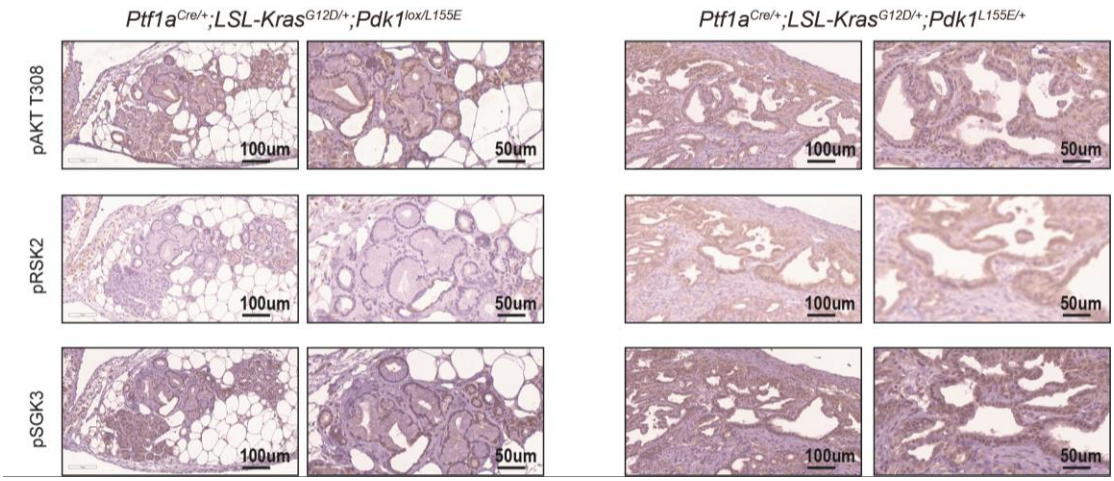

Figure 10. *Pdk1*^{L155E} and *Pdk1*^{K465E} mutations related signaling pathway *in vivo*

Representative immunohistochemical images of *Ptf1a*$^{Cre/+}$*;LSL-Kras*$^{G12D/+}$ mice (n=3), *Ptf1a*$^{Cre/+}$*;LSL-Kras*$^{G12D/+}$*; Pdk1*$^{lox/K465E}$ mice (n=3), *Ptf1a*$^{Cre/+}$*;LSL-Kras*$^{G12D/+}$*;Pdk1*$^{lox/L155E}$ mice (n=1) , and *Ptf1a*$^{Cre/+}$*;LSL-Kras*$^{G12D/+}$*;Pdk1*$^{L155E/+}$ mice (n=2) at endpoint. pAKT T308, pRSK2 S227, and pSGK3 were tested in three indicated group. Scale bars 100 μm for micrographs, 50 μm for insets.

4.5 Inducible induction of PDK1^{K465E} and PDK1^{L155E} mutations *in vivo* and *in vitro*

DRS mouse models genetic strategies are shown in Figure 11A. *Pdx1-Flp;FSF-Kras*$^{G12D/+}$*;FSF-R26*^{CreER}*;Pdk1*$^{lox/K465E}$*;p53*$^{frt/wt}$ (DRS-PDK1$^{lox/K465E}$; p53$^{frt/wt}$) mice and *Pdx1-Flp;FSF-Kras*$^{G12D/+}$*;FSF-R26*^{CreER}*;Pdk1*$^{lox/L155E}$*;p53*$^{wt/wt}$ (DRS-PDK1$^{lox/L155E}$;p53$^{wt/wt}$) mice were generated for this thesis (Figure 11A). To test tamoxifen-induced CreER^{T2} mediated recombination in the DRS system (Schönhuber et al., 2014), the floxed double color fluorescent tdTomato-EGFP Cre reporter line (*R26*$^{mT-mG}$) (Muzumdar et al., 2007), in which the expression of *tdTomato* was replaced by *EGFP* following Cre-mediated excision, was used (Figure 11B). *Pdx1-Flp;FSF-Kras*$^{G12D/+}$*; FSF-R26*$^{CreER/+}$*;R26*$^{mT-mG}$ mice were aged, and after PDAC formation, tumor cell lines were isolated. These animals had not been exposed to tamoxifen (TAM), so the floxed *tdTomato* reporter allele remained non-recombined in these cells. *In vitro* treatment of TAM led to the recombination of the *R26*$^{mT-mG}$ reporter, and therefore the fluorescence changed from *tdTomato* (red) to *EGFP* (green) expression within 24 hours of treatment (Figure 11B) (Schönhuber et al., 2014). Mock (EtOH) treated cells showed no recombination (Figure 12A), excluding Cre activity in

the absence of tamoxifen.

In the DRS-PDK1^{K465E} and DRS-PDK1^{L155E} mice, an *frt*-flanked *Trp53* allele (*p53^{frt}*) was present to enable *p53* deletion and accelerate tumorigenesis (Lee et al., 2012). The *p53^{frt}* allele will be knocked out after Flp is expressed. *p53* status (*p53^{frt}* or *p53^{wt}*; *p53^{frt}* recombined or *p53^{frt}* not recombined) was tested before the experiments (Figure 11C, D). After DRS-PDK1$^{lox/K465E}$;p53$^{frt/wt}$ and DRS-PDK1$^{lox/L155E}$;p53$^{wt/wt}$ mice were aged and developed PDAC, the cell lines were isolated.

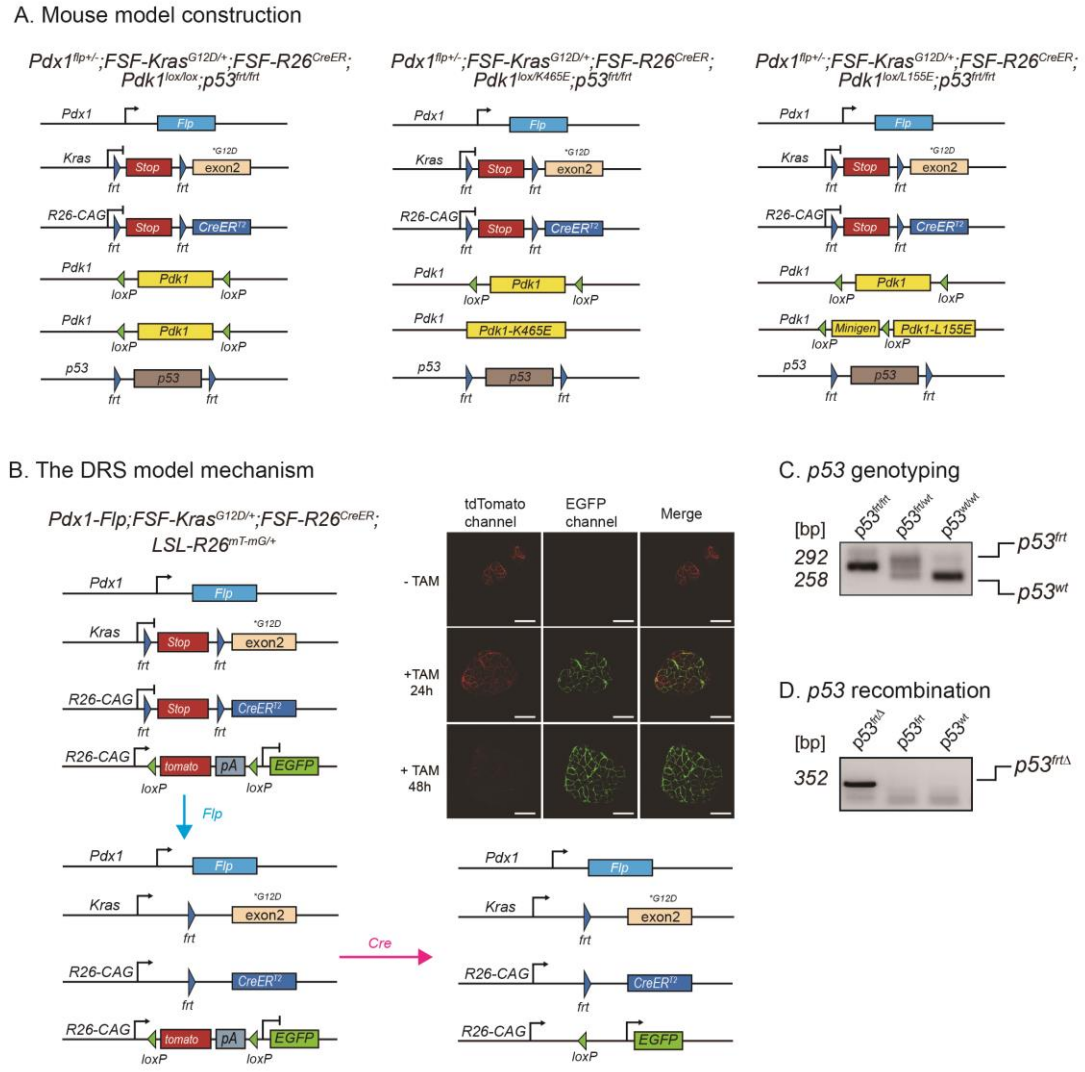

Figure 11. DRS mouse model constructions for spatial or temporal manipulation of established KRAS^{G12D}-induced PDAC cells in the *Pdx1-Flp* lineage

(A) Mouse model construction of *Pdx1-Flp;FSF-Kras$^{G12D/+}$;FSF-R26^{CreER}; Pdk1$^{lox/lox}$; p53$^{frt/frt}$* (left); *Pdx1-Flp, FSF-Kras$^{G12D/+}$;FSF-R26^{CreER};Pdk1$^{lox/K465E}$;p53$^{frt/frt}$* (middle); and *Pdx1-Flp;FSF-Kras$^{G12D/+}$;FSF-R26^{CreER};Pdk1$^{lox/L155E}$; p53$^{frt/frt}$* (right). Genetic strategy to delete *Pdk1* in established PanIN lesions by time-specific TAM-mediated CreER^{T2}

activation. Pdx1-Flp activated expression of *Kras*^{G12D} induces PanIN lesions, and CreER^{T2} is activated in the *Flp* lineage by TAM administration to delete *Pdk1*.

(B) Genetic strategy in *Pdx1-Flp;FSF-Kras*$^{G12D/+}$*;FSF-R26*^{CreER}*;R26*$^{mT\text{-}mG}$ mice or PDAC cells to induce *EGFP* expression by tamoxifen mediated CreER^{T2} activation before TAM treatment (left). *EGFP* expression after TAM induced Cre-loxP recombination (bottom right). PDAC cells isolated from a *Pdx1-Flp;FSF-Kras*$^{G12D/+}$*; FSF-R26*^{CreER}*;R26*$^{mT\text{-}mG}$ mouse, which has not been treated with tamoxifen, were incubated with 0.1 µM TAM *in vitro*. tdTomato channel (red color, unrecombined cells) and Cre-induced EGFP channel (green color, recombined cells) were analyzed by confocal microscopy at indicated time points (top right). Scale bars 50 µm. (Images provided by Nina Schönhuber, Doctoral dissertation, 2014).

(C) Interpretation of *p53* genotyping PCR results. The corresponding graphic representation of each possible allele. The PCR product of *p53*^{frt} (292 bp), *p53*^{wt} (258 bp). bp, base pair.

(D) Interpretation of *p53*^{frt} recombination PCR results. The corresponding graphic representation of each possible allele. The PCR product of *p53*$^{frt\Delta}$ (352 bp), *p53*^{frt} (no band), and *p53*^{wt} (no band). bp, base pair; Δ, recombined allele.

After treated with TAM/EtOH, both *Pdk1*^{lox} recombination and *Pdk1*^{L155E} recombination of the cell lines became complete and stable after day 2 of treatment (Figure 12A). To understand the PH-domain and PIF-pocket domain mutations related pathway, phosphorylation of AKT, RSK and S6 was tested in two different cell lines of DRS-PDK1$^{lox/K465E}$;p53$^{frt/wt}$ and DRS-PDK1$^{lox/L155E}$;p53$^{wt/wt}$ (Figure 12B). For *Pdk1*^{K465E} mutation, it showed no influence on the RAS/RAF/MEK/ERK pathway confirmed by the unchanged phosphorylation of pRSK1 S380 (Figure 12B). It also did not influence the PIF-pocket dependent pathway as confirmed by the lack of variation of pRSK2 S227 and pS6R S235 phosphorylation, nor the mTORC2/AKT pathway as verified by the unchanged pAKT S473 (Figure 12B). Although multiple western blots were performed, the immunoblot result of pAKT T308 was not detectable. Thus, the regulation of the PI3K/PDK1/AKT pathway was difficult to assess. For *Pdk1*^{L155E} mutation, the PIF-pocket domain related pathway was inhibited significantly, confirmed by pRSK2 S227 and pS6R S235 downregulation. The RAS/RAF/MEK/ERK pathway was not significantly changed, as no changes of the phosphorylation of RSK1 S380. Since no variation of pAKT S473 was observed, the mTORC2/AKT pathway was not influenced neither. In conclusion, PIF-pocket domain of PDK1 is essential for the activation of RSK2 and S6R, but the effects of PH-domain remain unclear.

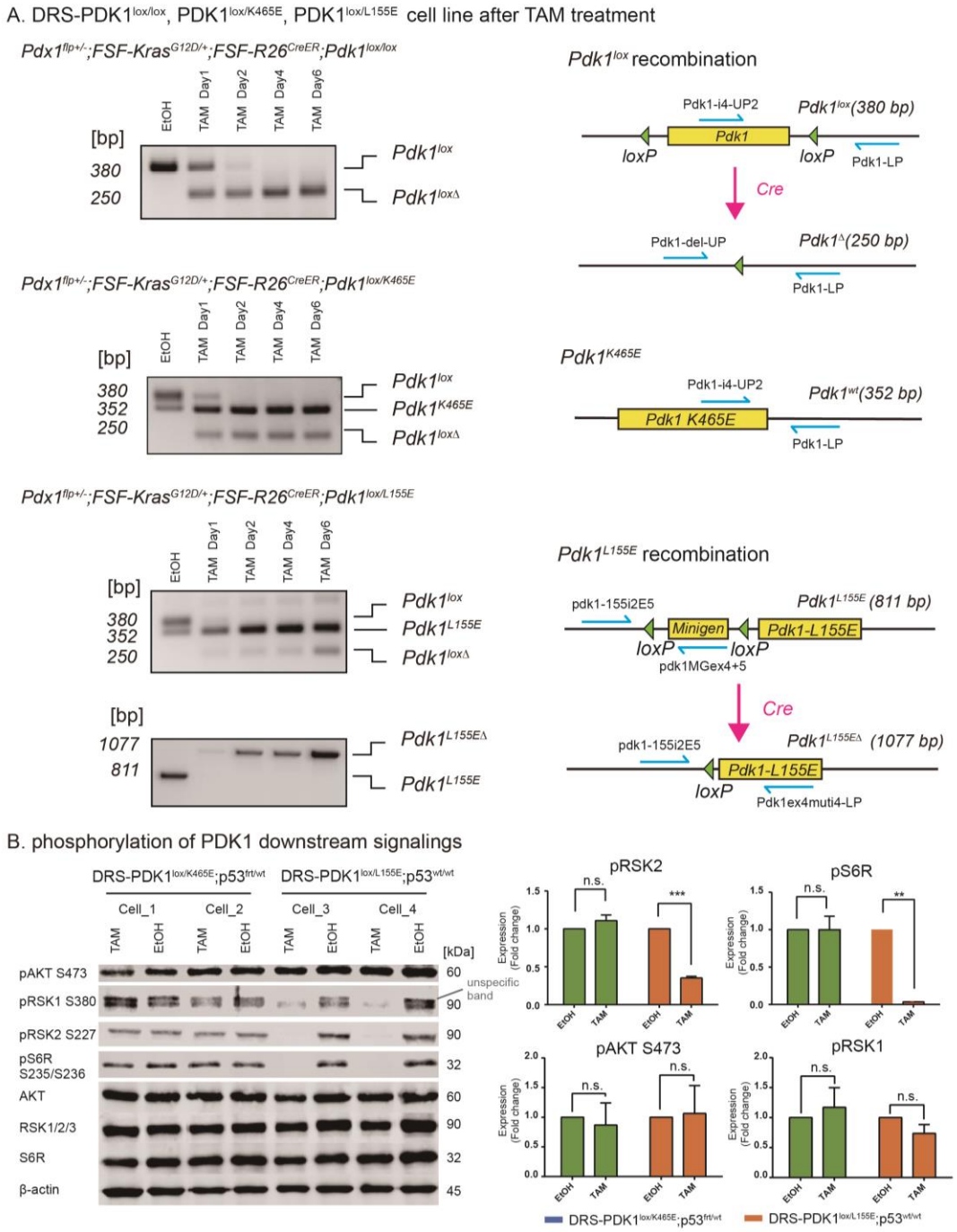

Figure 12. Analysis of PH-domain and PIF-pocket dependent downstream signaling in vitro

(A) Recombination test after TAM treatment of *Pdx1-Flp;FSF-Kras$^{G12D/+}$;FSF-R26^{CreER};Pdk1$^{lox/lox}$* (top); *Pdx1-Flp; FSF-Kras$^{G12D/+}$;FSF-R26^{CreER};Pdk1$^{lox/K465E}$* (middle) and *Pdx1-Flp;FSF-Kras$^{G12D/+}$;FSF-R26^{CreER};Pdk1$^{lox/L155E}$* (bottom) cells. The corresponding graphic representation of each possible allele (right). bp, base pair; Δ, recombined allele.

(B) Phosphorylation rate of PDK1 downstream signaling. Cell_1 to Cell_4 were different cell lines from the indicated genotype. DRS-PDK1$^{lox/K465E}$;p53$^{frt/wt}$ and DRS-PDK1$^{lox/L155E}$;p53$^{wt/wt}$. Immunoblot analysis of PI3K/PDK1/AKT pathway activation and PIF-pocket domain dependent pathway activation of PDAC cell lines after 8 days 500 nM TAM or vehicle (EtOH) treatment (left). β-actin was used as a loading control. The unspecific band was marked.

Phosphorylation rate after the quantification and normalization (right). Expression reported in fold changes compared to Ctrl (EtOH treated cell lines). kDa, 1,000 Daltons; **, $p<0.01$; ***, $p<0.001$; n.s., not significant; mean ± SD, two-way ANOVA.

4.6 *Pdk1^{K465E}* and *Pdk1^{L155E}* mutations impair PDAC cell proliferation and colony formation *in vitro*

To assess the effects of the two different PDK1 mutants on cell viability and colony formation, we used the DRS to inducibly activate the mutations *in vitro* via TAM treatment. *p53^{frt}* recombination was tested as routine before the TAM/EtOH treatment. The recombination for each cell line treated with TAM/EtOH was tested, and in TAM treated cell lines, complete *Pdk1^{lox}* recombination and *Pdk1^{L155E}* recombination were observed as shown in Figure 12A. MTT and clonogenic assays were used to test proliferation and colony formation, respectively. The cell growth and colony formation of DRS-PDK1^{K465E};p53^{wt} cell lines were significantly impaired after TAM treatment (Figure 13A). For DRS-PDK1^{L155E};p53^{wt} cell lines, the experiment was repeated and yielded similar results (Figure 13B). Thus, PDK1^{K465E} and PDK1^{L155E} can block PDAC cell proliferation and colony formation.

To assess the role of p53 in PDK1 downstream signaling, DRS-PDK1^{K465E};p53^{frt} and DRS-PDK1^{L155E};p53^{frt} mice were generated. These animals develop PDAC within a year due to the Flp mediated deletion of the *frt* flanked *p53* tumor suppressor. After these mice developed tumors, primary pancreatic tumor cell lines were isolated for further experiments. The status of *p53^{frt}* were tested as shown in Figure 13C and Figure 14E. *p53* was deleted in all the cell lines with *p53$^{frt/frt}$* or *p53$^{frt/wt}$* that used in our experiments. When one *p53* is mutated, the other *p53^{wt}* allele is usually lost, known as loss of heterozygosity (LOH) (Baker et al., 1990). MTT and clonogenic assay on DRS-PDK1^{K465E};p53^{frt} and DRS-PDK1^{L155E};p53^{frt} cell lines were performed after treatment with TAM/EtOH. Notably, the impairment caused by *Pdk1^{K465E}* mutation in cell proliferation and colony formation observed in the *p53* wild-type setting (Fig. 13) was completely blocked in *p53* deleted cell lines (Figure 14B). This was not the case for *Pdk1* completely deleted cells and cells harboring the *Pdk1^{L155E}* mutation (Fig. 14). Results of MTT and clonogenic assays showed that proliferation and colony formation

of TAM treated cell lines were strongly inhibited compared to the same cell lines treated with EtOH (Figure 14A, C). In conclusion, *Pdk1*^{L155E} and *Pdk1*^{K465E} mutations block PDAC cell proliferation and colony formation; however, *p53* deletion is able to bypass the growth arrest specifically in the DRS-PDK1^{K465E} model.

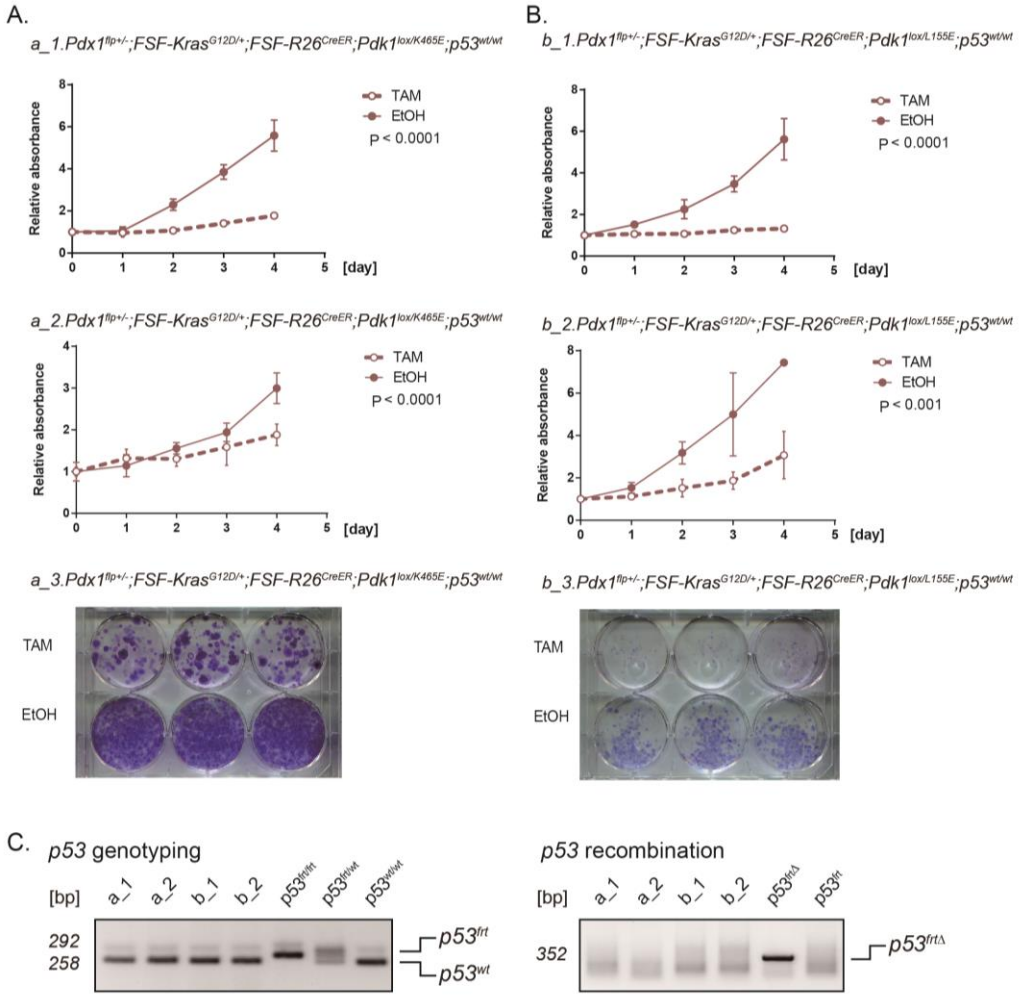

Figure 13. *Pdk1*^{K465E} and *Pdk1*^{L155E} mutations impair proliferation and colony formation of *p53* wild-type PDAC cells *in vitro*

(A) a_1 to a_2 depict two distinct *Pdx1-Flp;FSF-Kras*$^{G12D/+}$*;FSF-R26*^{CreER}*;Pdk1*$^{lox/K465E}$*;p53*$^{wt/wt}$ cell lines. MTT assays of TAM treated cell lines compared to placebo control (EtOH) treated lines (top left). mean ± SD, two-way ANOVA. a_3 includes representative images of clonogenic assays of cells treated with TAM (upper row) and EtOH (lower row) (bottom left).

(B) b_1 to b_2 depict two distinct *Pdx1-Flp;FSF-Kras*$^{G12D/+}$*;FSF-R26*^{CreER}*;Pdk1*$^{lox/L155E}$*;p53*$^{wt/wt}$ cell lines. MTT assays of TAM treated cell lines compared to EtOH treated lines (top right). mean ± SD, two-way ANOVA. b_3 includes representative images of the clonogenic assay of cells treated with TAM (upper row) and EtOH (lower row) (bottom right).

(C) *p53*^{frt} genotyping PCR (left) and the corresponding graphic representation of PCR products of a_1, a_2, b_1, and b_2 cell lines: *p53*^{frt} (292 bp), *p53*^{wt} (258 bp). *p53*^{frt} recombination PCR (right) and the corresponding graphic

representation of PCR products of a_1, a_2, b_1, and b_2 cell lines: $p53^{frt\Delta}$ (352 bp), $p53^{frt}$ not recombined (no band). bp, base pair; Δ, recombined allele.

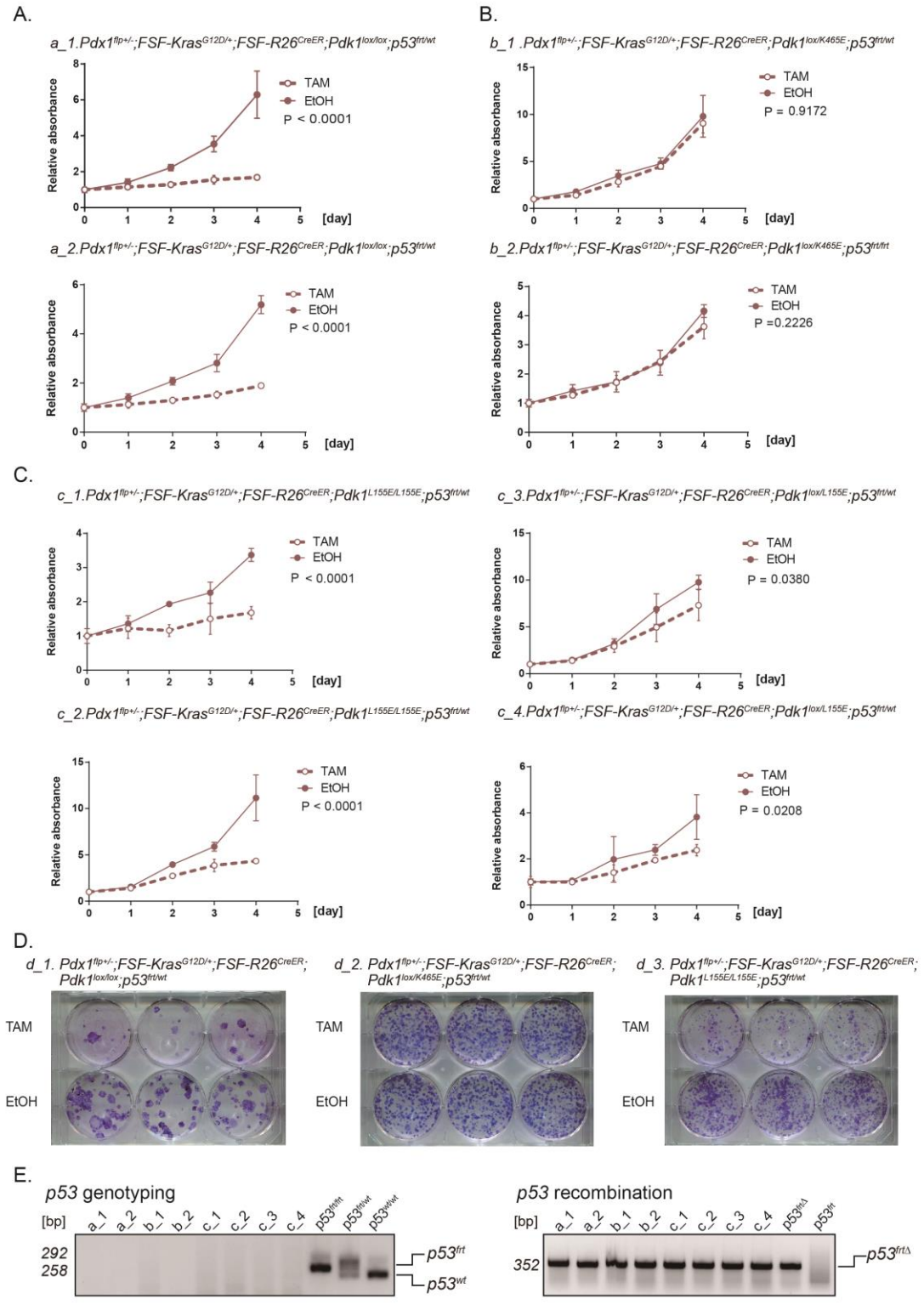

Figure 14. Context specific effects of *Pdk1*^{K465E} and *Pdk1*^{L155E} mutations on proliferation and colony formation in *p53* deficient PDAC cells *in vitro*

(A) a_1 to a_2 depict two distinct *Pdx1-Flp;FSF-Kras*$^{G12D/+}$*;FSF-R26*^{CreER}*;Pdk1*$^{lox/lox}$*;p53*$^{frt/wt}$ cell lines. MTT assays of TAM treated cell lines compared to EtOH treated lines. mean ± SD, two-way ANOVA.

(B) b_1 to b_2 depict two distinct *Pdx1-Flp;FSF-Kras*$^{G12D/+}$*;FSF-R26*^{CreER}*;Pdk1*$^{lox/K465E}$*;p53*$^{frt/wt}$ and *Pdx1-Flp;FSF-Kras*$^{G12D/+}$*;FSF-R26*^{CreER}*;Pdk1*$^{lox/K465E}$*;p53*$^{frt/frt}$ cell lines. MTT assays of TAM treated cell lines compared to EtOH treated ones. mean ± SD, two-way ANOVA.

(C) c_1 to c_2 depict two distinct *Pdx1-Flp;FSF-Kras*$^{G12D/+}$*;FSF-R26*^{CreER}*;Pdk1*$^{L155E/L155E}$*;p53*$^{frt/wt}$ cell lines and c_3 to c_4 depict two distinct *Pdx1-Flp;FSF-Kras*$^{G12D/+}$*;FSF-R26*^{CreER}*;Pdk1*$^{lox/L155E}$*;p53*$^{frt/wt}$ cell lines. MTT assays of TAM treated cell lines compared to EtOH treated lines. mean ± SD, two-way ANOVA.

(D) d_1, d_2 and d_3 are representative images of clonogenic assays of *Pdx1-Flp;FSF-Kras*$^{G12D/+}$*; FSF-R26*^{CreER}*;Pdk1*$^{lox/lox}$*;p53*$^{frt/wt}$ cells, *Pdx1-Flp;FSF-Kras*$^{G12D/+}$*;FSF-R26*^{CreER}*;Pdk1*$^{lox/K465E}$*;p53*$^{frt/wt}$ cells, and *Pdx1-Flp;FSF-Kras*$^{G12D/+}$*;FSF-R26*^{CreER}*;Pdk1*$^{L155E/L155E}$*;p53*$^{frt/wt}$ cells treated with TAM (upper row) and EtOH (lower row) (bottom).

(E) *p53*^{frt} genotyping PCR (left) and the corresponding graphic representation of PCR products of a_1, a_2, b_1, b_2, c_1, c_2, c_3, and c_4 cell lines: *p53*^{frt} (292 bp), *p53*^{wt} (258 bp). *p53*^{frt} recombination PCR (right) and the corresponding graphic representation of PCR products of each cell lines: *p53*$^{frt\Delta}$ (352 bp), *p53*^{frt} not recombined (no band). bp, base pair; Δ, recombined allele.

4.7 Longitudinal analysis of PIF-pocket domain and PH-domain dependent downstream signaling *in vitro*

We analyzed in the following experiments the biological behavior changes of PDAC cells regulated by *Pdk1*^{L155E} or *Pdk1*^{K465E} mutation in *p53* wild-type and deleted cells. Time series analysis was used to stepwise dissect the precise changes over time. As the flow chart shows, the samples and cell images were collected after treatment with TAM/EtOH on day 1, day 2, day 4, day 6, and day 8 (Figure 15A). Medium with TAM or EtOH was exchanged every 2 days. No obvious morphological changes were observed in all the cell lines (Figure 15B). As verified by the recombination test for the first 6 days, the recombination was complete and stable at approximately 2 days after start of the treatment (Figure 12A). The *p53*^{frt} status of each cell lines used for longitudinal analysis of PIF-pocket domain and PH-domain was tested. As shown in Figure 15C, *p53* was deleted in cell lines with *p53*$^{frt/frt}$ and *p53*$^{frt/wt}$. The *p53*^{wt} allele was lost because of LOH.

The PDK1 related signaling pathways were tested in DRS-PDK1^{L155E} and DRS-PDK1^{K465E} PDAC cell lines using phosphorylation specific antibodies for key PDK1 downstream signaling molecules. The activation of mTORC2/AKT pathway and the PI3K/PDK1/AKT pathway was confirmed by assessing AKT S473, GSK3 S9, and

S6K1 T389 phosphorylation; the RAS/RAF/MEK/ERK pathway was analyzed by ERK T202/Y204 and RSK1 S380 phosphorylation; and activation of the PIF-pocket dependent pathway was investigated by testing for RSK2 S227 and S6R S235/S236 phosphorylation (Biondi et al., 2000; Biondi et al., 2001; Biondi et al., 2002).

Growth factors and mitogens induce the activation of p70 S6K and the subsequent phosphorylation of the S6R protein (Peterson and Schreiber, 1998). The activity of p70 S6K is controlled by multiple phosphorylation events, of which the phosphorylation at T229 by PDK1 and T389 by mTOR are most critical for its function (Pullen et al., 1998). Meanwhile, S6R S235/S236 is not only one of the downstream phosphorylation targets of S6K1, but also an target of RSK2 (Al-Ali et al., 2017; Roux et al., 2007).

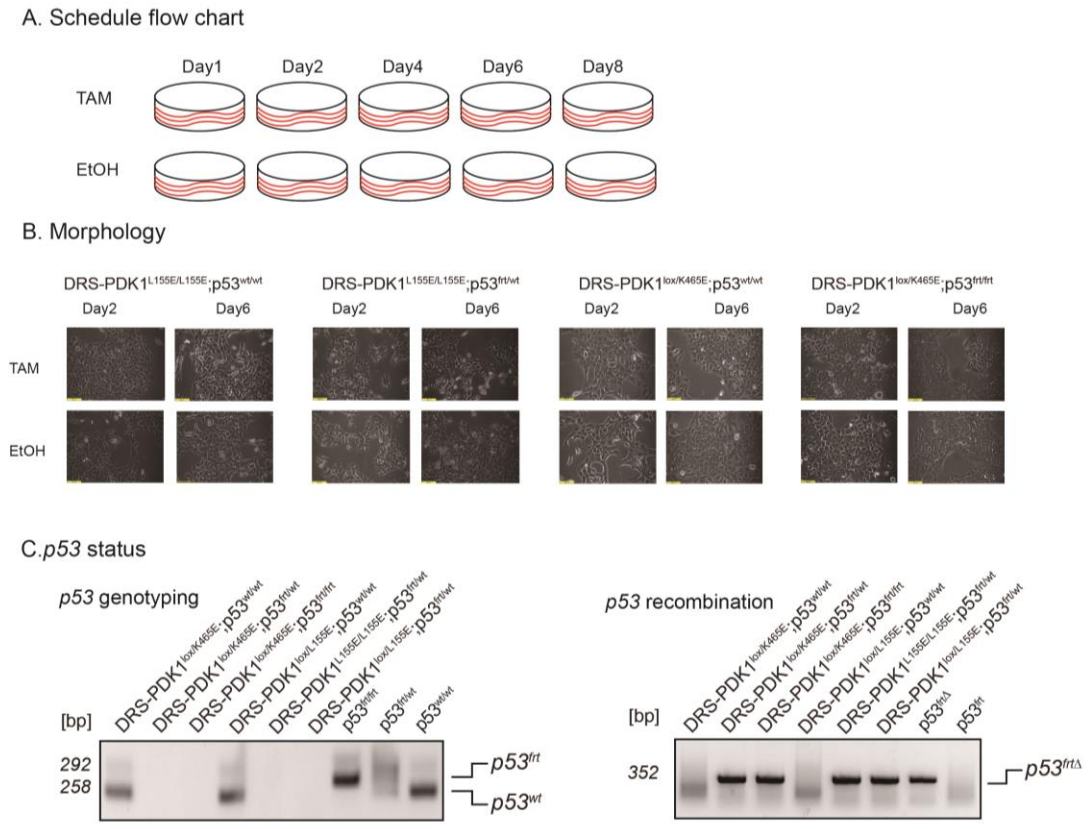

Figure 15. Time series DRS cell lines treated with TAM or EtOH

(A) The schedule flow of cell lines treated with TAM or placebo (EtOH); DNA samples and protein samples for further experiments and cell images were collected at day 1, day 2, day 4, and day 6.

(B) Representative images of cells at day 2 and day 6. Four cell lines are shown. DRS-PDK1$^{L155E/L155E}$;p53$^{wt/wt}$ (*Pdx1-Flp;FSF-Kras$^{G12D/+}$;FSF-R26^{CreERT2};Pdk1$^{L155E/L155E}$;p53$^{wt/wt}$*), DRS-PDK1$^{L155E/L155E}$;p53$^{frt/wt}$ (*Pdx1-Flp; FSF-Kras$^{G12D/+}$;FSF-R26^{CreERT2};Pdk1$^{L155E/L155E}$;p53$^{frt/wt}$*), DRS-PDK1$^{lox/K465E}$;p53$^{wt/wt}$ (*Pdx1-Flp;FSF-Kras$^{G12D/+}$;*

FSF-R26^{CreERT2}*;Pdk1*$^{lox/K465E}$*;p53*$^{wt/wt}$) and DRS-PDK1$^{lox/K465E}$;p53$^{frt/frt}$, (*Pdx1-Flp;FSF-Kras*$^{G12D/+}$*;FSF-R26*^{CreERT2}*; Pdk1*$^{lox/K465E}$*;p53*$^{frt/frt}$). The morphological changes in cell lines were analyzed via visual inspection. Scale bar 100um.

(C) *p53*^{frt} genotyping PCR (left) and the corresponding graphic representation of PCR products of cell lines used for longitudinal analysis: *p53*^{frt} (292 bp), *p53*^{wt} (258 bp). *p53*^{frt} recombination PCR (right) and the corresponding graphic representation of PCR products of each cell lines: *p53*$^{frt\Delta}$ (352 bp), *p53*^{frt} not recombined (no band). bp, base pair; Δ, recombined allele.

To longitudinal analysis the PIF-pocket domain related pathway, western blot was performed using proteins extracted from both *p53* wild-type and *p53* deleted DRS-PDK1^{L155E} cells. The *Pdk1*^{lox} recombination test and *Pdk1*^{L155E} recombination test were performed to validate the corresponding DNA level changes at each timepoint, and we observed that the *Pdk1*^{lox} deletion and *Pdk1*^{L155E} allele recombining completed around Day 2 (Figure 16). For DRS-PDK1^{L155E};p53^{wt} cells, with *Pdk1*^{L155E} mutation and *p53* wild-type, the phosphorylation of RSK2 S227, S6R S235/S236 and S6K1 T389 was blocked (Figure 16A). In contrast, the phosphorylation of AKT S473, GSK3, ERK T202/Y204, RSK1 S380 was not significantly changed (Figure 16A). For DRS-PDK1^{L155E};p53^{frt} cells, with *Pdk1*^{L155E} mutation and *p53* deletion, the inhibition of RSK2 S227, S6R S235/S236 and S6K1 T389 phosphorylation are shown in Figure 16B, C. However, the AKT S473, GSK3, RSK1 S380 phosphorylation showed high variability and the ERK T202/Y204 was up regulated after *p53* deletion (Figure 16B, C).

In conclusion, PIF-pocket domain of PDK1 is essential for the RSK2 S227, S6R S235/S236, and S6K1 T389 phosphorylation with or without *p53* deletion.

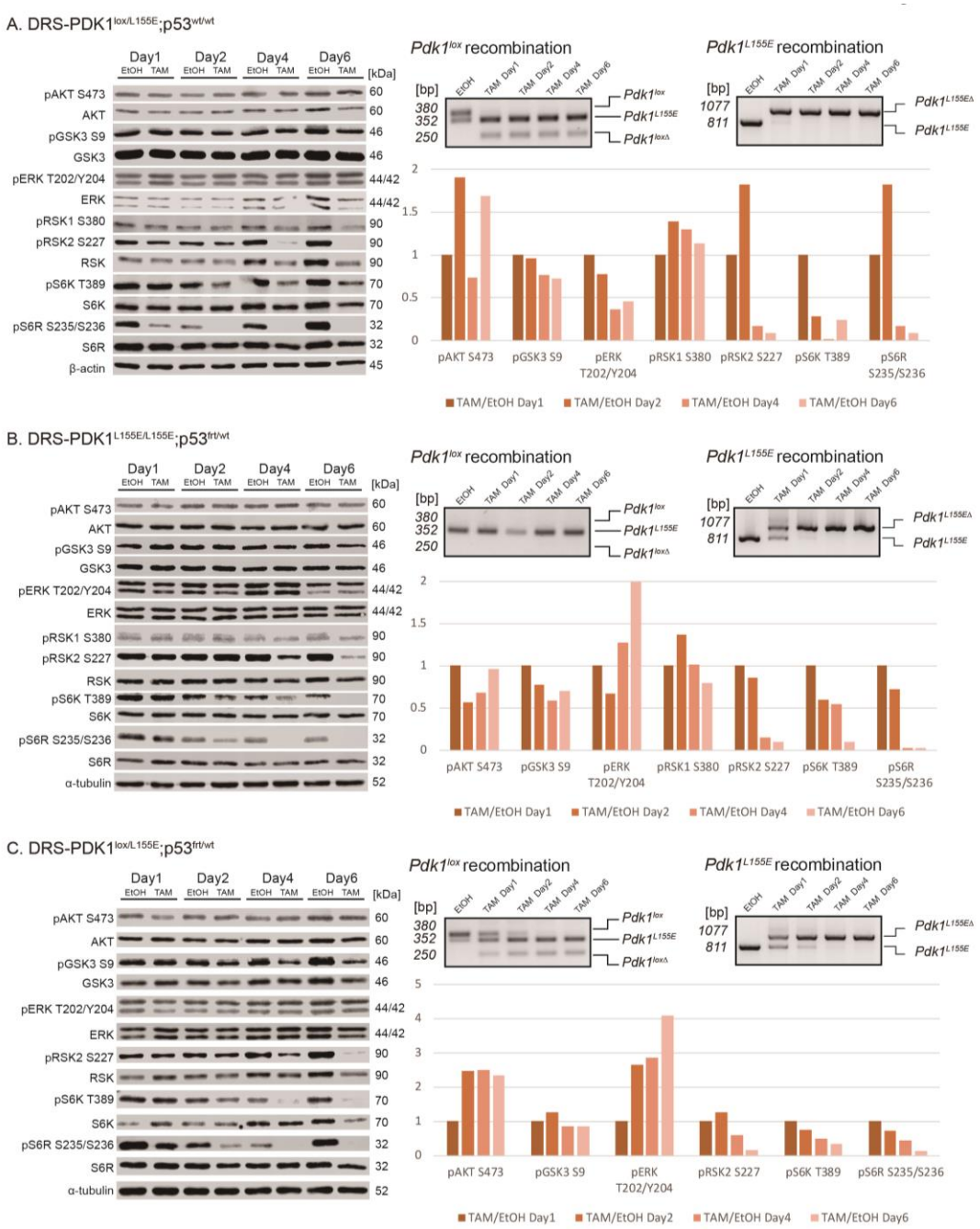

Figure 16. Logitudinal analysis of PIF-pocket domain of PDK1 downstream signaling in *p53* wild-type and mutant PDAC cells

(A) Immunoblot analysis of tamoxifen (TAM) treated DRS-PDK1$^{lox/L155E}$;p53$^{wt/wt}$ cell lines compared to ethanol (EtOH) treated controls. α-tubulin or β-actin served as loading controls. Each column containing 6 days of samples represented one cell line (left). *Pdk1^{lox}* recombination test and *Pdk1^{L155E}* recombination test with TAM and EtOH treatment (top right). kDa, 1,000 Daltons; bp, base pair; △, recombined allele. Each day's phosphorylation rate was calculated by dividing the value of TAM treated sample by the value of EtOH treated sample, and the rate on the first day was set as control. The fold change of protein phosphorylation rate compared to that of TAM and EtOH treated sample is shown in the column graph on the right panel (bottom right). The left y-axis demonstrates the fold change relative to control.

(B) Immunoblot analysis of related signaling in TAM treated DRS-PDK1$^{L155E/L155E}$;p53$^{frt/wt}$ cell lines compared to EtOH treated controls. *Pdk1^{lox}* recombination PCR and *Pdk1^{L155E}* recombination PCR test. kDa, 1,000 Daltons; bp, base pair; Δ, recombined allele.

(C) Immunoblot analysis of related signaling in TAM treated DRS-PDK1$^{lox/L155E}$;p53$^{frt/wt}$ cell lines compared to EtOH treated controls. *Pdk1^{lox}* recombination PCR and *Pdk1^{L155E}* recombination PCR test. kDa, 1,000 Daltons; bp, base pair; Δ, recombined allele.

To longitudinal analysis the PH-domain related pathway, western blot was performed using proteins extracted from both *p53* wild-type and *p53* deleted DRS-PDK1^{K465E} cells. The *Pdk1^{lox}* recombination test was performed to validate the corresponding DNA level changes as well. We observed that the DRS-PDK1^{K465E};p53^{wt} cells, with *Pdk1^{K465E}* mutation and wild-type *p53*, *Pdk1^{lox}* deletion completed around Day 1, while DRS-PDK1^{K465E};p53^{frt} cells, with *Pdk1^{K465E}* mutation and *p53* deletion, the *Pdk1^{lox}* deletion completed during day 2 to day 4 (Figure 17).

For DRS-PDK1^{K465E};p53^{wt} cells, with *Pdk1^{K465E}* mutation and wild-type *p53*, AKT S473, GSK3, ERK T202/Y204, RSK1 S380, RSK2 S227, S6K1 T389 and S6R S235/S236 phosphorylation was unchanged (Figure 17A). For DRS-PDK1^{K465E};p53^{frt} cells, with *Pdk1^{K465E}* mutation and *p53* deletion, no obvious and consistent changes was found neither (Figure 17B, C).

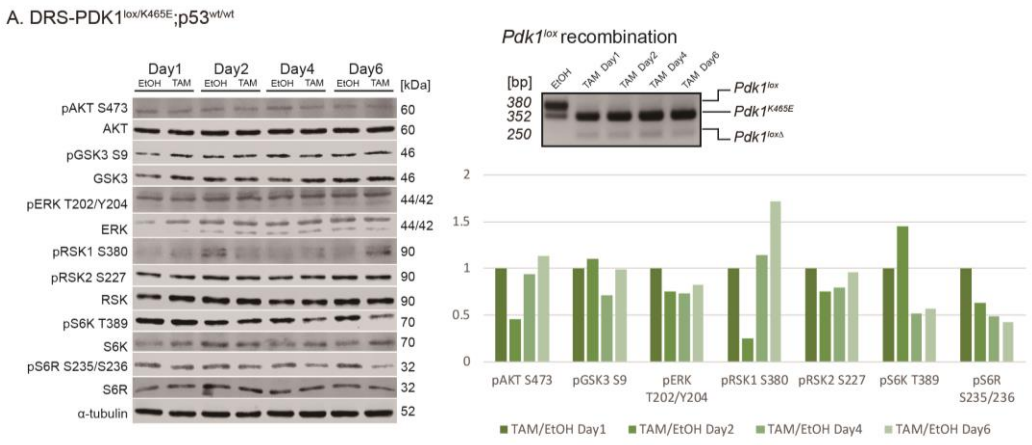

(Figure 17 continued on next page)

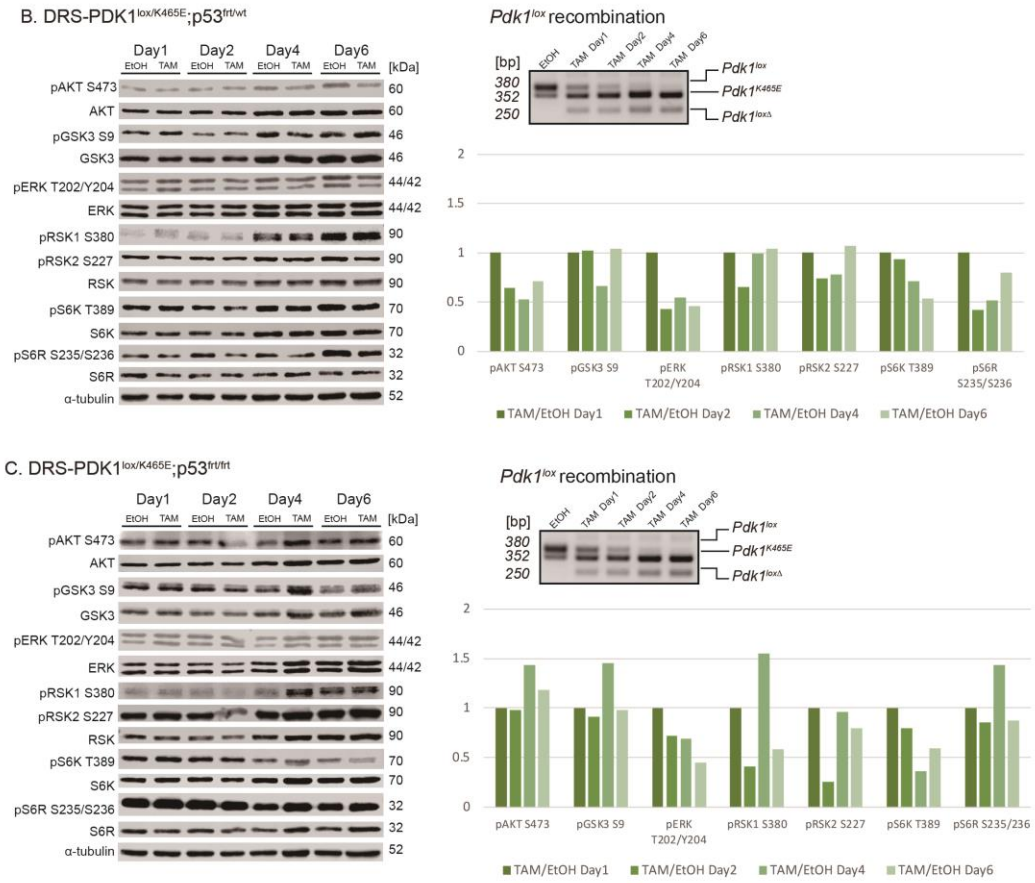

Figure 17. Longitudinal analysis of PH-domain of PDK1 downstream signaling in *p53* wild-type and deficient PDAC cells

(A) Immunoblot analysis of related signaling in tamoxifen (TAM) treated DRS-PDK1$^{lox/K465E}$;p53$^{wt/wt}$ cell lines compared to ethanol (EtOH) treated controls. α-tubulin or β-actin served as loading controls. Each column containing 6 days of samples represented one cell line (left). *Pdk1^{lox}* recombination test with TAM and EtOH treatment (top right). kDa, 1,000 Daltons; bp, base pair; Δ, recombined allele. Each day's phosphorylation rate was calculated by dividing the value of TAM treated sample by the value of EtOH treated sample, and the rate on the first day was set as control. The fold change of protein phosphorylation rate compared to that of TAM and EtOH treated sample is shown in the column graph on the right panel (bottom right). The left y-axis demonstrates the fold change relative to control.

(B) Immunoblot analysis of related signaling in TAM treated DRS-PDK1$^{lox/K465E}$;p53$^{frt/wt}$ cell lines compared to EtOH treated controls and *Pdk1^{lox}* recombination PCR test. kDa, 1,000 Daltons; bp, base pair; Δ, recombined allele.

(C) Immunoblot analysis of related signaling in TAM treated DRS-PDK1$^{lox/K465E}$;p53$^{frt/frt}$ cell lines compared to EtOH treated controls and *Pdk1^{lox}* recombination PCR test. kDa, 1,000 Daltons; bp, base pair; Δ, recombined allele.

5. Discussion

5.1 Roles of *Pdk1^{L155E} and Pdk1^{K465E}* mutation in KRAS driven pancreatic tumor initiation and development.

KRAS mutations were found in more than 90% of PDAC (Morris et al., 2010). Different paths to inhibit RAS signaling are currently under investigation in the hope of finding a successful treatment (Gillson et al., 2020). However, all clinical attempts to directly interfere with KRAS oncoprotein activity have failed, and KRAS is still widely considered undruggable (Berndt et al., 2011). Other strategies currently being pursued include indirect approaches, such as targeting proteins that facilitate RAS membrane association or downstream effector signaling. Former researchers in our lab proved that PI3K/PDK1 signaling was a key effector of oncogenic *Kras* in the pancreas, mediating cell plasticity, ADM, and PDAC formation (Eser et al., 2013). Thus, our current goal is to dissect the PDK1 downstream function in the RAS related pathways. To do this in established tumors, our research group has developed a novel inducible dual-recombinase system (DRS) by combining Flp/frt and Cre/loxP. This model enables the genetic validation of therapeutic targets in autochthonous tumors *in vivo,* and in this project, in which the primary cell lines were isolated, it provided a stable cell line model to dissect gene function and its downstream signaling *in vitro*. *Pdk1^{L155E} and Pdk1^{K465E}* mutations were used in this thesis, as these mutations alter 2 main domains, which control the major functions of PDK1 and its two main downstream signaling pathways (Bayascas et al., 2008; Mora et al., 2004).

5.1.1 Role of the PIF-pocket domain of PDK1 for KRAS-driven tumorigenesis

The constitutive homozygous mutation of *Pdk1^{L155E}* in mice is lethal for the embryo, thus a ”minigen” method is used to enable tissue specific expression of this mutant that abolishes the PIF-pocket domain of PDK1 (Bayascas et al., 2006). The minigen cassette, containing a wild-type *Pdk1* allele, was knocked into the endogenous *Pdk1*

locus. Thereby, the PIF-pocket domain of PDK1 is inactivated, resulting in a lack of RSK2, S6K, S6R, SGK3, and PKC activation/phosphorylation (Biondi et al., 2000; Biondi et al., 2001; Biondi et al., 2002). The activity of pS6K is controlled by multiple phosphorylation events, of which the phosphorylation at T229 by PDK1 and T389 by mTOR are most critical for its function (Alessi et al., 1997; Pullen et al., 1998). The activation of S6K and RSK2 subsequently phosphorylates the S6R protein (Al-Ali et al., 2017; Peterson and Schreiber, 1998; Roux et al., 2007). Thus, decreased S6R S235/S236 phosphorylation might be a consequence of S6K1 T389 (PI3K/PDK1/AKT/mTORC1 pathway) or S6K1 T229 and RSK2 S227 (PIF-pocket dependent pathway) downregulation.

Based on the KC mouse model, KCPDK1^{L155E} mice were generated to study tumorigenesis. After Cre was expressed, the minigen and/or *Pdk1^{lox}* were recombined in the pancreas. Thereafter, the *Pdk1^{L155E}* mutation is expressed. In our project, KCPDK1^{L155E} mice died much earlier than normal KC mice. The lifetime of KCPDK1$^{lox/L155E}$ mice was 128 days, and for KCPDK1$^{L155E/L155E}$ mice, 138 days. The reasons for termination of the experiment was an impaired heath status of the animals, which could be due to pancreatic atrophy in figure 8B. None of them died of tumor indicating that PDAC development is impaired in these mutants.

Several studies have revealed that the inactivation of the PIF-pocket dependent pathway in the brain or liver leads to mental or metabolism diseases. There is increasing evidence that SGK1 is involved in the development and complications of diabetes and neurological disorders (Lang et al., 2009; Lang et al., 2010). Loss-of-function mutations in the gene encoding RSK2 are responsible for the Coffin–Lowry syndrome which causes severe mental problems (Hanauer and Young, 2002). S6Ks play important roles in cell growth, proliferation, and cell differentiation by regulating ribosome biogenesis, protein synthesis, cell cycle progression, and metabolism (Shin et al., 2011). In my thesis, the PIF-pocket dependent pathway is blocked specifically in the pancreas. Therefore, effects on the brain and liver can be excluded.

Timepoint KCPDK1^{L155E} mice and KCPDK1^{K465E} mice showed similar pancreas weight

and body weight changes to wild-type animals. Although, the KCPDK1^{L155E} mice did not show a statistically significant reduction in ADM lesions as KCPDK1^{K465E} mice do, PanIN lesions development was significantly inhibited in KCPDK1^{L155E} mice at 6 months and 1 year old.

To investigate the molecular mechanisms of the phenotype of KCPDK1^{L155E} mice, pancreatic tissues from KC, KCPDK1$^{lox/K465E}$, KCPDK1$^{L155E/+}$, and KCPDK1$^{lox/L155E}$ were collected for immunohistochemistry analysis. We discovered that pRSK2 S227 staining of KCPDK1$^{lox/L155E}$ pancreata was negative, but pAKT T308 and pSGK3 T320 was positive in all groups of IHC staining *in vivo*.

Our data suggest that the PIF-pocket domain of PDK1 does not block ADM but can inhibit the PanIN formation. On a molecular level, the PIF-pocket domain dependent RSK2 pathway can not be activated in PDK1^{L155E} mutant mice *in vivo*.

5.1.2 The PH-domain of PDK1 is essential for KRAS-driven PDAC tumorigenesis

The *Pdk1*^{K465E} mutation was used by researchers previously to abrogate phosphoinositide binding in the PH-domain so that the PI3K/PDK1/AKT pathway would be inhibited without affecting the function of the PIF-pocket domain (Bayascas et al., 2008). Since *Pdk1* deletion was found essential for ADM and PanIN formation and Wu et al. suggests that AKT activity is critical for ADM *in vitro*. (Wu et al., 2014), we hypothesized that the PH-domain of PDK1 most likely adjusted the tumorigenesis via the PI3K/PDK1/AKT pathway.

In our project, the *Pdk1*^{K465E} mutant allele was crossed in KC mouse model to study tumorigenesis. As described in the survival curve, the survival time of KCPDK1^{K465E} mice was prolonged significantly. The lifetime of KCPDK1$^{lox/K465E}$ mice was 704.5 days, significantly longer than KC mice (455 days). By the time of human endpoint, the tumor incidence rate for KCPDK1$^{lox/K465E}$ mice was 40%, and for KCPDK1$^{K465E/K465E}$ mice, 10%. This result indicates the tumor incidence rate of KCPDK1^{K465E} mice was decreased compared with KC mice, which is 88% as described in Figure 5C. After

summarizing the survival curve and tumor incidence rate, we concluded that the PH-domain dependent pathway is important for PDAC tumor initiation or development.

However, the lifetime of KCPDK1$^{K465E/K465E}$ mice is 516 days, which is not significantly longer than KC mice. The reason why KCPDK1$^{K465E/K465E}$ mice had shorter lifespans than KCPDK1$^{lox/K465E}$ mice or wild-type mice is that *Pdk1*^{K465E} mutation regulated pathways affect other important physiological processes of other cells, such as neurology cells and endocrine cells, and cause related diseases (Dummler et al., 2006). That was also proved by our data in Figure 5C.

Timepoint mice were also analyzed to assess tumorigenesis. In the first 6 months, the percentage of pancreas weight/body weight was similar to wt mice but significantly reduced relative to KC mice. Although ADM and PanIN lesions still existed in pancreas tissue in the first 6 months, as confirmed by HE and AB staining results, the number of ADM and PanIN lesions were significantly less in KCPDK1^{K465E} mice.

ADM has long been suggested to be an initiating event in human and murine PDAC formation (Aichler et al., 2012; Caldwell et al., 2012; Morris et al., 2010; Reichert and Rustgi, 2011). To study tumorigenesis *in vitro*, we included 3-month-old KC mice and wt mice (control) in an ADM assay and determined ADM. Consistently, PH-domain of PDK1 is essential for ADM of acinar cells isolated from KCPDK1^{K465E} mice.

Previous studies have reported that AKT T308 phosphorylation in PI3K/PDK1/AKT pathway is abrogated by *Pdk1*^{K465E} mutation (Bayascas et al., 2008). However, AKT T308 phosphorylation tested by IHC showed no difference. Altogether, these results suggest that there might be no obvious regulation of the PI3K/PDK1/AKT pathway by the PH-domain of PDK1 *in vivo*. The reason may be other crosstalk pathways that could fully recover the inactivation of this pathway regulated by *Pdk1*^{K465E} mutation.

Taken together, inactivation of the PH-domain significantly inhibits ADM and PanIN formation. Although this study did not confirm the pathway which inhibited ADM and PanIN formation in KCPDK1^{K465E} mice, it did substantiate the importance of the PH-domain of PDK1. Future research should, therefore, concentrate on the

investigation of the mechanisms.

5.2 Mouse models to test PDAC tumor maintenance

In this study, a novel dual-recombinase system combining the established Cre/loxP with the Flp/frt recombination system was used to manipulate the genetically engineered mouse models for the study of tumor maintenance (Schönhuber et al., 2014). In our project, we crossed the *Pdk1^{lox}, Pdk1^{L155E},* and *Pdk1^{K465E}* alleles into the DRS mice. After we generated enough mice and aged the mice until they processed to tumor, we euthanized the mice and isolated primary murine cell lines from PDAC. With these primary cell lines, we could study the tumor cells *in vitro*.

As we mentioned both KCPDK1^{L155E} and KCPDK1^{K465E} mutations block the ADM and PanIN formation partially. Next, we tested if tumor maintenance was also influenced by the PDK1 downstream signaling pathway.

5.2.1 The PIF-pocket domain of PDK1 is fundamental for KRAS-driven PDAC cell proliferation and maintenance, and independent of the *p53* status

Many researchers have proven that the PIF-pocket domain of PDK1 is crucial in many aspects. Biondi et al. (2001) reported that the PIF-binding pocket in PDK1 is essential for the activation of S6K and SGK, but not PKB. Haga (2009) demonstrated that in hepatocytes, the PDK1/S6K pathway mediates protein synthesis and cell proliferation (Haga et al., 2009).

PDAC tumor cell proliferation and colony formation were tested by MTT and clonogenic assay. We found that *Pdk1^{L155E}* mutation blocked PDAC cell proliferation and colony formation, apart from *p53* deletion.

Afterward, we longitudinal analyzed the key proteins of PDK1 downstream signaling and proved that the RSK2 S227, S6R S235/S236, and S6K1 T389 phosphorylation was inhibited in *Pdk1^{L155E}* mutated cells. Thereby, PIF-pocket domain is essential for RSK2 and S6 activation.

S6K T389 was strongly impaired in *Pdk1^{L155E}* mutated cells as well. As Pullen (1998)

reported, S6K T389 was regulated by the PI3K/AKT/mTORC1 pathway (Alessi et al., 1997; Pullen et al., 1998). But considering AKT S473 was not changed in our experiment, we have to suppose that S6K T389 phosphorylation was regulated by the PIF-pocket as well. Importantly, these effects were not influenced by the *p53* status.

However, ERK T202/Y204 phosphorylation was overactivated in *p53* deleted cell lines. The relationship between ERK and the PDK1 pathway is not clear after *p53* deletion. Some researchers contend that ERK mediates cell behavior independent of *p53* (Bacus et al., 2001; Tang et al., 2002). In contrast, others found *p53* was an upstream regulator of ERK activation (Singh et al., 2007), or that *p53* initiated a feedback loop to regulate ERK activation (Sauer et al., 2010) .

In conclusion, independent of *p53* inactivation, the proliferation and colony formation of PDAC cells were inhibited by PIF-pocket deletion, and PIF-pocket domain of PDK1 is crucial for RSK2, S6 activation.

5.2.2 The PH-domain of PDK1 is indispensable for the maintenance of KRAS-driven *p53* wild-type PDAC

There are many downstream pathways that the PH-domain mutant *Pdk1*^{K465E} allele may influence. Zurashvili et al. reported that BDNF-mediated PKB activation reduced the activation of S6K, and PKB/mTORC1/BRSK pathway inhibition was affected by *Pdk1*^{K465E} mutation (Zurashvili et al., 2013). The authors found that the PH-domain was essential for neuronal differentiation, but not survival. In contrast, Najafov et al. reported that AKT was efficiently activated by PIF-pocket dependent PtdIns (3,4,5) P3 mechanisms itself (Najafov et al., 2012).

We tested PDAC tumor cell proliferation and colony formation by MTT and clonogenic assay. The results showed that the PH-domain was essential for tumor cell proliferation and colony formation of *p53* wild-type tumors. To assess the effect of the *p53* status, we tested the *p53* deleted DRS-PDK1^{K465E};p53^{frt} cell lines as well. Notably, the reduction of proliferation and colony formation was completely blocked in the *p53* deleted DRS-PDK1^{K465E};p53^{frt} cell line.

Levine reported that *p53* was found to suppress the IGF-1/AKT and mTORC1 pathways (Levine et al., 2006). Sabbatini and McCormick provided the first direct and unambiguous link between *p53* mediated apoptosis and the PI3K/PDK1/AKT signaling pathway (Sabbatini and McCormick, 1999).

In our experiments, the phosphorylation status of key proteins downstream of PDK1 was tested on day 1, day 2, day 4, and day 6 after inactivation of the PH-domain to dissect the precise changes induced by the *Pdk1*^{K465E} mutation. We discovered that no significant changes were observed in TAM treated DRS-PDK1^{K465E};p53^{wt} and DRS-PDK1^{K465E};p53^{frt} cell lines compared with EtOH treated lines.

In conclusion, the PH-domain of PDK1 is indispensable for the maintenance of KRAS-driven *p53* wild-type PDAC. However, *p53* deletion is able to bypass the growth arrest in the PDK1^{K465E} model. And the key proteins downstream of PDK1, such as AKT S473, GSK3 S9, ERK T202/Y204, RSK1 S380, RSK2 S227, S6K1 T389, and S6R S235/S236 was not adjusted.

6. Summary

In this thesis, we analyzed the function of PIF-pocket and PH-domain mediated signaling in pancreatic cancer initiation and maintenance.

For tumor initiation, signaling via PIF-pocket domain of PDK1 is important for PanIN formation and PH-domain of PDK1 is essential for ADM and PanIN formation. Both two domains of PDK1 play an important role in tumorigenesis.

For tumor maintenance, we found that the PIF-pocket domain of PDK1 is fundamental for KRAS-driven PDAC cell proliferation and maintenance, and this is independent of the *p53* status. In contrast, the PH-domain of PDK1 is indispensable for the maintenance of KRAS-driven *p53* wild-type PDAC as well, however, p53 deletion is able to bypass the growth arrest.

The signaling pathways mediated by PIF-pocket domain of PDK1 is via RSK2 S227, S6K1 T389, and S6R S235/S236 phosphorylation, however, the PH-domain mediated pathway is not clear and needs further investigation.

7. Reference

Aichler, M., Seiler, C., Tost, M., Siveke, J., Mazur, P. K., Da Silva-Buttkus, P., Bartsch, D. K., Langer, P., Chiblak, S., Durr, A*., et al.* (2012). Origin of pancreatic ductal adenocarcinoma from atypical flat lesions: a comparative study in transgenic mice and human tissues. J Pathol *226*, 723-734.

Al-Ali, H., Ding, Y., Slepak, T., and Wu, W. (2017). The mTOR Substrate S6 Kinase 1 (S6K1) Is a Negative Regulator of Axon Regeneration and a Potential Drug Target for Central Nervous System Injury. *37*, 7079-7095.

Alessi, D. R., James, S. R., Downes, C. P., Holmes, A. B., Gaffney, P. R., Reese, C. B., and Cohen, P. (1997). Characterization of a 3-phosphoinositide-dependent protein kinase which phosphorylates and activates protein kinase Balpha. Curr Biol *7*, 261-269.

Ariston Gabriel, A. N., Jiao, Q., Yvette, U., Yang, X., Al-Ameri, S. A., Du, L., Wang, Y. S., and Wang, C. (2020). Differences between KC and KPC pancreatic ductal adenocarcinoma mice models, in terms of their modeling biology and their clinical relevance. Pancreatology *20*, 79-88.

Bacus, S. S., Gudkov, A. V., Lowe, M., Lyass, L., Yung, Y., Komarov, A. P., Keyomarsi, K., Yarden, Y., and Seger, R. (2001). Taxol-induced apoptosis depends on MAP kinase pathways (ERK and p38) and is independent of p53. Oncogene *20*, 147-155.

Baker, S. J., Preisinger, A. C., Jessup, J. M., Paraskeva, C., Markowitz, S., Willson, J. K., Hamilton, S., and Vogelstein, B. (1990). p53 gene mutations occur in combination with 17p allelic deletions as late events in colorectal tumorigenesis. Cancer Res *50*, 7717-7722.

Bardeesy, N., Aguirre, A. J., Chu, G. C., Cheng, K. H., Lopez, L. V., Hezel, A. F., Feng, B., Brennan, C., Weissleder, R., Mahmood, U*., et al.* (2006). Both p16(Ink4a) and the p19(Arf)-p53 pathway constrain progression of pancreatic adenocarcinoma in the mouse. Proc Natl Acad Sci U S A *103*, 5947-5952.

Basturk, O., Hong, S. M., Wood, L. D., Adsay, N. V., Albores-Saavedra, J., Biankin, A. V., Brosens, L. A., Fukushima, N., Goggins, M., Hruban, R. H*., et al.* (2015). A Revised Classification System and Recommendations From the Baltimore Consensus Meeting for Neoplastic Precursor Lesions in the Pancreas. Am J Surg Pathol *39*, 1730-1741.

Bayascas, J. R., Sakamoto, K., Armit, L., Arthur, J. S., and Alessi, D. R. (2006). Evaluation of approaches to generation of tissue-specific knock-in mice. J Biol Chem *281*, 28772-28781.

Bayascas, J. R., Wullschleger, S., Sakamoto, K., Garcia-Martinez, J. M., Clacher, C., Komander, D., van Aalten, D. M., Boini, K. M., Lang, F., Lipina, C*., et al.* (2008). Mutation of the PDK1 PH-domain inhibits protein kinase B/Akt, leading to small size and insulin resistance. Mol Cell Biol *28*, 3258-3272.

Berndt, N., Hamilton, A. D., and Sebti, S. M. (2011). Targeting protein prenylation for cancer therapy. Nat Rev Cancer *11*, 775-791.

Biankin, A. V., Waddell, N., Kassahn, K. S., Gingras, M. C., Muthuswamy, L. B., Johns, A. L., Miller, D. K., Wilson, P. J., Patch, A. M., Wu, J*., et al.* (2012). Pancreatic cancer genomes reveal aberrations in axon guidance pathway genes. Nature *491*, 399-405.

Biondi, R. M., Cheung, P. C., Casamayor, A., Deak, M., Currie, R. A., and Alessi, D. R. (2000). Identification of a pocket in the PDK1 kinase domain that interacts with PIF and the C-terminal residues of PKA. Embo j *19*, 979-988.

Biondi, R. M., Kieloch, A., Currie, R. A., Deak, M., and Alessi, D. R. (2001). The PIF-binding pocket in PDK1 is essential for activation of S6K and SGK, but not PKB. Embo j *20*, 4380-4390.

Biondi, R. M., Komander, D., Thomas, C. C., Lizcano, J. M., Deak, M., Alessi, D. R., and van Aalten, D. M. (2002). High resolution crystal structure of the human PDK1 catalytic domain defines the regulatory phosphopeptide docking site. Embo j *21*, 4219-4228.

Bosetti, C., Rosato, V., Li, D., Silverman, D., Petersen, G. M., Bracci, P. M., Neale, R. E., Muscat, J., Anderson, K., Gallinger, S.*, et al.* (2014). Diabetes, antidiabetic medications, and pancreatic cancer risk: an analysis from the International Pancreatic Cancer Case-Control Consortium. Ann Oncol *25*, 2065-2072.

Bourne, H. R., Sanders, D. A., and McCormick, F. (1990). The GTPase superfamily: a conserved switch for diverse cell functions. Nature *348*, 125-132.

Bradford, M. M. (1976). A rapid and sensitive method for the quantitation of microgram quantities of protein utilizing the principle of protein-dye binding. Anal Biochem *72*, 248-254.

Bray, F., Ferlay, J., Soerjomataram, I., Siegel, R. L., Torre, L. A., and Jemal, A. (2018). Global cancer statistics 2018: GLOBOCAN estimates of incidence and mortality worldwide for 36 cancers in 185 countries. CA Cancer J Clin *68*, 394-424.

Bryant, K. L., and Stalnecker, C. A. (2019). Combination of ERK and autophagy inhibition as a treatment approach for pancreatic cancer. *25*, 628-640.

Caldwell, M. E., DeNicola, G. M., Martins, C. P., Jacobetz, M. A., Maitra, A., Hruban, R. H., and Tuveson, D. A. (2012). Cellular features of senescence during the evolution of human and murine ductal pancreatic cancer. Oncogene *31*, 1599-1608.

Cantley, L. C. (2002). The phosphoinositide 3-kinase pathway. Science *296*, 1655-1657.

Castellano, E., and Downward, J. (2011). RAS Interaction with PI3K: More Than Just Another Effector Pathway. Genes Cancer *2*, 261-274.

Christenson, E. S., Jaffee, E., and Azad, N. S. (2020). Current and emerging therapies for patients with advanced pancreatic ductal adenocarcinoma: a bright future. The Lancet Oncology *21*, e135-e145.

Chuvin, N., Vincent, D. F., Pommier, R. M., Alcaraz, L. B., Gout, J., Caligaris, C., Yacoub, K., Cardot, V., Roger, E., Kaniewski, B.*, et al.* (2017). Acinar-to-Ductal Metaplasia Induced by Transforming Growth Factor Beta Facilitates KRAS(G12D)-driven Pancreatic Tumorigenesis. Cellular and molecular gastroenterology and hepatology *4*, 263-282.

Corcoran, R. B., Contino, G., Deshpande, V., Tzatsos, A., Conrad, C., Benes, C. H., Levy, D. E., Settleman, J., Engelman, J. A., and Bardeesy, N. (2011). STAT3 plays a critical role in KRAS-induced pancreatic tumorigenesis. Cancer Res *71*, 5020-5029.

Dummler, B., Tschopp, O., Hynx, D., Yang, Z. Z., Dirnhofer, S., and Hemmings, B. A. (2006). Life with a single isoform of Akt: mice lacking Akt2 and Akt3 are viable but display impaired glucose homeostasis and growth deficiencies. Mol Cell Biol *26*, 8042-8051.

Eser, S., Reiff, N., Messer, M., Seidler, B., Gottschalk, K., Dobler, M., Hieber, M., Arbeiter, A., Klein, S., Kong, B.*, et al.* (2013). Selective requirement of PI3K/PDK1 signaling for Kras oncogene-driven pancreatic cell plasticity and cancer. Cancer Cell *23*, 406-420.

Eser, S., Schnieke, A., Schneider, G., and Saur, D. (2014). Oncogenic KRAS signaling in pancreatic cancer. Br J Cancer *111*, 817-822.

Esposito, I., Konukiewitz, B., Schlitter, A. M., and Kloppel, G. (2012). [New insights into the origin of pancreatic cancer. Role of atypical flat lesions in pancreatic carcinogenesis]. Pathologe *33 Suppl 2*, 189-193.

Field, J., Broek, D., Kataoka, T., and Wigler, M. (1987). Guanine nucleotide activation of, and competition between, RAS proteins from Saccharomyces cerevisiae. Mol Cell Biol *7*, 2128-2133.

Gannon, M., Herrera, P. L., and Wright, C. V. (2000). Mosaic Cre-mediated recombination in pancreas using the pdx-1 enhancer/promoter. Genesis *26*, 143-144.

Gillson, J., Ramaswamy, Y., Singh, G., Gorfe, A. A., Pavlakis, N., Samra, J., Mittal, A., and Sahni, S. (2020). Small Molecule KRAS Inhibitors: The Future for Targeted Pancreatic Cancer Therapy? *12*.

Guerra, C., and Barbacid, M. (2013). Genetically engineered mouse models of pancreatic adenocarcinoma. Molecular oncology *7*, 232-247.

Haga, S., Ozaki, M., Inoue, H., Okamoto, Y., Ogawa, W., Takeda, K., Akira, S., and Todo, S. (2009). The survival pathways phosphatidylinositol-3 kinase (PI3-K)/phosphoinositide-dependent protein kinase 1 (PDK1)/Akt modulate liver regeneration through hepatocyte size rather than proliferation. Hepatology (Baltimore, Md) *49*, 204-214.

Hanahan, D., and Coussens, L. M. (2012). Accessories to the crime: functions of cells recruited to the tumor microenvironment. Cancer Cell *21*, 309-322.

Hanauer, A., and Young, I. D. (2002). Coffin-Lowry syndrome: clinical and molecular features. Journal of medical genetics *39*, 705-713.

Hassid, B. G., Lucas, A. L., Salomao, M., Weng, C., Liu, F., Khanna, L. G., Kumar, S., Hwang, C., Chabot, J. A., and Frucht, H. (2014). Absence of pancreatic intraepithelial neoplasia predicts poor survival after resection of pancreatic cancer. Pancreas *43*, 1073-1077.

Hingorani, S. R., Petricoin, E. F., Maitra, A., Rajapakse, V., King, C., Jacobetz, M. A., Ross, S., Conrads, T. P., Veenstra, T. D., Hitt, B. A.*, et al.* (2003). Preinvasive and invasive ductal pancreatic cancer and its early detection in the mouse. Cancer Cell *4*, 437-450.

Hirsch, J., Dieguez, G., and Cockrum, P. (2020). Comparing total cost of care for Medicare FFS patients with pancreatic cancer by chemotherapy regimen. Journal of Clinical Oncology *38*, e19394-e19394.

Hruban, R. H., Adsay, N. V., Albores-Saavedra, J., Anver, M. R., Biankin, A. V., Boivin, G. P., Furth, E. E., Furukawa, T., Klein, A., Klimstra, D. S.*, et al.* (2006). Pathology of genetically engineered mouse models of pancreatic exocrine cancer: consensus report and recommendations. Cancer Res *66*, 95-106.

Hruban, R. H., Canto, M. I., Goggins, M., Schulick, R., and Klein, A. P. (2010). Update on familial pancreatic cancer. Advances in surgery *44*, 293-311.

Hruban, R. H., Goggins, M., Parsons, J., and Kern, S. E. (2000). Progression model for pancreatic cancer. Clin Cancer Res *6*, 2969-2972.

Hruban, R. H., Takaori, K., Klimstra, D. S., Adsay, N. V., Albores-Saavedra, J., Biankin, A. V., Biankin, S. A., Compton, C., Fukushima, N., Furukawa, T.*, et al.* (2004). An illustrated consensus on the classification of pancreatic intraepithelial neoplasia and intraductal papillary mucinous neoplasms. Am J Surg Pathol *28*, 977-987.

Iodice, S., Gandini, S., Maisonneuve, P., and Lowenfels, A. B. (2008). Tobacco and the risk of pancreatic cancer: a review and meta-analysis. Langenbeck's archives of surgery *393*, 535-545.

Jackson, E. L., Willis, N., Mercer, K., Bronson, R. T., Crowley, D., Montoya, R., Jacks, T., and Tuveson, D. A. (2001). Analysis of lung tumor initiation and progression using conditional expression of oncogenic K-ras. Genes Dev *15*, 3243-3248.

Jiang, H., and Hegde, S. (2016). Targeting focal adhesion kinase renders pancreatic cancers responsive to checkpoint immunotherapy. *22*, 851-860.

Jones, S., Zhang, X., Parsons, D. W., Lin, J. C., Leary, R. J., Angenendt, P., Mankoo, P., Carter, H., Kamiyama, H., Jimeno, A.*, et al.* (2008). Core signaling pathways in human pancreatic cancers revealed by global genomic analyses. Science *321*, 1801-1806.

Kanda, M., Matthaei, H., Wu, J., Hong, S. M., Yu, J., Borges, M., Hruban, R. H., Maitra, A., Kinzler, K., Vogelstein, B., and Goggins, M. (2012). Presence of somatic mutations in most early-stage pancreatic intraepithelial neoplasia. Gastroenterology *142*, 730-733 e739.

Kawaguchi, Y., Cooper, B., Gannon, M., Ray, M., MacDonald, R. J., and Wright, C. V. (2002). The role of the transcriptional regulator Ptf1a in converting intestinal to pancreatic progenitors. Nat Genet *32*, 128-134.

Kelber, J. A., Reno, T., Kaushal, S., Metildi, C., Wright, T., Stoletov, K., Weems, J. M., Park, F. D., Mose, E., Wang, Y.*, et al.* (2012). KRas induces a Src/PEAK1/ErbB2 kinase amplification loop that drives metastatic growth and therapy resistance in pancreatic cancer. Cancer Res *72*, 2554-2564.

Laemmli, U. K. (1970). Cleavage of structural proteins during the assembly of the head of bacteriophage T4. Nature *227*, 680-685.

Laklai, H., Miroshnikova, Y. A., Pickup, M. W., Collisson, E. A., Kim, G. E., Barrett, A. S., Hill, R. C., Lakins, J. N., Schlaepfer, D. D., Mouw, J. K.*, et al.* (2016). Genotype tunes pancreatic ductal adenocarcinoma tissue tension to induce matricellular fibrosis and tumor progression. *22*, 497-505.

Lang, F., Görlach, A., and Vallon, V. (2009). Targeting SGK1 in diabetes. Expert opinion on therapeutic targets *13*, 1303-1311.

Lang, F., Strutz-Seebohm, N., Seebohm, G., and Lang, U. E. (2010). Significance of SGK1 in the regulation of neuronal function. The Journal of physiology *588*, 3349-3354.

Lawlor, M. A., Mora, A., Ashby, P. R., Williams, M. R., Murray-Tait, V., Malone, L., Prescott, A. R., Lucocq, J. M., and Alessi, D. R. (2002). Essential role of PDK1 in regulating cell size and development in mice. Embo J *21*, 3728-3738.

Lee, C. L., Moding, E. J., Huang, X., Li, Y., Woodlief, L. Z., Rodrigues, R. C., Ma, Y., and Kirsch, D. G. (2012). Generation of primary tumors with Flp recombinase in FRT-flanked p53 mice. Dis Model Mech *5*, 397-402.

Levine, A. J., Feng, Z., Mak, T. W., You, H., and Jin, S. (2006). Coordination and communication between the p53 and IGF-1-AKT-TOR signal transduction pathways. Genes Dev *20*, 267-275.

Li, J., Li, Y., Cao, G., Guo, K., Zhang, L., and Ma, Q. (2013). Early manifestations of pancreatic cancer: the effect of cancer-nerve interaction. Medical hypotheses *81*, 180-182.

Liu, D., Zhang, Y., Dang, C., Ma, Q., Lee, W., and Chen, W. (2007). siRNA directed against TrkA sensitizes human pancreatic cancer cells to apoptosis induced by gemcitabine through an inactivation of PI3K/Akt-dependent pathway. Oncol Rep *18*, 673-677.

Mann, K. M., Ying, H., Juan, J., Jenkins, N. A., and Copeland, N. G. (2016). KRAS-related proteins in pancreatic cancer. Pharmacology & therapeutics *168*, 29-42.

Martincorena, I., and Campbell, P. J. (2015). Somatic mutation in cancer and normal cells. Science *349*, 1483-1489.

Massihnia, D., Avan, A., Funel, N., Maftouh, M., van Krieken, A., Granchi, C., Raktoe, R., Boggi, U., Aicher, B., Minutolo, F.*, et al.* (2017). Phospho-Akt overexpression is prognostic and can be used to tailor the synergistic interaction of Akt inhibitors with gemcitabine in pancreatic cancer. Journal of hematology & oncology *10*, 9.

Matthaei, H., Schulick, R. D., Hruban, R. H., and Maitra, A. (2011). Cystic precursors to invasive pancreatic cancer. Nature reviews Gastroenterology & hepatology *8*, 141-150.

Meloche, S., and Pouysségur, J. (2007). The ERK1/2 mitogen-activated protein kinase pathway as a master regulator of the G1- to S-phase transition. Oncogene *26*, 3227-3239.

Moodie, S. A., Willumsen, B. M., Weber, M. J., and Wolfman, A. (1993). Complexes of Ras.GTP with Raf-1 and mitogen-activated protein kinase kinase. Science *260*, 1658-1661.

Mora, A., Komander, D., van Aalten, D. M., and Alessi, D. R. (2004). PDK1, the master regulator of AGC kinase signal transduction. Seminars in cell & developmental biology *15*, 161-170.

Morris, J. P. t., Wang, S. C., and Hebrok, M. (2010). KRAS, Hedgehog, Wnt and the twisted developmental biology of pancreatic ductal adenocarcinoma. Nat Rev Cancer *10*, 683-695.

Mullis, K., Faloona, F., Scharf, S., Saiki, R., Horn, G., and Erlich, H. (1986). Specific enzymatic amplification of DNA in vitro: the polymerase chain reaction. Cold Spring Harb Symp Quant Biol *51 Pt 1*, 263-273.

Muzumdar, M. D., Tasic, B., Miyamichi, K., Li, L., and Luo, L. (2007). A global double-fluorescent Cre reporter mouse. Genesis *45*, 593-605.

Najafov, A., Shpiro, N., and Alessi, D. R. (2012). Akt is efficiently activated by PIF-pocket- and PtdIns(3,4,5)P3-dependent mechanisms leading to resistance to PDK1 inhibitors. Biochem J *448*, 285-295.

Nakhai, H., Sel, S., Favor, J., Mendoza-Torres, L., Paulsen, F., Duncker, G. I., and Schmid, R. M. (2007). Ptf1a is essential for the differentiation of GABAergic and glycinergic amacrine cells and horizontal cells in the mouse retina. Development *134*, 1151-1160.

Neuzillet, C., Tijeras-Raballand, A., Ragulan, C., and Cros, J. (2019). Inter- and intra-tumoural heterogeneity in cancer-associated fibroblasts of human pancreatic ductal adenocarcinoma. *248*, 51-65.

Offield, M. F., Jetton, T. L., Labosky, P. A., Ray, M., Stein, R. W., Magnuson, M. A., Hogan, B. L., and Wright, C. V. (1996). PDX-1 is required for pancreatic outgrowth and differentiation of the rostral duodenum. Development *122*, 983-995.

Peterson, R. T., and Schreiber, S. L. (1998). Translation control: connecting mitogens and the ribosome. Curr Biol *8*, R248-250.

Pullen, N., Dennis, P. B., Andjelkovic, M., Dufner, A., Kozma, S. C., Hemmings, B. A., and Thomas, G. (1998). Phosphorylation and activation of p70s6k by PDK1. Science *279*, 707-710.

Pylayeva-Gupta, Y., Grabocka, E., and Bar-Sagi, D. (2011). RAS oncogenes: weaving a tumorigenic web. Nat Rev Cancer *11*, 761-774.

Raimondi, S., Lowenfels, A. B., Morselli-Labate, A. M., Maisonneuve, P., and Pezzilli, R. (2010). Pancreatic cancer in chronic pancreatitis; aetiology, incidence, and early detection. Best practice & research Clinical gastroenterology *24*, 349-358.

Rangarajan, A., and Weinberg, R. A. (2003). Opinion: Comparative biology of mouse versus human cells: modelling human cancer in mice. Nat Rev Cancer *3*, 952-959.

Reichert, M., and Rustgi, A. K. (2011). Pancreatic ductal cells in development, regeneration, and neoplasia. J Clin Invest *121*, 4572-4578.

Roux, P. P., Shahbazian, D., Vu, H., Holz, M. K., Cohen, M. S., Taunton, J., Sonenberg, N., and Blenis, J. (2007). RAS/ERK signaling promotes site-specific ribosomal protein S6 phosphorylation via RSK and stimulates cap-dependent translation. J Biol Chem *282*, 14056-14064.

Sabbatini, P., and McCormick, F. (1999). Phosphoinositide 3-OH kinase (PI3K) and PKB/Akt delay the onset of p53-mediated, transcriptionally dependent apoptosis. J Biol Chem *274*, 24263-24269.

Sauer, B. (1987). Functional expression of the cre-lox site-specific recombination system in the yeast Saccharomyces cerevisiae. Mol Cell Biol *7*, 2087-2096.

Sauer, L., Gitenay, D., Vo, C., and Baron, V. T. (2010). Mutant p53 initiates a feedback loop that involves Egr-1/EGF receptor/ERK in prostate cancer cells. Oncogene *29*, 2628-2637.

Schönhuber, N., Seidler, B., Schuck, K., Veltkamp, C., Schachtler, C., Zukowska, M., Eser, S., Feyerabend, T. B., Paul, M. C., Eser, P.*, et al.* (2014). A next-generation dual-recombinase system for time- and host-specific targeting of pancreatic cancer. Nat Med.

Schneider, G., Siveke, J. T., Eckel, F., and Schmid, R. M. (2005). Pancreatic cancer: basic and clinical aspects. Gastroenterology *128*, 1606-1625.

Senecoff, J. F., Rossmeissl, P. J., and Cox, M. M. (1988). DNA recognition by the FLP recombinase of the yeast 2 mu plasmid. A mutational analysis of the FLP binding site. J Mol Biol *201*, 405-421.

Shin, S., Wolgamott, L., Yu, Y., Blenis, J., and Yoon, S. O. (2011). Glycogen synthase kinase (GSK)-3 promotes p70 ribosomal protein S6 kinase (p70S6K) activity and cell proliferation. Proc Natl Acad Sci U S A *108*, E1204-1213.

Singh, S., Upadhyay, A. K., Ajay, A. K., and Bhat, M. K. (2007). p53 regulates ERK activation in carboplatin induced apoptosis in cervical carcinoma: a novel target of p53 in apoptosis. FEBS letters *581*, 289-295.

Son, J., Lyssiotis, C. A., Ying, H., Wang, X., Hua, S., Ligorio, M., Perera, R. M., Ferrone, C. R., Mullarky, E., Shyh-Chang, N.*, et al.* (2013). Glutamine supports pancreatic cancer growth through a KRAS-regulated metabolic pathway. Nature *496*, 101-105.

Tang, D., Wu, D., Hirao, A., Lahti, J. M., Liu, L., Mazza, B., Kidd, V. J., Mak, T. W., and Ingram, A. J. (2002). ERK activation mediates cell cycle arrest and apoptosis after DNA damage independently of p53. J Biol Chem *277*, 12710-12717.

Tauriello, D. V. F., and Batlle, E. (2016). Targeting the Microenvironment in Advanced Colorectal Cancer. Trends in cancer *2*, 495-504.

Vojtek, A. B., Hollenberg, S. M., and Cooper, J. A. (1993). Mammalian Ras interacts directly with the serine/threonine kinase Raf. Cell *74*, 205-214.

Warne, P. H., Viciana, P. R., and Downward, J. (1993). Direct interaction of Ras and the amino-terminal region of Raf-1 in vitro. Nature *364*, 352-355.

Wittinghofer, A., and Pai, E. F. (1991). The structure of Ras protein: a model for a universal molecular switch. Trends Biochem Sci *16*, 382-387.

Wu, C. Y., Carpenter, E. S., Takeuchi, K. K., Halbrook, C. J., Peverley, L. V., Bien, H., Hall, J. C., DelGiorno, K. E., Pal, D., Song, Y.*, et al.* (2014). PI3K Regulation of RAC1 Is Required for Kras-Induced Pancreatic Tumorigenesis in Mice. Gastroenterology.

Wullschleger, S., Sakamoto, K., Johnstone, L., Duce, S., Fleming, S., and Alessi, D. R. (2011). How moderate changes in Akt T-loop phosphorylation impact on tumorigenesis and insulin resistance. Dis Model Mech *4*, 95-103.

Ying, H., Kimmelman, A. C., Lyssiotis, C. A., Hua, S., Chu, G. C., Fletcher-Sananikone, E., Locasale, J. W., Son, J., Zhang, H., Coloff, J. L.*, et al.* (2012). Oncogenic Kras maintains pancreatic tumors through regulation of anabolic glucose metabolism. Cell *149*, 656-670.

Zamboni, G., Hirabayashi, K., Castelli, P., and Lennon, A. M. (2013). Precancerous lesions of the pancreas. Best practice & research Clinical gastroenterology *27*, 299-322.

Zhang, X. F., Settleman, J., Kyriakis, J. M., Takeuchi-Suzuki, E., Elledge, S. J., Marshall, M. S., Bruder, J. T., Rapp, U. R., and Avruch, J. (1993). Normal and oncogenic p21ras proteins bind to the amino-terminal regulatory domain of c-Raf-1. Nature *364*, 308-313.

Zhang, Y., Lazarus, J., Steele, N. G., Yan, W., and Lee, H. J. (2020). Regulatory T-cell Depletion Alters the Tumor Microenvironment and Accelerates Pancreatic Carcinogenesis. *10*, 422-439.
Zurashvili, T., Cordón-Barris, L., Ruiz-Babot, G., Zhou, X., Lizcano, J. M., Gómez, N., Giménez-Llort, L., and Bayascas, J. R. (2013). Interaction of PDK1 with phosphoinositides is essential for neuronal differentiation but dispensable for neuronal survival. Mol Cell Biol *33*, 1027-1040.

8. Acknowledgements

I would like to thank everyone who helped me to the success of this MD thesis.

First of all, I thank Prof. Dr. Dieter Saur for giving me the opportunity to work on this interesting project, for his constructive advice, valuable comments on the project and revision of the thesis. He is an excellent supervisor with intelligence and diligence.

I also thank PD Dr. Günter Schneider for his kindness being a member of my Doctoral committee and for the discussion and analysis of experiments.

Furthermore, I owe my gratitude to Dr. Felix Hesse for sharing pathological data in his doctoral dissertation, to Dr. Nina Schönhuber for the help of the pre-experiments of this project, to Magdalena Zukowska and Markus Raspe for the excellent technical support.

I am also grateful to all other colleagues for discussion and the nice atmosphere in the lab.

Last but not least, I thank my family and my friends who always supported me.